Republic of Iraq
Ministry of Higher Education
And Scientific Research
AL-Qadisiyah University
College of Education
Physics Department

Interfacial Shear Strength and Energy Release Rate Measurement for Fiber-Matrix Materials Drag-Out from Polymer composite.

A Thesis
Submitted to Physics Department/College of Education
AL-Qadisiyah University in Partial Fulfillment of
Requirements for the Degree of Master of Science in
Physics

By
Elaf Adel Abd Ali AL-Bderey
B.Sc. AL-Qadisiyah University 2014

Supervisors
Asst. Brof .Dr. Hisham Mohammed ali Hasan AL-Barmany

201٧ A. D.   1438 A. H.

CERTIFICATION OF THE SUPERVISOR

I certify that this thesis entitled **"Interfacial Shear Strength and Energy Release Rate Measurement for Fiber-Matrix Materials Drag-Out from Polymer composite"** Was Prepared By **"Elaf Adel Abd Ali"** under my supervision at Department of Physics, Faculty of education, University of AL-Qadisiyah, as a partial fulfillment for the requirements for the Degree of Master in physics science.

Signature:

Name: Dr.Hisham Mohammed ali Al-Barmany (Supervisor)

Title: Assistant Professor

Address: University of AL-Qadisiyah

Date:

Based on the recommendation of (Assi.Prof.Dr. Hisham Mohammed Ali Hasan) I refer this thesis to the masters defense committee for their opinion.

Signature:

Name: Dr. Abd AL-Hussain Abbas Khudhaier

Title: Assistant Professor

Address: Physics Department/Faculty of

Education /University of AL-Qadisiyah

Date:

CERTIFICATION OF LINGUISTIC EVALUATOR

I certify that thesis entitled **"Interfacial Shear Strength and Energy Release Rate Measurement for Fiber-Matrix Materials Drag-Out from Polymer composite"** was prepared by **"Elaf Adel Abd Ali"** was evaluated linguistically, and I forward it for debate by the examination committee.

Signature:

Name: Jenan Atiya

Title: Lecturer

Address: Department of English /College of Education /University of AL-Qadisiyah

Date: 6/10/2016

CERTIFICATION OF SCIENTIST EVALUATOR

I certify that thesis entitled **"Interfacial Shear Strength and Energy Release Rate Measurement for Fiber-Matrix Materials Drag-Out from Polymer composite."** was prepared by **"Elaf Adel Abd Ali"** was evaluated scientifically, and I forward it for debate by the examination committee.

Signature: Burhan

Name: Burhan Rashid Alshafaay

Title: Assist. professor

Date 15/1/2017

Examining Committee Certification

We, the member of examining committee, certify that we have read this thesis entitled "**Interfacial Shear Strength and Energy Release Rate Measurement for Fiber-Matrix Materials Drag-Out from Polymer composite** "and examined the student " **Elaf Adel Abd Ali** " in its contentsand that, in our opinion it is adequate for the partial fulfillment of the Requirements for the degree of Master of Sciencein Physics.

Signature:

Name: Prof. Abbas Fadhel Essa

Address: University of Wasit College of science

Date: 11/4/2019
(Chairman)

Signature:

Name: Asst. Prof. Hayder M. Abduljalil

Address: University of Babylon
College of science
Date: 10 - 4 - 2017
(Member)

Signature:

Name: Asst. Prof. Raheem A. Jaber

Address: University of Al- Qadisiayh,
College of Education
Date: ٢٧/٤/٢٠.
(Member)

Signature:

Name: Asst. Prof. Hisham Mohammed ali Al-Barmany
Address: University of Al-Qadisiyah College Computer Science and Information Technology
Date: 12 - ٢ - 2017
(Member and Supervisor)

Approved by the Deanery of the College of Education

Signature

Name: Prof. Dr. Khalid Jawad Kadhim Al-Adilee
Rank: Professor
Position: Dean of College of Education   Date: / /

بسم الله الرحمن الرحيم

﴿ وَكَذَلِكَ أَوْحَيْنَا إِلَيْكَ رُوحًا مِنْ أَمْرِنَا مَا كُنْتَ تَدْرِي مَا الْكِتَابُ وَلَا الْإِيمَانُ وَلَكِنْ جَعَلْنَاهُ نُورًا نَهْدِي بِهِ مَنْ نَشَاءُ مِنْ عِبَادِنَا وَإِنَّكَ لَتَهْدِي إِلَى صِرَاطٍ مُسْتَقِيمٍ ﴾

صَدَقَ اللهُ الْعَلِيُّ الْعَظِيمُ

الآية (٥٢) سورة الشورى

DEDICATION

To whom left me ......my mother

To whom given me hope ......my father

ACKNOWLEDGEMENT

In the name of ALLAH, the most compassionate the most merciful.
Praise be to ALLAH and pray and peace be on his prophet
Mohammed his relatives and companions and on all those who follow
him.
First, I would like to express my sincere gratitude to my supervisor;

Asst. Prof.Dr.Hisham Mohammed Ali Hasan AL-Barmany for their

remarkable suggestion, encouragement and guidance through the

research; I am really indebted to him.

My thanks to the Deanship of the College of Education and the

presidency of the department of Physics AL-Qadisiyah University for

them available to me the opportunity to complete my studies.

Also extend my thanks to the professors of the Department of Physics

and single out Dr. Salim Azara Hussein and the department staff and

graduate students in the department.

I would like to extend my gratitude of the chemistry department for

their cooperation in the examination of samples.

Finally, thanks to my family, I express my deepest appreciation for

their Love, help, understanding, and support.

Elaf Adel

Abstract

A drag-out test of different single fiber-matrix materials of U-shaped specimens have been used to calculate the interfacial shear strength and the energy release rate at interface in post cure with three values of temperature (25^oC, 50^oC, 75^oC) which include the effect of thermal stress and friction. Steel molds are used to make polysiloxane molds of different embedded lengths. These polysiloxane molds used to cure two kinds of matrices, epoxy and polyester after fixing single fiber. The fibers used are glass fiber, carbon fiber, Kevlar and polyethylene fiber of different embedded lengths and diameters with each kind of matrix. A force displacement curve for low range force specimen obtained from drag-out test. Matched between drag-out test analysis and Nairn model for microbond test done in order to calculate the interfacial shear strength and the energy release rate of debond fiber at interface. The results have been shown to increase the post cure, lead to increased adhesion, as well as increased energy release rate. The best composite has been obtained epoxy-kevlar fiber.

I

Contents

List of Symbol

Symbol	Definition
a	**Crack length**
$C_T(a)$	**Stress-transfer function**
E_A, E_F	**Axial modulus of fiber**
E_m	**Axial modulus of matrix**
E_T	**Transfer modulus of fiber**
F_d	**Peak force in force-displacement curve**
F_{knik}	**Knick force in force-displacement curve**
G_A	**Shear modulus of fiber**
G_m	**Shear modulus of fiber**
$G(a)$	**Energy release rate of crack length a**
$G_\infty(l_e)$	**Energy release rate of long droplet limit**
H	**Cross head displacement in drag-out test**
$l_{1/2}$	**Half free length of U-shape specimen**
l_e	**Embedded fiber length**
r_f	**Fiber radius**
r_m	**Matrix radius**
V_1	**Fiber volume fraction**
V_2	**Matrix volume fraction**
α_A	**Axial thermal expansion of fiber**
α_m	**Thermal expansion of matrix**
α_T	**Transverse thermal expansion coefficient of fiber**
β	**Shear-lag parameter**
ε_f	**Strain in fiber**
ε_m	**Strain in matrix**
υ_A	**Axial poisson ratio of fiber**
υ_m	**Axial poisson ratio of matrix**
υ_T	**Transverse poisson ratio of fiber**
σ_f	**Tensile stress on fiber**
σ_m	**Tensile stress on matrix**
τ_{ifss}	**Interfacial shear strength**
W	**External work**
k	**Frictional stress transfer**
FRP	**Fiber reinforce polymer**

Chapter One
Introduction

1-1 Introduction:

In history of man using bricks made of clay and reinforced with straw are an early example of application of composites. The individual constituents, clay and straw, could not serve the function by themselves but did when put together. Some believe that the straw was used to keep the clay from cracking, but others suggest that it blunted the sharp cracks in the dry clay. Historical examples of composites are abundant in the literature. Significant examples include the use of reinforcing mud walls in houses with bamboo shoots, glued laminated wood by Egyptians (1500 B.C.), and laminated metals in forging swords (A.D. 1800). In the 20th century, modern composites were used in the 1930s when glass fibers reinforced resins [1].

1-2 Composite Materials:

A composite is a structural material that consists of two or more combined constituents that are combined at a macroscopic level and are insoluble in each other. The first combined is called the reinforcing and the second called the matrix [1]. In other word materials system composed of a mixture or combination of two or more micro- or macro constituents that differ in chemical composition [1,2].

On the basis of matrix phase, composites can be classified into metal matrix composites, ceramic matrix composites, and polymer matrix composites as shown in Fig (1-1). The classifications according to types of reinforcement are particulate composites (composed of particles), fibrous composites (composed of fibers), and laminate composites (composed of laminates). Fibrous composites can be further subdivided on the basis of natural/biofiber or synthetic fiber. Biofiber encompassing composites are

referred to as biofiber composites. They can be again divided on the basis of matrix, that is, no biodegradable matrix and biodegradable matrix. Bio-based composites made from natural/biofiber and biodegradable polymers are referred to as green composites. These can be further subdivided as hybrid composites and textile composites. Hybrid composites comprise of a combination of two or more types of fibers [3,4].
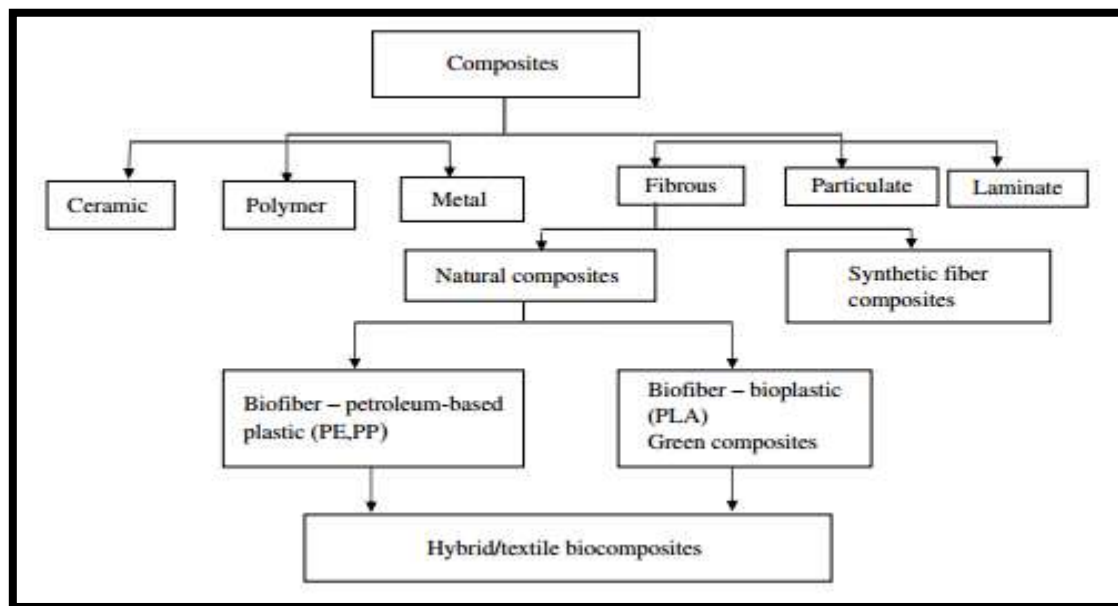
Fig (1-1) Classification of composites [3].

1- Particulate composites consist of particles immersed in matrices such as alloys and ceramics. They are usually isotropic because the particles are added randomly. Particulate composites have advantages such as improved strength, increased operating temperature, oxidation resistance, etc. Typical examples include use of aluminum particles in rubber; silicon carbide particles in aluminum; and gravel, sand, and cement to make concrete.

2- Flake composites consist of flat reinforcements of matrices. Typical flake materials are glass, mica, aluminum, and silver. Flake composites provide advantages such as high out-of-plane flexural modulus,higher strength, and low cost. However, flakes cannot be oriented easily and only a limited number of materials are available for use.

3-Fiber composites consist of matrices reinforced by short (discontinuous) or long (continuous) fibers. Fibers are generally an isotropy and examples include carbon and aramids [1].

One of modern composites is fiber reinforcing polymers (FRP), these composites consist of fibers with high stiffness, and high strength and small diameters reinforce a polymer matrix to use in many cases as a substitute for the traditional metals. The high specific stiffness and strength as well as the cheap cost for manufacturing the polymer matrix give polymer composite materials a huge market and research attention [2,5,6]

There are two types of polymer matrix materials the first is thermosetting resins the most usually used resins are epoxy, unsaturated polyester and vinyl ester. The liquid resin is converted into a hard rigid solid by chemical cross-linking, which leads to the formation of a tightly bound three-dimensional network. This is usually done while the composite is being formed. The mechanical properties depend on the molecular units making up the network and on the length and density of the cross-links. The former is determined by the initial chemicals used and the latter by control of the cross-linking processes in the cure. Curing can be achieved at room temperature, but it is usual to use a cure schedule which involves heating at once or more temperatures for predetermined times to achieve optimum cross -linking and hence optimum properties.

The second types are thermoplastic unlike thermosetting resins, thermoplastics are not cross-linked. They derive their strength and stiffness from the ingrained properties of the monomer units and the very high molecular weight [6,7].

The most important difference from thermosetting ones is the fact that no chemical reaction occurs during processing. The thermoplastic matrix is heated over its softening or melting temperature, thus enabling the forming; subsequently, the part is cooled. This implies both advantages and disadvantages compared to thermosetting [8].

1-3 Testing Types:

1-3-1 Microbond and Pull-out Test:

Microbond and pull-out test a single fiber embedded in droplet matrix and fiber is pull out by force from the matrix. The analyses for the microbond test and the pull-out test are very similar as in Fig (1-5), but there are two important differences.

1-In the microbond test, the fiber is pulled while the top of the matrix is restrained. The force on the fiber is balanced by a restraining force on the matrix. The net stress on the free droplet below the loading point is zero. While in the pull-out test the fiber is pulled while the matrix droplet is typically restrained on the opposite end. This loading from both ends leads to a non-zero net stress throughout the specimen.

2-The amount of matrix material used. Microbond specimens typically use a small amount of matrix while pull-out tests use much more matrix. There are two terms in the final energy release rate analysis that depend on the rate of stress transfer between the matrix and the fiber. In the microbond

test, these stress-transfer terms can be determined sufficiently accurately by shear-lag methods. In the pull-out test, the shear-lag methods have to be modified or replaced to get good stress-transfer results. The stress-transfer terms are only important when there is significant friction on the interface or when the total embedded fiber length is small. If friction is low and the embedded fiber length is long, the energy release rate in both the microbond test and in the pull-out test can be determined without need for any stress-transfer analysis [9].
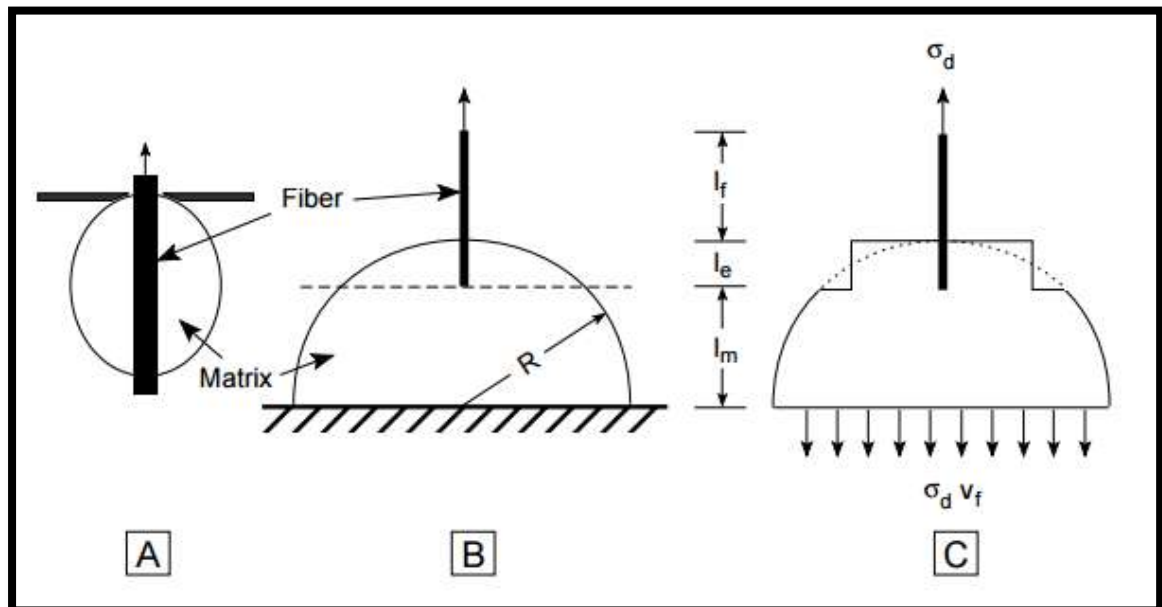
 Fig. (1-2) (A) Microbond test (B) Pull-out test (C) The conversion of the embedded fibre zone to equivalent, concentric fibre and matrix cylinders. [9].

1-3-2 Drag-Out Test

The drag out configuration involves a sample that has a free length and two embedded fiber areas which explain in Fig (1-6). A force is applied at a point on the free length in a direction perpendicular to the fiber. In drag-out test a specimen of U-shaped matrix is use to calculate the

interfacial shear strength and the energy release rate between single fiber and matrix. The drag-out test can be used with flexible fibers in situations where the fibers have both ends embedded in the matrix. From the analysis of drag-out test a relation between the drag-out force and pull-out component force could be obtained and then the data generated in drag-out test use as input in theoretical Nairn model to evaluate the interfacial shear strength and the energy release rate at interface [10].
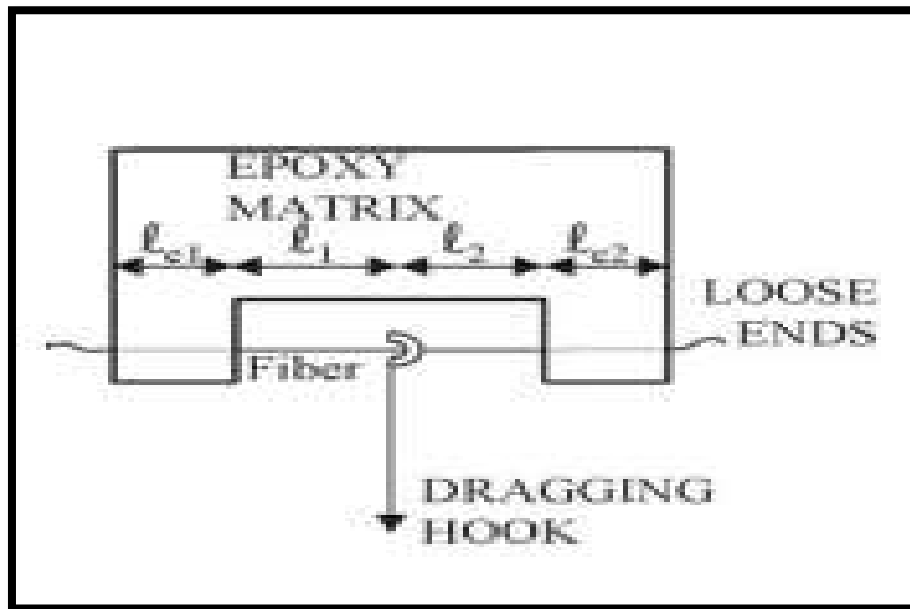
Fig (1-3) Drag-out single fiber test [10].

1-4 Thermal Stress

Thermal stresses are stresses induced in a body as a result of changes in temperature. An understanding of the origins and nature of thermal stresses is important because these stresses can lead to fracture or undesirable plastic deformation. Thermal stresses will be introduced. The magnitude of the stress ∂ resulting from a temperature change from T_0 to T_f is $\sigma = E\alpha_1(T_0 - T_f) = E\alpha_1\Delta T$

Where E is the modulus of elasticity and α_1 is the linear coefficient of thermal expansion [11].

When a solid body is heated or cooled, the internal temperature distribution will depend on its size and shape, the thermal conductivity of the material, and the rate of temperature change. Thermal stresses may be established as a result of temperature gradients across a body, which are frequently caused by rapid heating or cooling, in that the outside changes temperature more rapidly than the interior differential dimensional changes serve to restrain the free expansion or contraction of adjacent volume elements within the piece. For example upon heating, the exterior of a specimen is hotter and, therefore, will have expanded more than the interior regions, hence, compressive surface stresses are induced and are balanced by tensile interior stresses. The interior–exterior stress conditions are reversed for rapid cooling such that the surface is put into a state of tension [11].

1-5 Literature Review

Scheer and Nairn (1995), [21] researchers study several stress analysis methods were used to find the energy release rate for initiation of an interfacial crack in a microbond specimen. First, in this paper used a recently derived variational mechanics analysis of the stresses in a microbond specimen. Previous studies for analysis of crack growth have used shear-lag methods. For a second analysis, use present a new, and more complete, shear-lag analysis of the microbond specimen. Calculated energy release rate was used to predict the debonding stress as a function of the droplet length. The predictions were compared to two experimental results. new analyses that include residual thermal stresses were found to be the best.

Nairn, et al. (1996), [13] researchers consider fragmentation experiments as a set of experimental results for fiber break density as a function of applied strain. This paper explores the potential for using fracture mechanics or energy methods in interpreting fragmentation experiments. Researchers found that energy does not control fiber fracture; instead, fiber fracture releases much more energy than required to fracture the fiber. The excess released energy can lead to other damage mechanisms such as interfacial debonding. By assuming that all the excess released energy causes interfacial debonding and balancing energy using the energy release rate for debonding, researchers were able to determine interfacial toughness from fragmentation experiments. A reliable determination of interfacial toughness requires prior knowledge of interphase stress-transfer properties, fiber failure properties, actual damage mechanisms, and the coefficient of friction at the interface.

Liu and Nairn (1999), [14] this researchers study the energy release rate model based on a generalized fracture mechanics of composites was developed for analyzing the microbond test. This model includes both friction at the fiber/matrix interface and residual thermal stresses. A series of microbond tests on macroscopic specimens were carried out for evaluating the model. In some specimens could observe debond crack growth. These results could be interpreted with a fracture mechanics R-curve which led to a measured interfacial fracture toughness. In many specimens, debond crack growth could not be observed. They developed an approximate method for determining interfacial fracture toughness even without knowledge of debond crack size. The macroscopic specimens were designed for studying the optimal approach to analysis of microbond

specimens. The geometry of the macroscopic specimens, however, could also be used to measure the mode II toughness of adhesive bonds.

Zhandarov, et al. (2000), [15] Researchers study single-fiber pull-out tests were used for investigation of interfacial bond strength or toughness and load transfer between polymeric matrices and glass fibers having different diameters. The interfacial bond strength was well characterized by ultimate interfacial shear strength whose values were nearly independent of fiber diameter. The same experiments were also analyzed by fracture mechanics methods to determine the interfacial toughness (G_{ic}). The critical energy release rate (G_{ic}) was a good material property for constant fiber diameter, but G_{ic} for initiation of debonding typically got smaller as the fiber diameter got larger. It was also possible to measure an effective shear-lag parameter, β, characterizing load transfer efficiency between the fiber and the matrix. β decreased considerably with the fiber radius; this decrease scaled roughly as expected from elasticity theory.

Nairn, (2000), [16] by partitioning the total stresses in a damaged composite into either mechanical and residual stresses or into initial and perturbation stresses, it was possible to derive two exact results for the energy release rate due to crack growth. These general results automatically include the effects of residual stresses, traction loaded cracks, and imperfect interfaces. These effects are normally not needed in fracture mechanics of homogeneous materials, but they are commonly needed for fracture mechanics of composites. The general results were used to consider mode I fraction in composites, fracture and thermal cracking for two-phase, isotropic composites, and interfacial fracture in the microbond and single-fiber, pull-out tests. The analysis of interfacial fracture illustrates the importance of including friction effects in the energy release rate and not as

part of the toughness of the composite. Many composite damage modes consist of a series of events instead of stable crack propagation. A new analysis method called finite fracture mechanics is proposed that predicts that the next event occurs when the total energy released by that event exceeds some critical value or toughness for that type of event. A finite fracture mechanics model for microcracking that can correlate the results from many laminates is described.

Nairn, et al. (2001), [17] Researchers study the energy release rate for propagation of a debond in either a single-fiber pull-out test or a microbond test was derived analytically. The key finding was that an accurate analysis can be derived by a global energy analysis that includes effects of residual stresses and interfacial friction but does not need to include the details of the stress state at the interfacial crack tip. The analytical results were verified by comparison to finite element analyses. The energy release rate expressions were used to determine interfacial fracture toughness from single-fiber pull-out tests or microbond tests. The experiments included both macrosized model microbond specimens (steel wire/epoxy) and micro-sized pull-out and microbond specimens (glass fiber/epoxy or vinyl ester). In all experiments, it was critical to correctly account for the true level of residual stresses in the specimen; it some experiments, the inclusion of friction was also critical.

Nuriel, et al. (2005) [10] researchers were developed an experiment to measure the interfacial adhesion in nanotube–polymer composites by 'dragging-out' a single nanotube from a polymer matrix using an atomic force microscope tip. To quantify the data, an approximate analysis was used. Here, this 'drag-out' configuration is reproduced at a larger scale, namely, using a single flexible fiber (polyethylene) bridging a polymer

(epoxy) hole. The data generated from this single fiber drag-out experiment was used as input in a new theoretical model that evaluates the interfacial shear adhesion at the fiber–matrix interface. Comparisons were made between the data generated from the single fiber drag-out and independent pull-out data produced in a classical microbond experiment with the same material system. The drag-out data compare fairly well with the microbond test data, and are found to be of the same order of magnitude as in the literature.

AL-Abdly,et al, (2008) [18] researchers tubular –shaped fiber reinforced composites were manufactured by using two types of resin epoxy (EP) and unsaturated polyester (UP), each was separately reinforced with glass, carbon and kevlar-49 fibers (filament and woven roving), hybrid reinforcement composites of these fibers were also prepared. The adhesion force test of the prepared specimens was carried out. These adhesion forces exhibited a peak value at a percent of hardener/resin (H/R)= 3% for UP matrix with all type of fiber arrangements while 30% was obtained for EP matrix. Such behavior was declined with increase in temperatures. Glass transition temperatures were determined from these measurements, and found to be 90°C for EP– glass and 83°C for UP –glass composites.

Hassan, (2008) [19] the characteristic of adhesion at the interface between polyethylene fiber and thermoset matrix composites could be studied by Kell-Tyson stress-based model and Nairn energy-based model including thermal stress and friction effect, which was more realistic than stress-based model as seen in the energy release rate of polyester-polyethylene fiber (38.273 J/m2) which was more shrinkage than epoxy where the energy release rate for epoxy-polyethylene fiber (34.952 J/m2), while the interfacial shear srength for polyester-polyethylene (0.77 MPa)

less than interfacial shear strength for epoxy-polyethylene fiber (0.811 MPa). The ultra high pollyethylene fiber molecule is inert and non-polar in nature, and thus chemical bonding with an adhesive is poor so the main adhesion was for thermal stress, which also explain that energy release rate was not depend on crack length (embedded length). In friction region the slip-hardening was due to soft surface of ultra high polyethylene fiber in comparison with matrix surface caused fiber surface fiber abrasion.

Al-Mullakhalaf, et al. (2011) [20] researchers study the debonding force between fiber and matrix for different fiber diameters through pull-out test technique where the fiber was embedded to a depth of (30) µm into the matrix. Kevlar 29 was selected as reinforcing fiber, and the tested diameters were (0.2, 0.4, 0.45, 0.5) mm, while the epoxy was of type Euxit 50. In the second stage of this research a panel of (4) mm thickness, and of three densities, which were (3, 4, and 5) fibers per centimeter, and the fiber reinforcement layer was located at the first third of the specimen thickness. Flexural, tensile, and fatigue tests were performed. The results showed that, in the pull-out test, the base area of the fiber should be less than the side area, which affect the debonding force.

Aruniit, et al. (2012) [21] researchers study examines the effect of different post cure parameters to a polymer matrix particulate reinforced composite material. The goal is to evaluate the importance of different factors and to suggest a well-balanced post cure mode that supports the application of the material. Polymer matrix composites are post cured at elevated temperature to increase the amount of cross linking to achieve better chemical and heat resistance and mechanical properties. Every material has an individual post cure process that depends from the raw materials. Post curing variables include temperature, duration of cure, the

time between initial curing and post curing and temperature profile gradient. There are several ways to determine the cure state of a polymer. It can be evaluated based on the mechanical and physical properties, residual styrene content, glass transition temperature, residual exotherm or solvent swelling test. For the determination of the suitable post cure parameters test slabs were casted and post cured with varying time and temperature. Glass transition temperature, residual exotherm, softening in ethanol, surface hardness, flexural strength and flexural modulus were determined. It is shown that the material should be cured at 60°C– 80°C. With higher temperature and extended time of cure the glass transition temperature raises but the material becomes too brittle.

Kumar, et al. (2015) [22] researchers curing cycle has a strong impact on the thermal and mechanical behavior of thermosetting polymers. The extent of cross-linking which is a strong function of curing temperature and time is directly linked to the glass transition temperature (T_g) of the thermosetting polymer. This transition temperature speaks about the transformation of the polymer from glassy state to rubbery state, hence decides the applicability of the material at certain temperature with certain degree of safety and reliability. The results revealed that the ILSS and T_g are significantly affected with post curing parameters. No significant change in ILSS was obtained at 80 °C over the entire curing time. In case of 110 ° C a smooth increment in ILSS was observed with time (even till 12 hrs). For samples post cured at 140 °C a rapid improvement in ILSS takes place with time followed by saturation. With all the possible combinations of curing temperature and time, optimum values are noticed at 140° C for 6 h.

Ramesh, et al. [23] researchers have been depending heavily on synthetic materials for various applications. In the present work, jute, banana and glass fibers are reinforced with epoxy resin in alternative positioning and various probabilities at different post curing temperature to form sandwich type composites. The composite block was cured at room temperature for 24h. The cold cured composite block was then post cured at various post curing temperature of 30°C, 60°C, 90°C, 120°C, 150°C and 180°C and 3KPa pressure in the hot press for 10minutes. The tensile and flexural properties of the composites obtained at different post curing temperature were studied. The morphology of the tensile fracture was studied using scanning electron microscopy analysis.

1-6 Aims of the Work

The aim of this work is to get the best adhesion between fiber and Matrix in the Interface area and study the effect of the cost cure on the adhesion, and calculated the energy release rate.

Chapter two

Mathematical

Model

2-1 Introduction:

Study of interface in composite system is essential for the development of an understanding the science and technology of composite materials. The important property of interface that can greatly affect the mechanical behavior is strength of adhesive bonding between the reinforcement and the matrix in composite materials, when load is applied to fiber reinforced composite. The load is transferred between the fiber and matrix through the interface. Several micromechanical test methods have been developed to determine the interface properties of composite by measuring the level of adhesion between a reinforcing fiber and resin matrix [21].

The level of fiber–matrix interfacial adhesion in composites is traditionally evaluated by means of a stress-based parameter. Recently, it was suggested that an interfacial energy parameter might constitute a valid alternative. From an overview of the literature regarding the single-fiber composite fragmentation test, it appears that energy-based approaches have already been proposed in the past, but were either not successful, or not fully developed. In this work recent energy balance scheme, proposed for the analysis of the initial interface debonding which occurs at fiber breaks during a fragmentation test, is presented and expanded here. The effects of thermal residual stress in the fiber, and of friction in the debonded area, are now incorporated in the energy balance model. It can use a different shear-lag parameter proposed by Nayfeh rather than the commonly used Cox parameter [29].

The analysis of test data falls into substantially different approaches for quantitative characterization of interfacial strength. The first approach is the stress-based in which the mechanical stress at

interface is determined and interfacial strength is characterized by certain value of interfacial stress at which the interface fails. The second approach is the energy-based which depend on shear-lag analysis that calculates the stresses along the interface and fracture mechanics and based on the determination of amount of energy releases in specimen during interfacial debonding per unit debonding area. It is assumed that interfacial failure occurs when energy release rate reaches its critical value, which is assuming to be a characteristic of the strength of the interface or interfacial toughness [23].

To calculate interfacial shear strength from equation definition is the ratio of maximum measured force (F) over the total interfacial are

$$\tau_{iss} = \frac{F}{2\pi r_f l_e}$$ …….. (2-1)

Where r_f is the fiber radius and l_e is the embedded fiber length. Physically this term is the average interfacial shear stress at the time of failure. It might be useful for qualitative work, but it has several limitations when one desires more rigorous interfacial characterization [30,31]

The interfacial shear strength cannot be an adequate characteristic of shear stress that actually exists at interface. The interfacial shear stress is smaller than maximum shear stress at moment of debonding which is obtained by the stress distribution of shear-lag analysis. Moreover the maximum force measured by micromechanical tests in micorbond, drag-out and pull-out are test affected by embedded length, internal stress and friction effect. In the energy-based approach which is dependent on Nairn and Co-worker model, the failure of interface in two popular interface tests microbond and pull-out [24,25,26].

It can be represented by a cylindrical single fiber surrounded by a hollow cylindrical of matrix or two concentric cylinders, a shear-lag analysis used to derive a system of equations for finding axial and shear stresses of two concentric cylinders and an energy release equation of crack propagation including internal stress and friction effect derived. In the experimental test the fiber is subjected to tensile stress which leads to a critical debonding shear stress (shear strength) that can be calculated from force-displacement curve in Fig (2-1)[27].
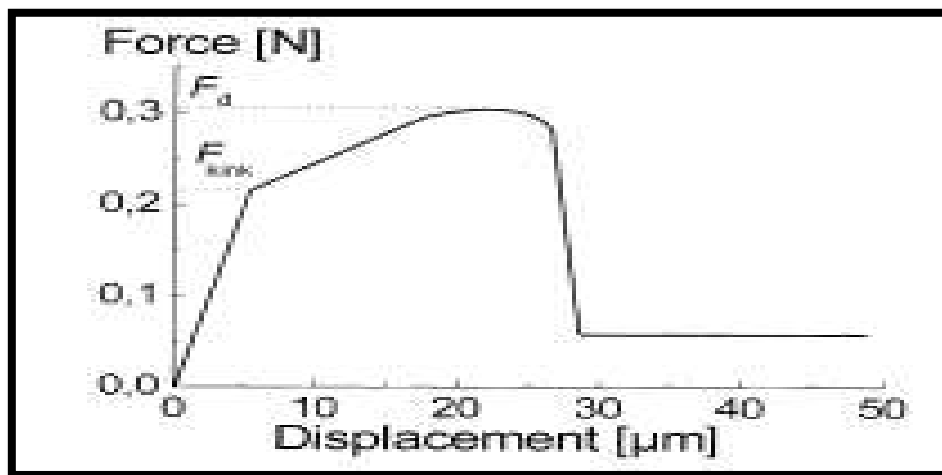

Fig (2-1) A typical force–displacement curve for Twaron–epoxy system from the pull-out test. The 'kink' indicates crack initiation [35]

From each force–displacement curve, a schematic is given in Fig (2-1) the force at a "kink" in the initial slope F_{kink}, the force of debonding (F_d) and the embedded length (l_e)[35].

2-2 Drag-out Test Analysis:

The drag out configuration involves a sample that has a free length and two embedded fiber areas. A force is applied at a point on the free length in a direction perpendicular to the fiber, as shown in Fig (2-2). The balance of forces for this configuration is shown in Fig (2-3). A hook

applies a tensile force (**F**) at a distance l_1 and l_2 from the left (A) and right (B) edges, respectively. (**H**) is the distance perpendicular to the baseline AB. The force causes a tension (**T$_i$**) in the fiber. The subscripts 1 and 2 refer to the left and right sides, respectively. The tension is a vector with a component (**P$_i$**) parallel to the baseline AB and a component (**R$_i$**) perpendicular to AB. The parallel component is equal to the pull-out force that acts to debond the fiber from the matrix [13].

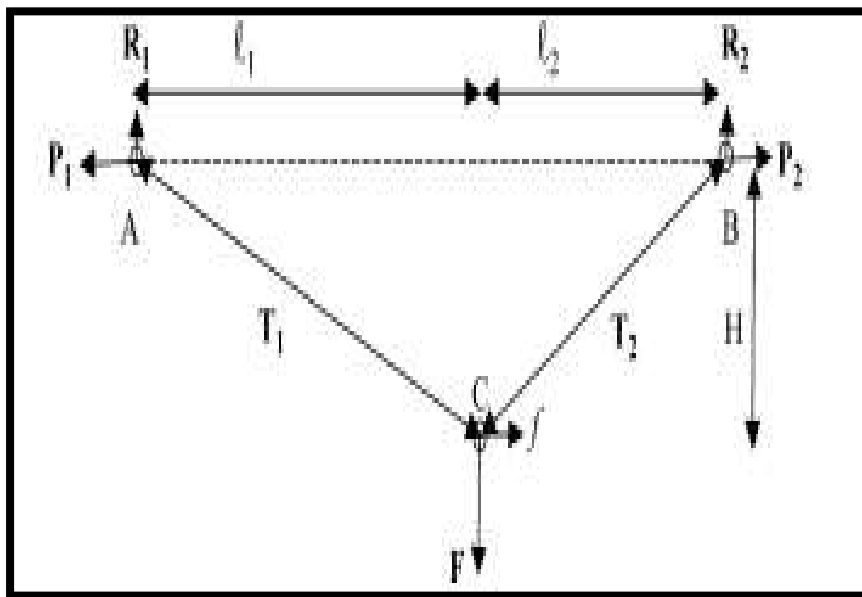**Fig (2-2) Force equilibrium for the drag-out configuration [13]**

If $l_1 \neq l_2$ then $P_1 \neq P_2$ and there is a horizontal balancing force f

$$p_1 = p_2 + f \qquad\qquad \text{.........(2-2)}$$

$$f = R_1 + R_2 \qquad\qquad \text{.........(2-3)}$$

From the torque balance get

$$R_1 l_1 = R_2 l_2 + fH \qquad\qquad \text{.........(2-4)}$$

Inserting Eqs (2-3) in (2-2)

$$R_1 l_1 = (F - R_1)l_2 + fH \qquad \qquad \text{………(2-5)}$$

$$R_1 = \frac{Fl_2 + fH}{l_1 + l_2} \qquad \qquad \text{……… (2-6)}$$

$$R_2 = \frac{Fl_1 - fH}{l_1 + l_2} \qquad \qquad \text{……… (2-7)}$$

The ratio between P and R is equal to the ratio between l and H

$$\frac{P_1}{R_1} = \frac{l_1}{H} \qquad \qquad \text{……… (2-8)}$$

And

$$\frac{P_2}{R_2} = \frac{l_2}{H} \qquad \qquad \text{……… (2-9)}$$

Isolating P in Eqs. (2-8) and (2-9) and inserting the expressions for R from Eqs. (2-6) and (2-7) gives:

$$P_1 = \frac{Fl_2 + fH}{l_1 + l_2} * \frac{l_1}{H} \qquad \qquad \text{………(2-10)}$$

And

$$P_2 = \frac{Fl_1 - fH}{l_1 + l_2} * \frac{l_2}{H} \qquad \qquad \text{………(2-11)}$$

If $l_1 = l_2 = l_{1/2}$ than $f = 0$ Eqs. (2-2), (2-8) and (2-9) become

$$R_1 = R_2 = \frac{F}{2} \qquad \qquad \text{……… (2-12)}$$

$$P_1 = P_2 = \frac{F}{2} * \frac{l_{1\backslash 2}}{H} \qquad \qquad \text{........ (2-13)}$$

The tension T in the fiber is:

$$T_1 = \sqrt{P_1^2 + R_1^2}$$ ……… (2-14)

$$T_2 = \sqrt{P_2^2 + R_2^2}$$ ……… (2-15)

Assuming that no interfacial debonding is present under a small applied force F, we have:

$$\sqrt{H^2 + l_1^2} = l_1 \left(1 + \frac{T_1}{AE}\right)$$ .... (2-16)

$$\sqrt{H^2 + l_2^2} = l_2 \left(1 + \frac{T_2}{AE}\right)$$ ……… (2-17)

The right-hand sides arise from the geometry, and the left side from Hooke's law

A is the fiber cross section and E is its Young's modulus.

If $l_1 = l_2 = l_{1/2}$ then $P_1 = P_2 = P$ and $T_1 = T_2 = T$

$$\sqrt{H^2 + l_{1\backslash2}^2} = l_{1\backslash2} \left(1 + \frac{\sqrt{p^2 + R^2}}{AE}\right)$$ .... (2-18)

From Eqs (2-9)

$$\sqrt{H^2 + l_{1\backslash2}^2} = l_{1\backslash2} \left(1 + \frac{\sqrt{R^2 \left(\frac{l_{1\backslash2}}{H}\right)^2 + R^2}}{AE}\right)$$ ……… (2-19)

In Eqs (2-3) $R_1 = R_2$ if $l_1 = l_2 = l_{1/2}$ then:

$$R = \frac{F}{2}$$

$$\sqrt{H^2 + l_{1\backslash2}^2} = l_{1\backslash2}\left(1 + \frac{F}{2AE}\sqrt{\left(\frac{l_{1\backslash2}}{H}\right)^2 + 1}\right) \qquad \ldots\ldots\ldots (2\text{-}20)$$

$$F = \frac{2AEH}{l_{1\backslash2}}\left(1 - \frac{l_{1\backslash2}}{\sqrt{H^2 + l_{1\backslash2}^2}}\right) \qquad \ldots\ldots\ldots (2\text{-}21)$$

From Eqs (2-8) if $l_1 = l_2 = l_{1/2}$ the pull-out force:

$$P = R\frac{l_{1\backslash2}}{H} = \frac{l_{1\backslash2}}{2} * \frac{F}{H} \qquad \ldots\ldots\ldots (2\text{-}22)$$

And

$$P = AE\left(1 - \frac{l_{1\backslash2}}{\sqrt{H^2 + l_{1\backslash2}^2}}\right) \qquad \ldots\ldots\ldots (2\text{-}23)$$

Where F is the applied force in drag-out test while P is the pull-out force component [13].

Equations (2-21), (2-23) are derived in elastic region and governed by Hooks law, before debonding between fiber and matrix occurs. The experimental data (drag-out force and the cross head displacement) indicates a knik point (F_{Knik}) (the drag-out force at crack initiation) while the drag-out force at peak is the maximum force in Fig (2-1) and the drag-out force at peak (F_d) point in which the crack equal approximately the length of embedded length as shown by Nairn[28].

2-3 Stress Analysis and Energy Release Rate

In Fig (2-3), show an idealized cylindrical model under test loading conditions. σ_f is the background fiber tensile stress or the stress on the fiber due to weight of the fiber below the droplet. σ_m is the stress applied to the droplet during the test. ξ and ζ represent the dimensionless radial and axial coordinates, respectively. The stresses on the top of the fiber and matrix cylinders are balanced with the σ_f stress on the bottom of the fiber. The net axial stress on any cross-section is $\sigma_0 = V_1\sigma_f$ where V_1 is the volume fraction of the fiber.
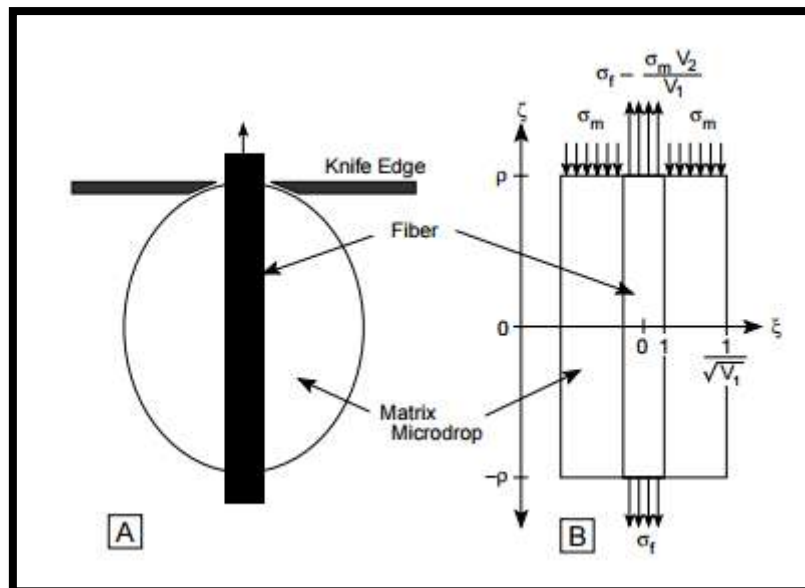

Fig (2-3) (A) microbond specimen of dimensionless length 2ρ, (B) Stress analysis [12].

A recent study has concluded that a critical energy release rate for interfacial crack growth failure criterion is more accurate than either an average shear or total energy failure criteria in predicting the failure load of microbond specimens. Recently derived variational mechanics analysis a new shear-lag analyses, two existing shear-lag analyses, and a simple

limiting model for long droplet lengths are all used to calculate the energy release rate for growth of an interfacial crack in the microbond specimen.

By assuming that debonding occurs when the energy release rate reaches a critical energy release rate, denoted as G_{ic}, predicted debond force as a function of droplet length for all[12,15].

2-3-1 Variation Mechanics stress Analysis

Used these equations because it is consistent with samples in the case around the drag-outt to pull-out. The droplet was assumed to be a cylinder on the fiber, the load was assumed to be applied uniformly over the top of the matrix cylinder. Axial ratio $\rho = l/2r_1$ where l is embeded length was analyzed by making only one assumption—that the axial stresses in the fiber and in the matrix cylinders depend only on the axial coordinate (z) and are independent of the radial coordinate (r), all stresses in the matrix and cylinder can be written in terms of a single unknown function, $\psi(\zeta)$, where $\zeta = z/r_1$ is a dimensionless axial coordinate normalized to the fiber radius, r_1. The stresses in the fiber are

$$\sigma_{zz,1} = \psi \qquad\qquad\qquad\qquad \text{……… (2-24)}$$

$$\tau_{rz,1} = -\frac{\xi\psi'}{2} \qquad\qquad\qquad\qquad \text{……… (2-25)}$$

$$\sigma_{rr,1} = \frac{\psi''}{16}\left(\xi^2(3+\upsilon_T)+\upsilon_m - \upsilon_T + \frac{2(1+\upsilon_m)\ln V_1}{V_2} - \frac{V_2 A_1}{V_1 A_0}\right) - \frac{V_2}{V_2}\left(\frac{A_3\psi + A_4\sigma_0 + A_5\Delta T}{A_0}\right)$$

$$\text{………. (2-26)}$$

$$\sigma_{\theta\theta,1} = \frac{\psi''}{16}\left(\xi^2(1+3\upsilon_T) + \upsilon_m - \upsilon_T + \frac{2(1+\upsilon_m)\ln V_1}{V_2} - \frac{V_2 A_1}{V_1 A_0}\right) - \frac{V_2}{V_1}\left(\frac{A_3\psi + A_4\sigma_0 + A_5\Delta T}{A_0}\right).$$

$$\ldots\ldots (2\text{-}27)$$

The stresses in the matrix are

$$\sigma_{zz,2} = \frac{\sigma_0}{V_2} - \frac{V_1\psi}{V_2} \qquad\qquad \ldots\ldots (2\text{-}28)$$

$$\tau_{rz,2} = \frac{V_1\psi'}{2V_2}\left(\xi - \frac{1}{\xi V_1}\right) \qquad\qquad \ldots\ldots (2\text{-}29)$$

$$\sigma_{rr,2} = \frac{\psi''}{16V_2}\left[(3+\upsilon_m)(1-\xi^2 V_1) + 2(1+\upsilon_m)\ln\xi^2 V_1 + \frac{V_2 A_1}{A_0}\left(1-\frac{1}{\xi^2 V_1}\right) + \left(1-\frac{1}{\xi^2 V_1}\right)\left(\frac{A_3\psi + A_4\sigma_0 + A_5\Delta T}{A_0}\right)\right]$$

$$\ldots\ldots (2\text{-}30)$$

$$\sigma_{\theta\theta,2} = \frac{\psi''}{16V_2}\left[(1+3\upsilon_m)(1-\xi^2 V_1) - 2(1-\upsilon_m)\ln\xi^2 V_1 + \frac{V_2 A_1}{A_0}\left(1+\frac{1}{\xi^2 V_1}\right) + \left(1+\frac{1}{\xi^2 V_1}\right)\left(\frac{A_3\psi + A_4\sigma_0 + A_5\Delta T}{A_0}\right)\right]$$

$$\ldots\ldots (2\text{-}31)$$

In these equations (2-24) and (2-25) refer to the fiber and matrix cylinders respectively, ν_m is the Poisson's ratio of the isotropic matrix, ν_T is the transverse Poisson's ratio of the transversely isotropic fiber, V_1 and V_2 are the volume fractions of the fiber and the matrix, A_1 to A_5 are material and geometry-specific constants[12].

σ_0 is the total stress applied in the z direction ($\sigma_0 = V1\sigma_f$ where σ_f is the background tensile stress), ΔT is the difference between the stress free temperature and the specimen temperature, and ξ is a dimensionless radial coordinate defined by $\xi = r/r_1$. By axisymmetry, the unspecified shear stresses are all zero. The stresses in Eqs (2-24)–(2-31) constitute an admissible stress state. By the principles of variational mechanics, the best approximation to the true stress state is found by finding the ψ (ζ)

that minimizes the total complementary strain energy. Depend only on mechanical properties of the fiber and matrix and on the geometry of the specimen physically, the constant ψ_0 is the far-field fiber stress or the stress that would exist in the fiber far from the ends of, an infinitely long droplet [12].

For energy release rate calculations, Need to calculate the total strain energy in the microbond specimen. Using the stresses in Eqs (2-24)–(2-31) to find the strain energy and integrating over the volume of the specimen gives the total strain energy. , the strain energy integral simplifies to

$$U(\rho) = \pi r_1^3 \int_{-\rho}^{\rho} d\zeta \left(C_{33}\psi^2 + 2C_{35}\psi\psi'' + C_{55}\psi''^2 + C_{44}\psi'^2 \right) \qquad \ldots\ldots\ldots (2\text{-}37)$$

In Eq. (2-37) assumed that $\sigma_f = \sigma_0 = 0$. This assumption follows the typical microbond experiment in which the background fiber stress σ_f is negligible. Eliminating σ_f leads to considerable simplification. If subsequent experiments show that σ_f is an important variable, the variational mechanics analysis can include its effects by rederiving the strain energy for non-zero σ_f. Substituting the known function $\psi(\zeta)$ and integrating gives[12]:

$$U(\rho) = 2C_{55}\rho\pi r_1^3 \left[\frac{D_3^2 \Delta T^2}{C_{33}^2} \left(\frac{C_{33}}{C_{55}} - \frac{X_e(\rho)}{\rho} \right) + \left(\frac{\sigma_m V_2}{2V_1} \right)^2 \left(\frac{X_e(\rho) + X_O(\rho)}{\rho} \right) \right] \quad \ldots(2\text{-}38)$$

2-3-2 Shear-Lag Stress Analysis:

The so-called "shear lag" method is often used for analysis of stress transfer problems in composites. The term "shear lag" can be traced, prior to its use in composites, to analysis of bending of I beams and T beams with wide flanges and to box beams. Simple beam theory

predicts that the axial displacements in the flanges of such beams are only a function of the distance from the neutral axis and independent of the distance from the web. This simple theory also predicts zero shear stress and zero shear strain in the flange. In reality, the true axial displacements "lag" behind the beam theory predictions. This "lag" is cause by load diffusion which can be viewed (using equilibrium arguments) as a consequence of non-zero shear stresses in the flange hence the term "shear-lag." In these beam analyses, "shear-lag" is an effect and not an analysis method. Many possible analysis methods can evaluate the "shear-lag" effect. These methods generally result in defining an effective flange width that is less than the actual flange width. [29,30].

A common problem analyzed by shear-lag methods is a solid fiber cylinder of radius r_1 embedded in a hollow matrix cylinder with inner radius r_1 and outer radius r_2

$$\frac{\partial^2 \tau_{rz}(r_1)}{\partial z^2} - \beta^2 \tau_{rz}(r_1) = 0 \qquad\qquad \text{.........(2-39)}$$

Where

$$\beta^2 = \frac{2}{r_1^2 E_A E_m} \left[\frac{E_A \upsilon_f + E_m \upsilon_m}{\dfrac{V_2}{4G_A} + \dfrac{1}{2G_m}\left(\dfrac{1}{V_2}\ln\dfrac{1}{V_1} - 1 - \dfrac{V_1}{2}\right)} \right] \qquad \text{......... (2-40)}$$

And V_1 and V_2 are the fiber and matrix volume fractions defined by

$$V_1 = \frac{r_1^2}{r_2^2} \qquad\qquad\qquad V_2 = \frac{r_2^2 - r_1^2}{r_2^2} \qquad \text{......... (2-41)}$$

E_A, E_m = Tensile Modulus

G_A, G_m = Axial shear modulus

The β^2 term Eq. (2-40), however, is very different than the one derived by Cox (1952) .The β^2 term here is identical to the one derived by Nayfeh and McCartney [31,.. ,34].

2-3-3 Energy Release Rate Analysis

The most widely used approach for analyzing failure in microbond specimens is to assume that the droplet shears off the fiber when the average shear stress at the interface, $\langle \tau_{rz}(\xi = 1) \rangle$, reaches the interfacial shear strength, τ_{ic}. By integrating the equations of stress equilibrium it is possible to derive an exact relation between $\langle \tau_{rz}(\xi = 1) \rangle$ and fiber force, F:

$$\langle \tau_{rz}(\xi = 1) \rangle = \frac{F}{2\pi r_1 l} \qquad \text{......... (2-42)}$$

The force, Fd, or the stress, $\sigma_d = -\sigma_m V_2 / V_1$,in the fiber at the instant of debonding as a function of droplet length are thus predicted to be linear

$$F_d = 2\pi r_1 l \tau_{ic} \quad \text{or} \quad \sigma_d = 4\tau_{ic}\rho \qquad \text{.........(2-43)}$$

There are two problems with Eq. (2-43). First, it is in poor agreement with experimental data over a wide range of droplet lengths. Second, despite that fact that Eq. (2-42) is an exact expression of stress equilibrium, the assumption that average shear stress determines failure is unrealistic. A variational stress analysis or a finite element analysis18 show that the shear stress is nonuniform and that there is a significant radial tensile stress concentration at the point where the fiber enters the droplet. It is probably incorrect to ignore these features of the stress state and attribute failure only to the level of average interfacial shear stress. It can be discuss a fracture mechanics method where debonding is predicted based on the energy release rate for initiation of an interfacial crack. The

highest interfacial stresses are at the point where the matrix is contacted by the microvise see in Fig (2-4) $\zeta = +\rho$. It is therefore logical to assume that debonding will be caused by initiation of an interfacial crack at $\zeta = +\rho$. This assumption agrees with experimental observations of microbond failures. In this section use the variational mechanics stress analysis and the shear-lag stress analysis to calculate the energy release rate for initiation of an interfacial crack G_i. By assuming that specimen failure occurs when G_i reaches the critical energy release rate for the interface, or the interfacial toughness, G_{ic}, further predict σ_d as a function of droplet length [17,35,36]

For a crack propagation analysis, we must consider a microbond specimen with an interfacial crack. Fig (2-4) shows an idealized microbond specimen with a crack of length a or dimensionless length 2δ where $\delta = a/2r_1$. The specimen is now divided into two regions—region I is the region within the interfacial crack and region II is the region with an intact interface. Our first step is to find the stresses and strain energies in each region. We begin by using the variational mechanics analysis.

Because the interfacial radial stress is tensile before crack formation, we assume the crack in Fig (2-4) opens and that the crack surfaces are stress free. The only possible stress state in region I in which σ_{zz} is independent of r is simple uniaxial tension. When σ_f is negligible, the axial stresses in the fiber and matrix are:

$$\sigma_{zz,1} = -\frac{\sigma_m V_2}{V_1} \qquad \text{and} \qquad \sigma_{zz,2} = \sigma_m \qquad \ldots\ldots\ldots(2\text{-}44)$$

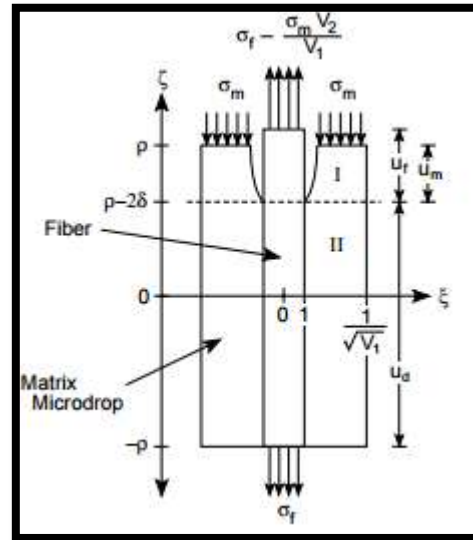**Fig (2-5) An idealized microbond specimen of dimensionless length 2ρ having an interfacial crack of dimensionless length 2δ emanating from the top of the droplet. Region I is the cracked region above the dashed line. Region II is the uncracked region below the dashed line [12].**

Using the general composite fracture mechanics methods and applying them to the geometry in Fig. (2-5) with an interfacial debond of length $_{(a)}$, the energy release rate for debond growth in both the pull-out and microbond specimens can be written as [12].

$$G(a) = \frac{r_f}{2} C_{33s}(\sigma_d - ka)^2 + \frac{r_f}{2} D_{3s}(2 + C_T'(a))(\sigma_d - ka)\Delta T +$$

$$\frac{r_f}{2}\left[\left(\frac{D_3^2}{C_{33}} + \frac{V_2(\alpha_T - \alpha_m)^2}{V_1 A_0} + \frac{2D_3 D_{3s}}{C_{33}} C_T'(a)\right)\Delta T^2 - kD_{3s} C_T(a)\Delta T\right] \quad .....(2\text{-}51)$$

$\Delta T =$ the different between stress free temperature and the specimen temperature

$C_T (a)$ = a stress-transfer function

Eq. (2-51) is essentially an exact result for debonding energy release rate in the concentric cylinders model including both the effects of residual thermal stresses and friction. Residual stresses are included by selecting

ΔT to match the true level of residual stresses in the specimen. Because rigorous modeling of coulomb friction is difficult, friction is included in an approximate manner. It is included by introducing a constant shear stress on the debond surface of τ_f. This frictional stress contributes to energy release rate by external work on the debond surfaces as the fiber and matrix slide by each other. In some experiments it is possible to measure τ_f and thus claim this approach can accurately include friction effects. The cumulative stress transfer function C_T (a) is defined [37...39]

$$C_T(a) = \int_0^{le-a} F(z)dz \qquad \text{......... (2-52)}$$

The model [9,12] ,suggested that an acceptable G(a=l) can be estimated by calculated G(a) from energy release rate curve for droplet has much larger than actual droplet. In reference [14] a well-behaved result got by calculation G(a) in long droplet limit or limit as $l_e \to \infty$ and the energy release rate G(a) in the limit as $l_e \to \infty$ could be calculated by found the limits on stress transfer function equations [40,41].

$$\lim_{le \to \infty} C_T(a) = \frac{1}{\beta} \quad \text{and} \quad \lim_{le \to \infty} C_T'(a) = 0$$

Substitute the results of above limits in Eq.(2-51)

$$G_\infty(a) = \frac{r_f}{2}\left[C_{33s}(\sigma_d - ka)^2 + D_{3s}(2\sigma_d - k(2a + \frac{1}{\beta})\Delta T + (\frac{D_3^2}{C_{33}} + \frac{V_2(\alpha_T - \alpha_m)^2}{V_1 A_0})\Delta T^2 \right]$$

$$\text{...... (2-53)}$$

σ_d = the axial stress at peak force in force- displacement curve

$$\sigma_d = \frac{F_d}{\pi r_f^2}$$

k = the fractional stress transfer = $\dfrac{2\tau_f}{r_f}$ and $\quad \tau_f = \dfrac{F_r}{2\pi r_f l_e}$

a= crack length = embedded length l_e at peak force (F_d)

$V_f = V_1$ = fiber volume fraction

$V_m = V_2$ = matrix volume fraction

$$V_1 A_0 = \frac{V_2(1-v_T)}{E_T} + \frac{V_1(1-v_m)}{E_m} + \frac{1+v_m}{E_m}$$

v_T = transverse poissons ratio of fiber

E_T = transverse modulus of fiber

E_m = modulus of matrix

v_m = poissons ratio of matrix

$$A_3 = -\left(\frac{v_A}{E_A} + \frac{V_1 v_m}{V_2 E_m} \right)$$

v_A = axial poisson ratio of fiber

E_A = axial modulus of fiber

$$C_{33} = \frac{1}{2}\left(\frac{1}{E_A} + \frac{V_1}{V_2 E_m} \right) - \frac{V_2 A_3^2}{V_1 A_0}$$

$$C_{33s} = \frac{1}{2}\left(\frac{1}{E_A} + \frac{V_1}{V_2 E_m} \right)$$

$$D_3 = -\frac{V_2 A_3}{V_1 A_0}\left[\alpha_T - \alpha_m \right] + \frac{1}{2}\left[\alpha_A - \alpha_m \right]$$

α_T = transverse thermal expansion coefficient of fiber

α_T = axial thermal expansion coefficient of fiber

α_m = matrix thermal expansion coefficient

$$D_{3s} = \frac{1}{2}(\alpha_A - \alpha_m) \ [42,43]$$

It can be used the equation (2-1) to calculated interfacial shear stress τ_{ifss} and the energy release rate $G_\infty(a)$ from equation (2-53) used for pull-out component so using equation (2-22) to find the pull-out force to any drag-out force in force-displacement curve in drag-out test.

Chapter Three

Experimental part

3-1 Properties of Materials used

3-1-1 Glass Fiber

Most glass fibers are based on silica (SiO_2), with additions of oxides of calcium, boron, sodium, iron and aluminum. These glasses are usually amorphous, although some crystallization may occur after prolonged heating at high temperatures, leading to a reduction in strength. Typical compositions of three types of glass popular for composites as shown in table (3-1) [4].

Table (3.1) Composition of glass fibers [4]

Composition %	E-Glass	C-Glass	S-Glass
Silicon oxide	52.4	64.4	64.4
Aluminum oxide	14.4	4.1	25
Boric oxide	10.6	4.7	-
Sodium oxide And Potassium oxide	0.8	9.6	0.3
Magnesium oxide	4.6	3.3	10.3
Calcium oxide	17.2	13.4	-
Barium oxide	-	0.9	-
Titanium dioxide	1.5	-	-
Iron	1	-	-

E-glass (E for electrical), draws well and has good strength, stiffness, electrical and weathering properties, and C-glass (C for corrosion) is preferred, having better resistance to corrosion than E-glass, but a lower strength. Finally, S-glass (S for strength) is more expensive

than E-glass, but has a higher, strength, Young's modulus and temperature resistance. Type of glass fiber shown in Fig (1-4) [4].

E-glass fibers, provided they are handled very carefully to avoid surface damage, have strength of 3.5 GPa and the variability in strength is small. The strength falls in humid air, owing to the adsorption of water on the surface.

A major factor determining the strength is the damage which fibers sustain when they rub against each other during processing operations. To minimize this damage, glass fibers are usually treated with a size at an early stage in manufacture. This is a thin coating applied to the fibers by spraying with water containing an emulsified polymer. The size serves several purposes

1- To protect the surface of the fibers from damage.
2- To bind the fibers together for ease of processing.
3- To lubricate the fibers so that they can withstand abrasion during subsequent processing operations.
4- To impart anti-static properties.
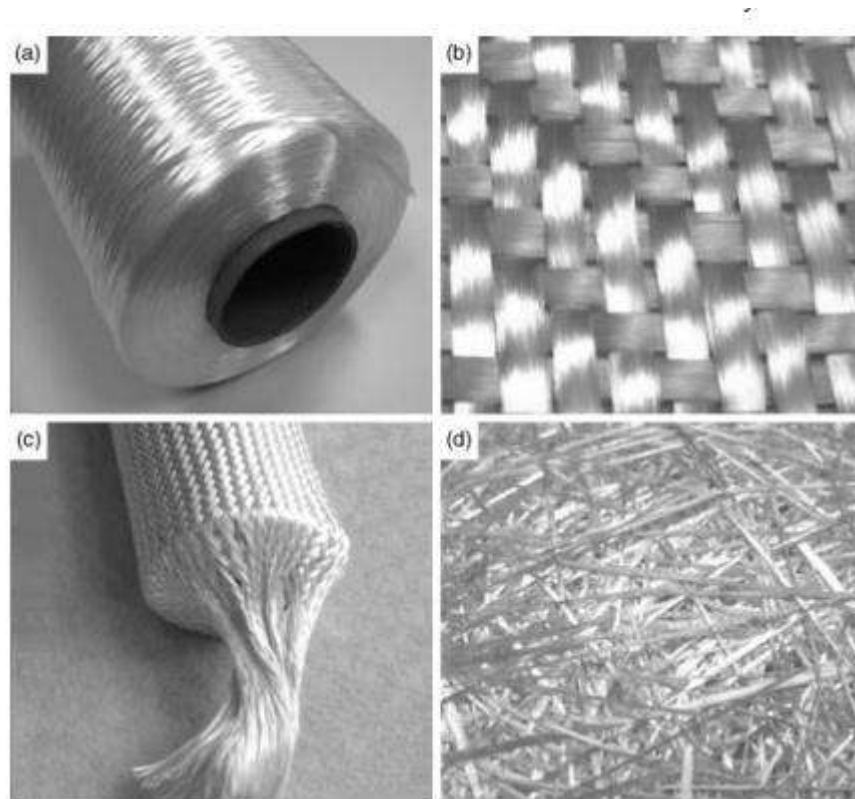5- To provide a chemical link between the glass surface and the matrix to increase the interface bond strength [44].

Fig (3-1) (a) rovingon coil, (b) woven fabric, (c) braided fabric, (d) chopped strand mat [3].

3-1-2 Carbon Fiber:

Carbon is a high-performance fiber material that is the most commonly used reinforcement the reasons for this are carbon fibers have the highest specific modulus and specific strength of all reinforcing fiber materials, they retain their high tensile modulus and high strength at elevated temperatures; high temperature oxidation, at room temperature, carbon fibers are not affected by moisture or a wide variety of solvents, acids, and bases [8].

Carbon fibers are produced by thermal decomposition of an organic (polymeric) fiber or ''precursor'' at high pressures and temperatures. The three most common precursors are:

1-Polyacrylonitrile (''PAN'').

2-Pitch (a by-product produced during the petroleum distillation process).

3-Rayon [45].

Carbon-reinforced polymer composites are currently being used extensively in sports and recreational equipment (fishing rods, golf clubs), filament-wound rocket motor cases, pressure vessels, and aircraft structural components—both military and commercial, fixed wing and helicopters (wing, body, stabilizer, and rudder components)[46].

3-1-3 Kevlar Fiber:

Kevlar is the DuPont trade name of poly(p-phenylene terephthalamide) (PPTA) and was first created in DuPont's labs in 1965 by Stephanie Kwolek and Herbert Blades. It is an organic fiber in the aromatic polyamide family. It possesses unique combination of high strength, high modulus, toughness and thermal stability. It can be spun into ropes or sheets of fabric that can be used in the construction of composite components. Kevlar is used in wide range of applications starting from bicycles to body armor, due to its high strength-to-weight ratio, and it is five times stronger than steel on an equal weight basis.

In 1965, scientists at DuPont discovered a new method of producing perfect polymer chain extension. The polymer poly-p-benzamide was found to form liquid crystalline solutions due to the simple repetitiveness of its molecular backbone. The key structural requirement for the backbone is the Para orientation on the benzene ring, which allows the formation of rod like molecular structures. These developments led to the current formulation of Kevlar. DuPont developed the fiber of poly(p-phenylene terepthalamide), which was introduced as

high strength Kevlar aramid fiber in 1971. In aramid fiber, the fiber-forming substance is a long-chain synthetic polyamide in which at least 85% of the amide linkages are attached directly two aromatic rings thus, in an aramid, most of the amide groups are directly connected to two aromatic rings, with nothing else intervening [46,47].

Kevlar Fiber Properties:

1- High thermal stability due to its aromatic.

2- Flame resist but capable of ignition.

3- Kevlar fiber possesses chemical subsidence low electrical conductivity compared with carbon fibers and glass fibers.

4- Kevlar fiber composites have highest specific strengths among all composite materials. Offer outstanding combinations of properties, such as high specific strength, toughness, creep resistance, and moderate cost, for specific applications [48].

3-1-4 Polyethylene Fiber:

Polyethylene has a high-strength; high-modulus polyethylene fiber called Spectra was evolution at Allied Signal Technologies during the 1980s. Spectra are based on ultra-high-molecular-weight polyethylene (UHMWPE). It has a specific gravity of 0.97, meaning that it is the only reinforcing fiber available that is lighter than water. Spectra is available in three classifications (Spectra 900, 1000 and 2000) and several grades are available in each class. The high specific strength of the fiber makes it particularly attractive for tensile applications. The glass transition temperature of UHMWPE is in the range of $0^{o}C$ to$20^{o}C$, and hence the fiber is in the rubbery state at room temperatures and exhibits time-

dependent (viscoelastic) behavior. This feature imparts outstanding impact resistance and toughness, but may lead to undesirable creep effects under long-term sustained loading. The melting temperature of the fiber is $147^{o}C$ [49,50].

A fiber of different diameter and embedded lengths were used

1- Carbon fiber AS4B with diameter o.22mm and 0.34mm and 0.43mm.

2- Kevlar fiber-49 with diameter 0.22mm and 0.34mm and 0.43mm.

3- E- Glass fiber with diameter 0.22mm and 0.34mm and 0.43mm.

4- Polyethylene fiber with diameter 0.45mm.

The mechanical and thermal properties are listed in table (3-1):

Table (3-2) the mechanical and thermal properties of reinforcement fiber [51,52]

Properties	Carbon fiber AS4	Kevlar fiber	E-glass fiber	Polyethylene Fiber
Tensile Modulus (E_A)(Gpa)	380	130	75	170
Transverse modulus (E_T)(Gpa)	40	10	75	117
Axial shear modulus (G_A)(Gpa)	20	15	32	5.61
Axial poisson ratio (υ_A)	0.22	0.2	0.17	0.32
Transverse poisson ratio(υ_T)	0.25	0.35	0.17	0.61
Axial coefficient of thermal expansion(α_A) $10^{-6}c^{-1}$	-0.7	-2	5	120
Transverse coefficient of thermal expansion(α_T) $10^{-6}c^{-1}$	10	-60	5	48

3-1-5 Epoxy matrix

Epoxy resin is widely used in structure and civil engineering applications and occupies a dominant position compared with other polymers. The major characteristics of epoxy resin systems provide an excellent combination of properties, including excellent abrasion resistance, very low shrinkage during and after cure, high mechanical strength, and excellent adhesion to most building materials, wide range of cure schedules to suit different climatic conditions and use performance can be achieved within hours.

In world today's, epoxy technologies have become firmly established in the construction sector, offering countless applications in all of the industrialized countries and in the Third World too. Products based on epoxies are used for an amazing variety of applications hard-wearing coatings and flooring resistant to water, chemicals and abrasion, thin-layer non-skid surfacing for roads and bridges; interlayer sealing membranes for bridges; mortars for repairs and load-bearing supports; grouts for the anchoring of crane rails and machines; adhesives for the structural bonding of prefabricated concrete elements; anchoring of reinforcing steel, rock bolts, pre-stressing anchors, etc. injection repair of cracks repair structures in general[53,45].
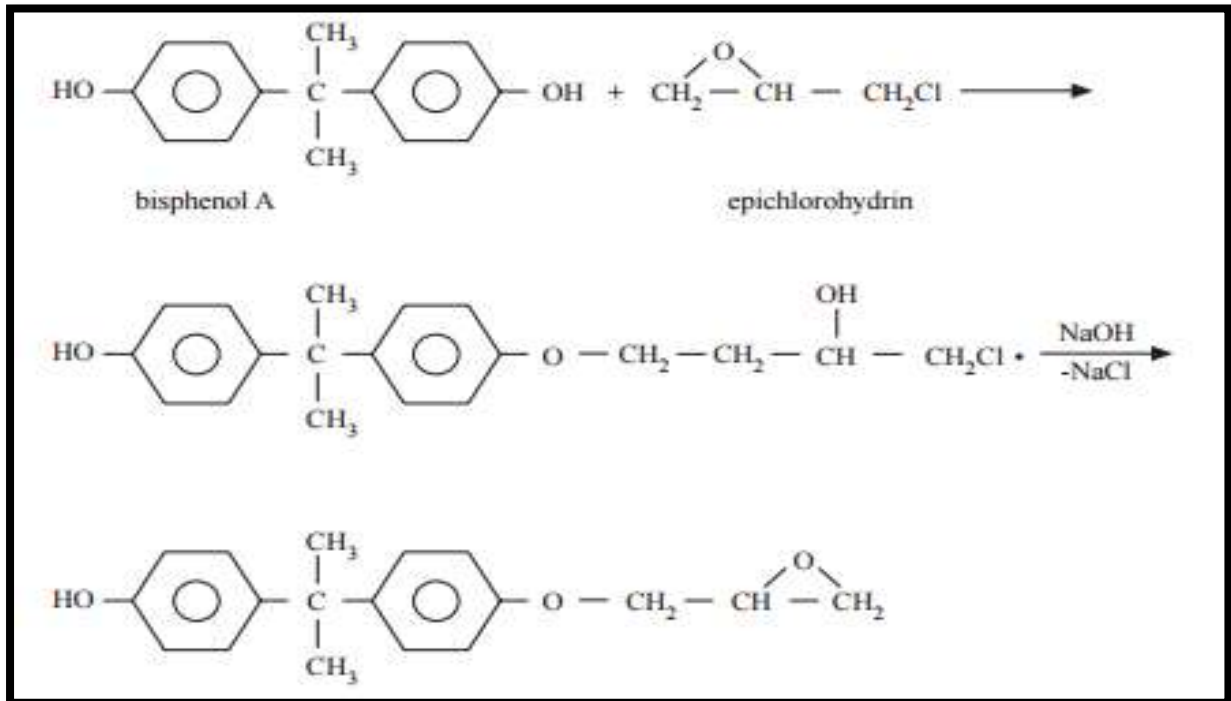
Fig.(3-2) Epoxy resins are normally prepared by the base-catalyzed reaction between an epoxide such as epichlorohydrin and a polyhydroxy compound such as bisphenol A [7].

The molar ratio of epichlorohydrin to bisphenol a can range from as high as 10:1 to as low as 1.2:1 as shown in Fig (3-2). This produces resins ranging from liquid to semisolid to solid and varying molecular weights and softening points [7].

3-1-6 Polyester Matrix:

Unsaturated polyesters are among the most important thermosetting polymers. The historical development of polyesters dates back to 1847, when Berzelius produced the first polyester product by reacting tartaric acid with glycerol. Carother, in 1920, prepared polyesters with well-defined polymeric structure. Several useful technologies are available today for various industries. The construction industry is among them [6,8].

Polyesters are composed of either adipic acid, dialkyl maleates or cyclic diols. Rigid polyesters are composed of phthalic acid or isophthalic acid as the saturated acid component, and fumaric acid or maleic acid as the unsaturated acid component, and propylene glycol or a mixture of this glycol with other glycols (diethylene glycol) as the glycol component as shown in Fig (3-3) . Styrene is a commonly used monomer to effect cross-linking either singly or in combination with other copolymerisable monomers, such as methyl acrylate, diethyl phthalate, a-methyl styrene and so on. The reaction of maleic anhydride with diethylene glycol is an example of a typical preparation of unsaturated polyesters [45].
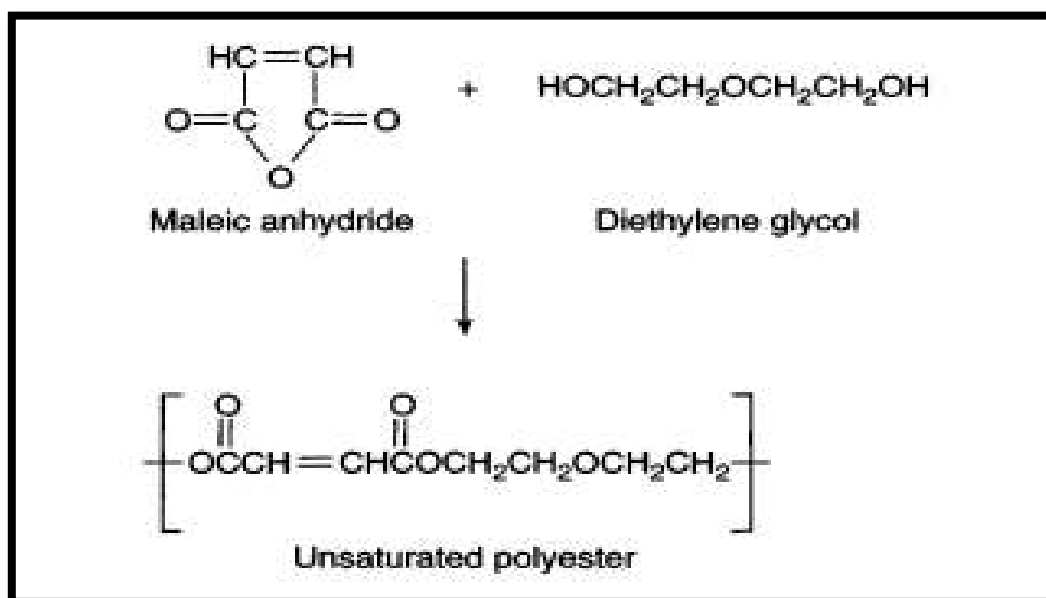

Fig (3-3) Typical preparation of unsaturated polyester [6].

The unsaturated polyester prepare industrially in two ways:

1- Fusion method. This method includes a poly condensation reaction at high temperature between glycols and dibasic acids or anhydrides.

2- Oxide method. This method includes the use of monoepoxide raw materials (ethylene or propylene oxide) and maleic anhydride or a mixture of maleic anhydride and saturated anhydrides. Glycols or

dibasic acids function as reaction initiators for the process. The oxide method provides a much faster reaction time and it is possible to control the molecular weight of the product by the quantity of starting ingredients [6].

The mechanical and thermal properties of matrixes which used are:

1- Epoxy resin type Quickmast 105 resin based injection on crack repair system made by the company (Don Construction Products. Ltd (DCP)).
2- Unsaturated Polyester Resin (Palatel A420) made by the company (Saudi International Resin. Ltd (SIR)).

The mechanical and thermal properties of these matrixes are listed in table (3-3).

Table (3-3) the mechanical and thermal properties of epoxy and polyester matrix [54, 55].

Properties	Epoxy	Polyester
Tensile modulus (E_m)(Gpa)	5	4
Axial shear modulus (G_m) (Gpa)	1.23	1.16
Axial poisons ratio (υ_m)	0.35	0.5
Axial coefficient of thermal expansion(α_m) $10^{-6} c^{-1}$	50	70

3-2 Sample Preparation

Sample preparation was with the molding hand, two molds were prepared first is steel and the second is rubber. The steel mold formed of three parts shown in Fig (3-4). The first part A shown in Fig (3-4-a) is a steel block containing a hole dimensions 45mm ,30mm and 18mm. The second part B formed of three steel U-shaped molds show in Fig (3-4-b) with dimensions length 40mm, height 27mm, width 18mm, embedded

lengths of 3mm, 4mm and 5mm from each side, the third part C which contains rectangular steel with two screw from each side, left and right and one screw from upper and lower side used to grip U-shaped steel mold part B Fig (3-4-d).

The second mold a polysiloxane (condensation silicones mixed with hardener) which approximately half of volume of hole of part A putted in the hole, by impression part B into part after (15-20) minute get on polysiloxane mold show in Fig (3-5-a). The polysiloxane mold cut by a razor blade and the razor cut was mad in the polysiloxane mold in which the fiber was to be placed, the fiber was placed straight in the cut as shown in Fig (3-5-b). The fiber protrudes over few millimeters outside the specimen. The matrix epoxy consisted of 100 parts hexandiodiglycidether resin and 34 parts by weigh of 3,3-diaminodicyclohexyl-methane as hardener while. The second kind of matrix materials polyester consist of 100 parts of weight of unsaturated polyester resin VIPAL VUP 4649(M) on the base of isophthalic acid and 2 parts of weight styrene as hardener after fiber fixed in polysiloxane mold. The two kinds of matrix materials must be carefully stirred and purred in to the polysiloxane mold to avoid the bubbles, 30 specimens cured at 75°C for 2 hours, 30 specimen cured at 50°C for 2 hours, 60 specimens (30 epoxy,30 polyester) cured at 25°C use in oven(Iso 9001 CERTIFIED) and leave it in polysiloxane molds for 5-7 days and then removed from polysiloxane mold Fig (3-2-c).
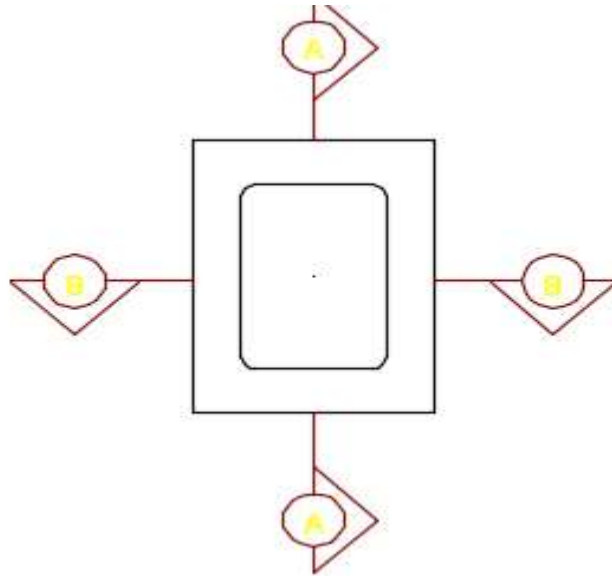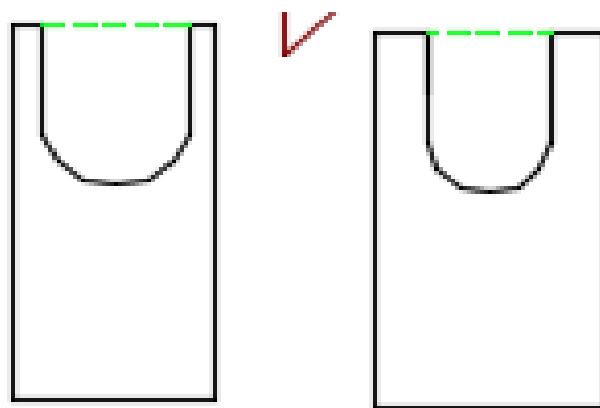
Fig (3-4-a) Part A of steel mold
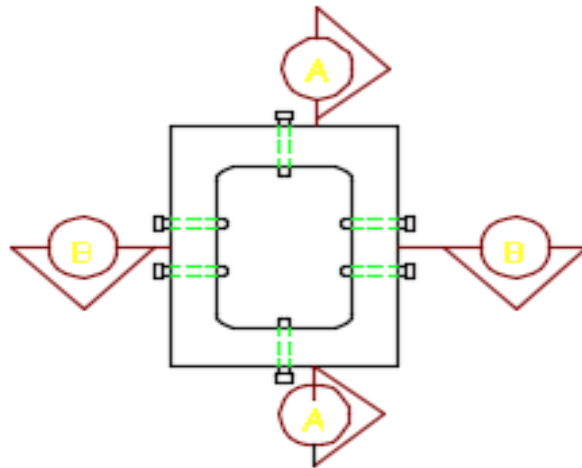

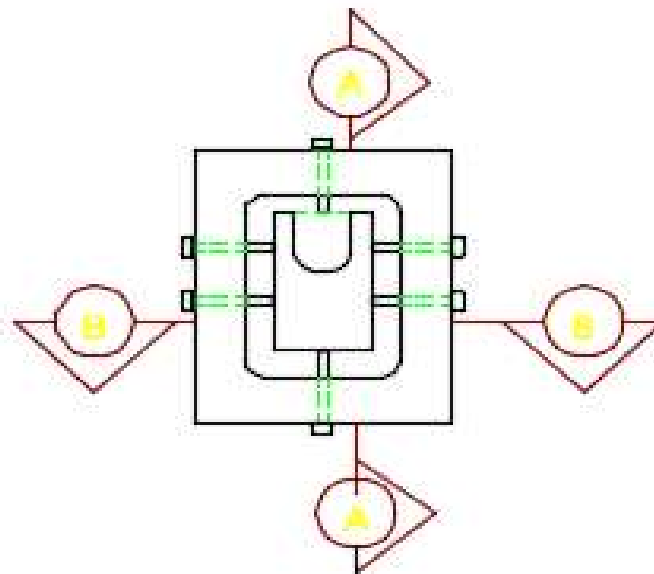**Fig (3-4-b) Part B of steel mold**

Fig (3-4-c) Part C fixer

Fig (3-4-d) Part C fixed part B

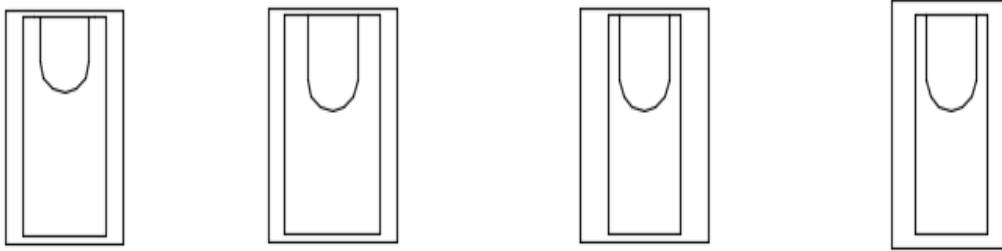**Fig (3-4) The parts of steel mold**.

Fig (3-5-a) Polysiloxane mold with different embedded lengths
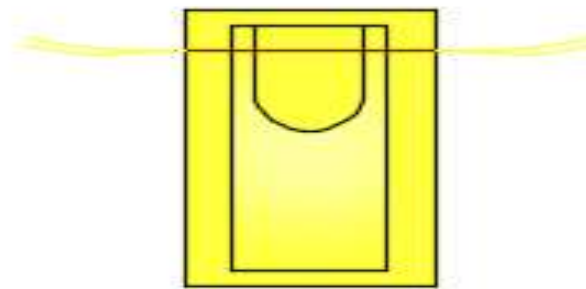

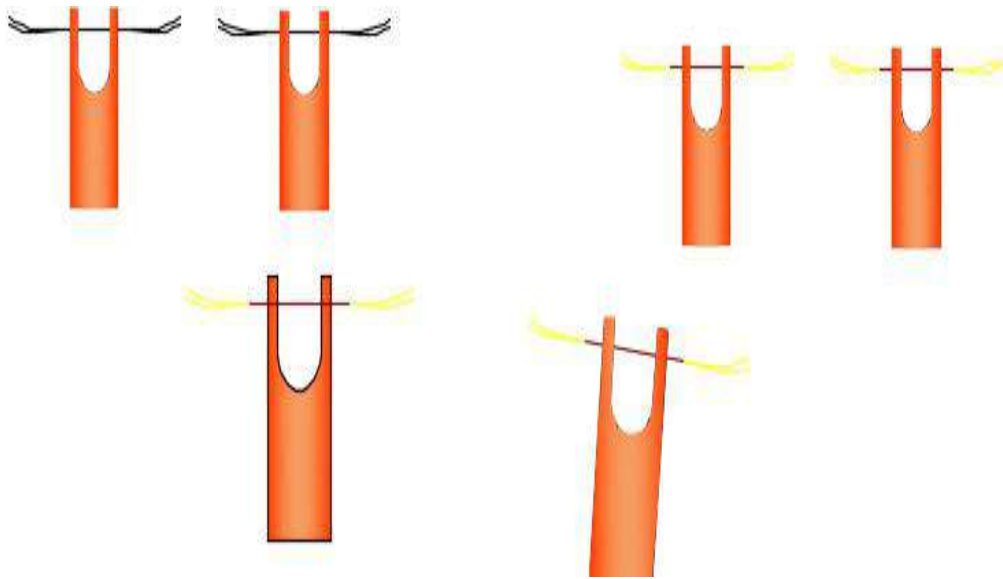**Fig (3-5-b) Kevlar fiber fixed in polysiloxane before matrix pours**

Fig (3-5-c) U-shape specimens after cured

Fig (3-5): polysiloxane molds and cured U-shaped specimens.

3-3 Samples Tested

Drag-out tensile test for specimens (polyester) had done tensile tester (ESM0301 motorized force tester mark-10) in the Department of Chemistry, University of Qadisiyah. Because of the maximum load 1.5 KN; therefore only the polyester samples could be measured, it has been installed lower grip (non movement) to install the sample on it. The upper grip been using steel hook, it is important to know that the steel hook is attached to free length fiber of the specimen at the center as shown in Fig (3-6). The speed of upper grip is (0.5 mm/min).

For high rang force (epoxy) samples have been measured at Babylon University College of Engineering, Department of polymer and petrochemical industries in the tester (Microcomputer controlled electronic universal testing machine model WDW-5E). The load rang between (0.5KN-5KN) with speed (0.5mm/min) shown Fig (3-7).

In the two device we applied the same Steps which is

1- Install hook in cross head(upper grip).
2- Install specimen in lower grip.
3- Install steel hook in the center of free fiber between embedded lengths.
4- Run screening device.

All specimens tested at 25°C after drag-out test done for each U-shaped specimen as force vs. cross head displacement curve recorder at x-y plotter, the force in Newten at x-axis and the displacement in millimeter at y-axis, used Microsoft excel to plot graphs.

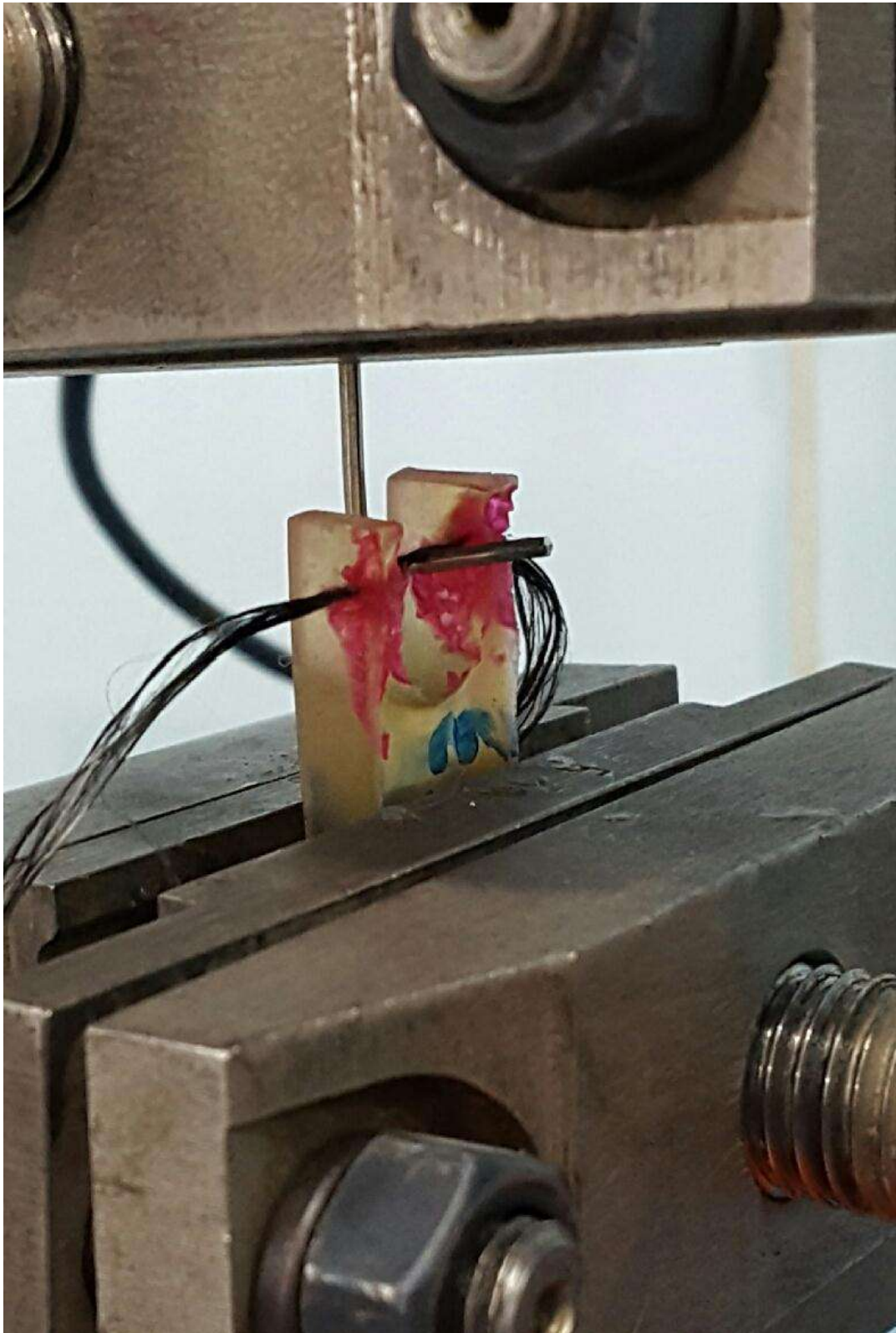**Fig (3-6) U-shape specimen in ESM0301 motorized force tester mark-10**

Fig (3-7) U-shape specimen in Microcomputer Controlled electronic Universal Testing machine model WDW-5E

Chapter Four

Results

and

Discussions

4-1 Introduction

In composite materials technology the adhesion between fibers and matrix is a key determination of the strength of the system, pull-out, microbond and drag-out tests were developed to measure the adhesion from the force required to pull-out embedded fibers from resin. Analytically there are two methods to calculate the strength of composite first, stress based model used to calculate the shear strength by dividing the maximum force by the adhesion area as in equation (2-1) and second, energy based model which depends on shear-lag theory and the energy release rate of crack propagated at the interface included the effect of thermal stress and friction. From the result of drag-out test, a general response for drag-out force versus cross head displacement for epoxy-glass fiber, epoxy-carbon fiber, epoxy-kevlar and epoxy-polyethylene at $(25^{o}C, 50^{o}C, 75^{o}C)$ and polyester-glass fiber, polyester -carbon, polyester-kevlar and polyester-polyethylene-fiber at $25^{o}C$ for different embedded lengths and diameters drawn as curves in Fig (4-1) to Fig (4-40).

4-2 Experimental Result from Drag-out Test

4-2-1Epoxy-glass fiber post cure at 25°C

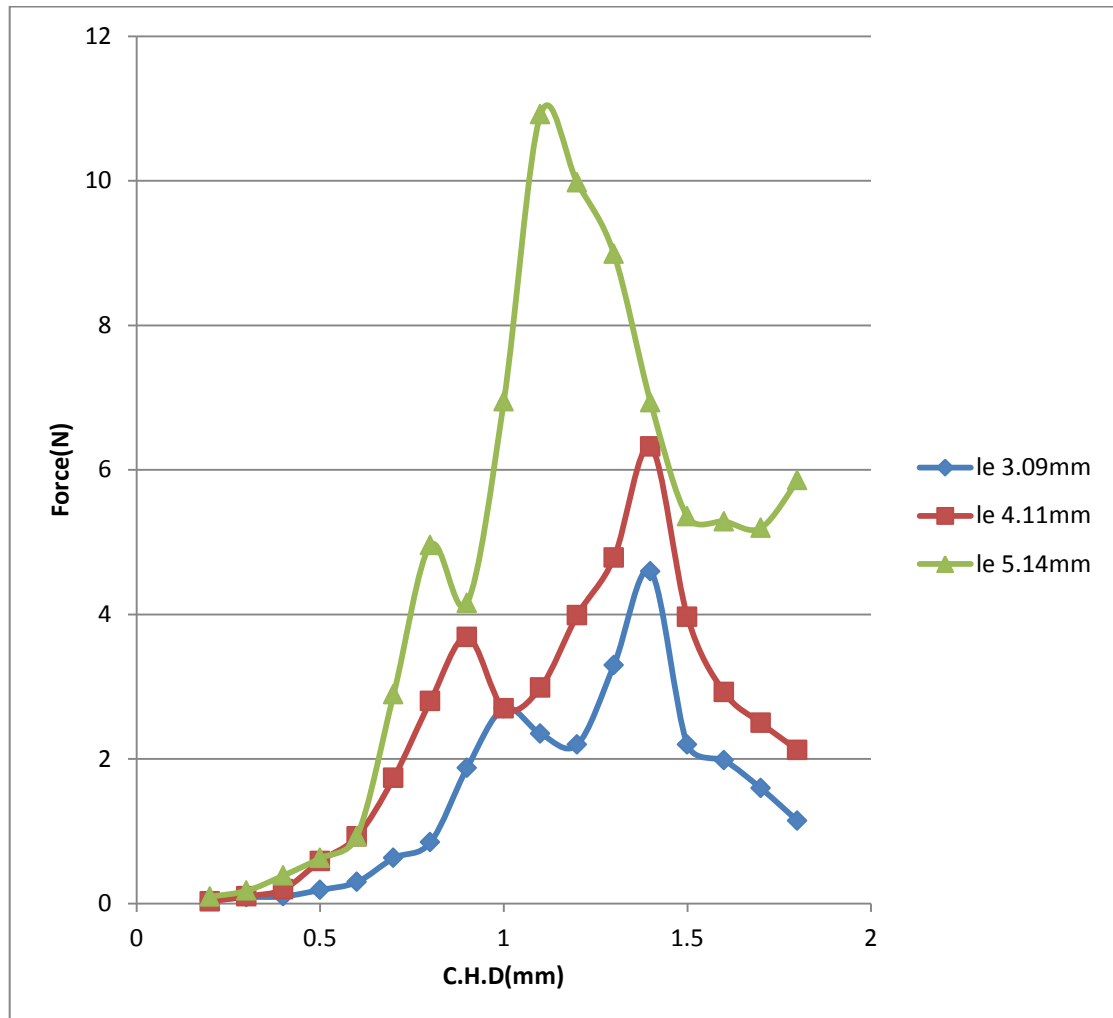Fig (4-1) show the results from drag-out test for epoxy-glass fiber post cure at 25°C of diameter 0.22mm.

Fig (4-1) The drag-out force vs. cross head displacement curve for epoxy-glass fiber post cures at 25°C of diameter (0.22mm).

The results from equation (2-1), (2-40) and (2-53) are listed in Table (4-1).

Table (4-1): The results from interfacial shear strength, shear-lag and energy release rate equations for epoxy glass fiber post cure at 25°C of diameter 0.22mm

Embedded length le(mm)	3.09	4.11	5.14
Drag-out deboned force at peak(N)	4.593	6.328	10.918
Drag-out friction force (N)	1.143	2.123	5.856
Pull-out debond force at peak(N)	15.682	25.781	33.183
Pull-out friction force (N)	8.283	12.619	19.823
IFSS at peak debond point (MPa)	11.348	14.081	16.347
Shear-lag parameter $\beta(\mu m)^{-1}$	0.00094	0.00094	0.00094
$G_\infty(l_e) J/m^2$	48.845	89.856	124.972
$G_\infty(l_e)$ at K=0 J/m^2	67.154	114.739	152.825

Fig (4-2) Shown the results drag-out test for epoxy-glass fiber post cure at 25°C of diameter 0.34mm.

Fig (4-2) The drag-out force vs. cross head displacements curve for epoxy-glass fiber post cure at 25°C of diameter (0.34mm).

The results from eqs. (2-1), (2-40) and (2-53) are listed in Table (4-2).

Table (4-2): The results from interfacial shear strength, shear-lag and energy release rate equations for epoxy-glass fiber post cure at 25°C of diameter 0.34mm

Embedded length le(mm)	3.09	4.11	5.14
Drag-out deboned force at peak(N)	14.867	20.673	23.957
Drag-out friction force (N)	8.121	13.198	16.287
Pull-out debond force at peak(N)	26.825	48.613	56.726
Pull-out friction force (N)	15.723	21.173	28.182
IFSS at peak debond point (MPa)	12.133	15.081	17.366
Shear-lag parameter $\beta(\mu m)^{-1}$	0.00072	0.00072	0.00072
$G_\infty(l_e)J/m^2$	127.971	136.829	232.384
$G_\infty(l_e)$ at K=0 J/m^2	164.812	182.823	275.601

Fig (4-3) Shown the results from drag-out test for epoxy-glass fiber post cure at 25°C of diameter 0.43 mm.
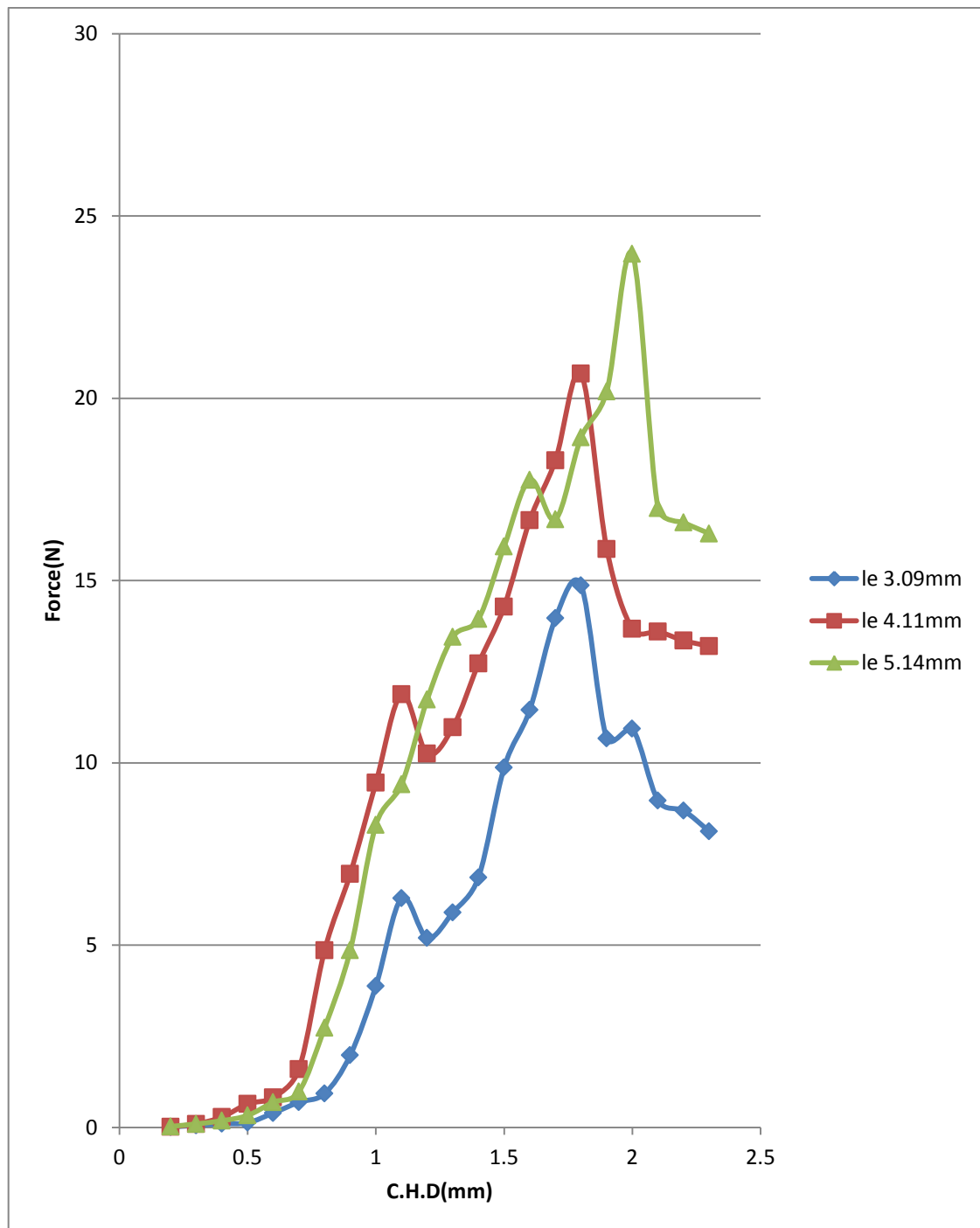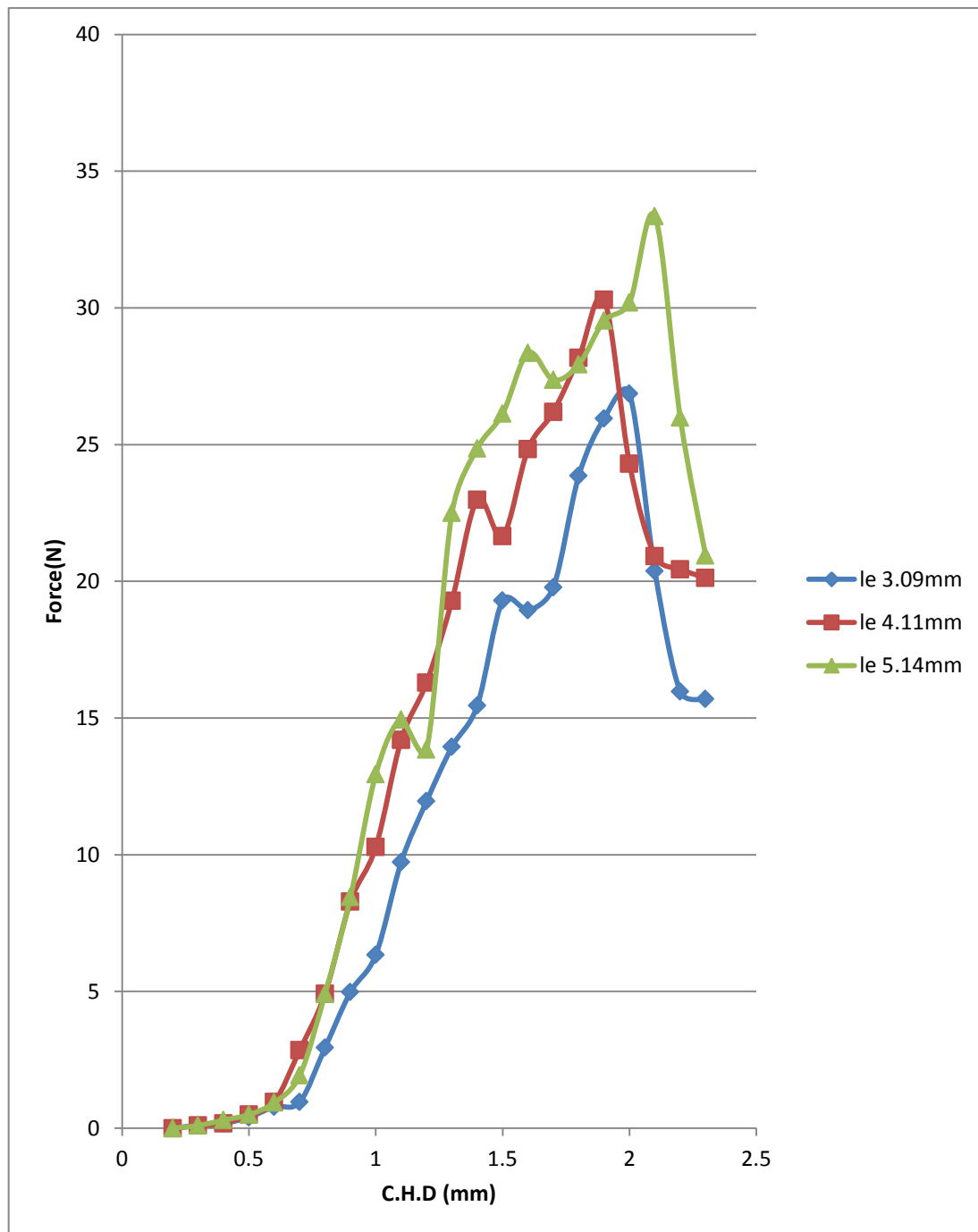

Fig (4-3) The drag-out force vs. cross head displacement curves for epoxy-glass fiber post cure at 25°C of diameter (0.43mm).

The results from equation (2-1), (2-40) and (2-53) are listed in Table (4-3)

Table (4-3): the results from interfacial shear strength, shear-lag and energy release rate equations for epoxy-glass fiber post cure at 25°C of diameter 0.43mm

Embedded length le(mm)	3.09	4.11	5.14
Drag-out deboned force at peak(N)	26.867	30.298	33.354
Drag-out friction force (N)	15.232	19.129	22.163
Pull-out debond force at peak(N)	55.812	65.182	74.723
Pull-out friction force (N)	25.723	31.737	38.825
IFSS at peak debond point (MPa)	14.377	15.827	19.821
Shear-lag parameter $\beta(\mu m)^{-1}$	0.00069	0.00069	0.00069
$G_\infty(l_e) J/m^2$	297.284	312.735	318.295
$G_\infty(l_e)$ at K=0 J/m^2	335.917	371.592	378.182

4-2-2 Epoxy –Carbon Fiber post cure at 25°C

Fig (4-4) Shown the results from drag-out test for epoxy-carbon fiber post cure at 25°Cof diameter 0.22mm.

Fig (4-4) The drag-out force vs. cross head displacement curves for epoxy-carbon fiber post cure at 25°C of diameter (0.22mm).

The results from equation (2-1), (2-40) and (2-53) are listed in table (4-4)

Table (4-4): the results from interfacial shear strength, shear-lag and energy release rate equations for epoxy-carbon fiber post cure at 25°C of diameter 0.22mm

Embedded length le(mm)	3.09	4.11	5.14
Drag-out deboned force at peak(N)	19.394	25.823	31.62
Drag-out friction force (N)	10.378	12.287	19.692
Pull-out debond force at peak(N)	27.934	34.834	48.498
Pull-out friction force (N)	19.725	22.834	31.834
IFSS at peak debond point (MPa)	18.723	21.845	22.872
Shear-lag parameter $\beta(\mu m)^{-1}$	0.00057	0.00057	0.00057
$G_{\infty}(l_e) J/m^2$	178.723	279.932	298.165
$G_{\infty}(l_e)$ at K=0 J/m^2	185.832	295.978	324.714

Fig (4-5) Shown the results from drag-out test for epoxy-carbon fiber post cure at 25°C of diameter 0.34mm.
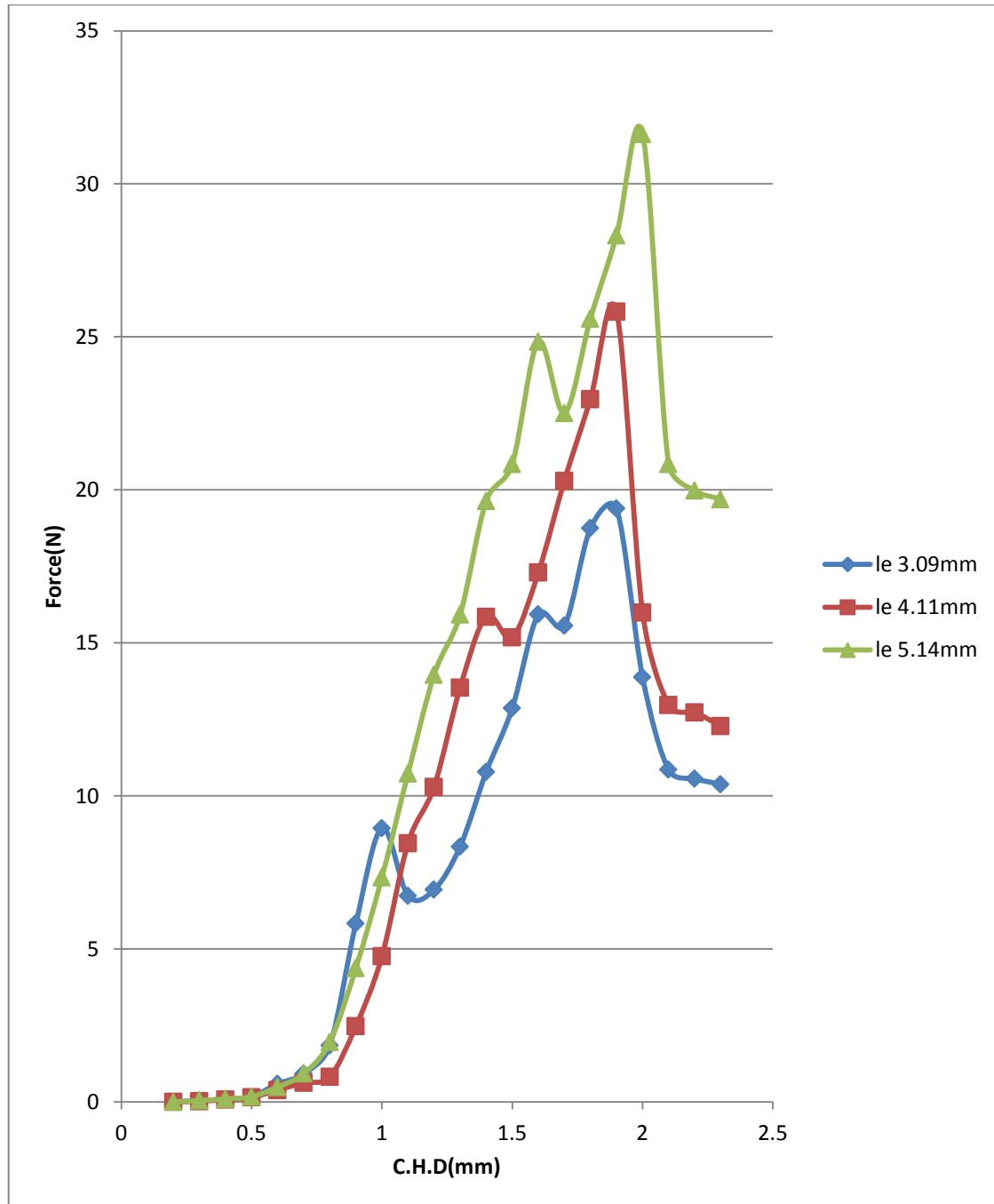

Fig (4-5) the drag-out force vs. cross head displacement curves for epoxy- carbon fiber post cure at 25°C of diameter (0.34mm).

The results from equation (2-1), (2-40) and (2-5۳) are listed in Table (4-5)

Table (4-5): the results from interfacial shear strength, shear-lag and energy release rate equations for epoxy-carbon fiber post cure at 25°C of diameter 0.34mm

Embedded length le(mm)	3.09	4.11	5.14
Drag-out deboned force at peak(N)	38.197	44.178	51.818
Drag-out friction force (N)	19.387	21.283	30.218
Pull-out debond force at peak(N)	47.945	74.926	89.823
Pull-out friction force (N)	36.823	52.718	63.287
IFSS at peak debond point (MPa)	23.845	25.089	26.834
Shear-lag parameter $\beta(\mu m)^{-1}$	0.00043	0.00043	0.00043
$G_\infty(l_e) J/m^2$	317.856	338.623	368.836
$G_\infty(l_e)$ at K=0 J/m^2	332.812	356.415	392.207

The results from drag-out test for epoxy-carbon fiber post cure at 25°C of diameter 0.43mm shown in Fig (4-6).
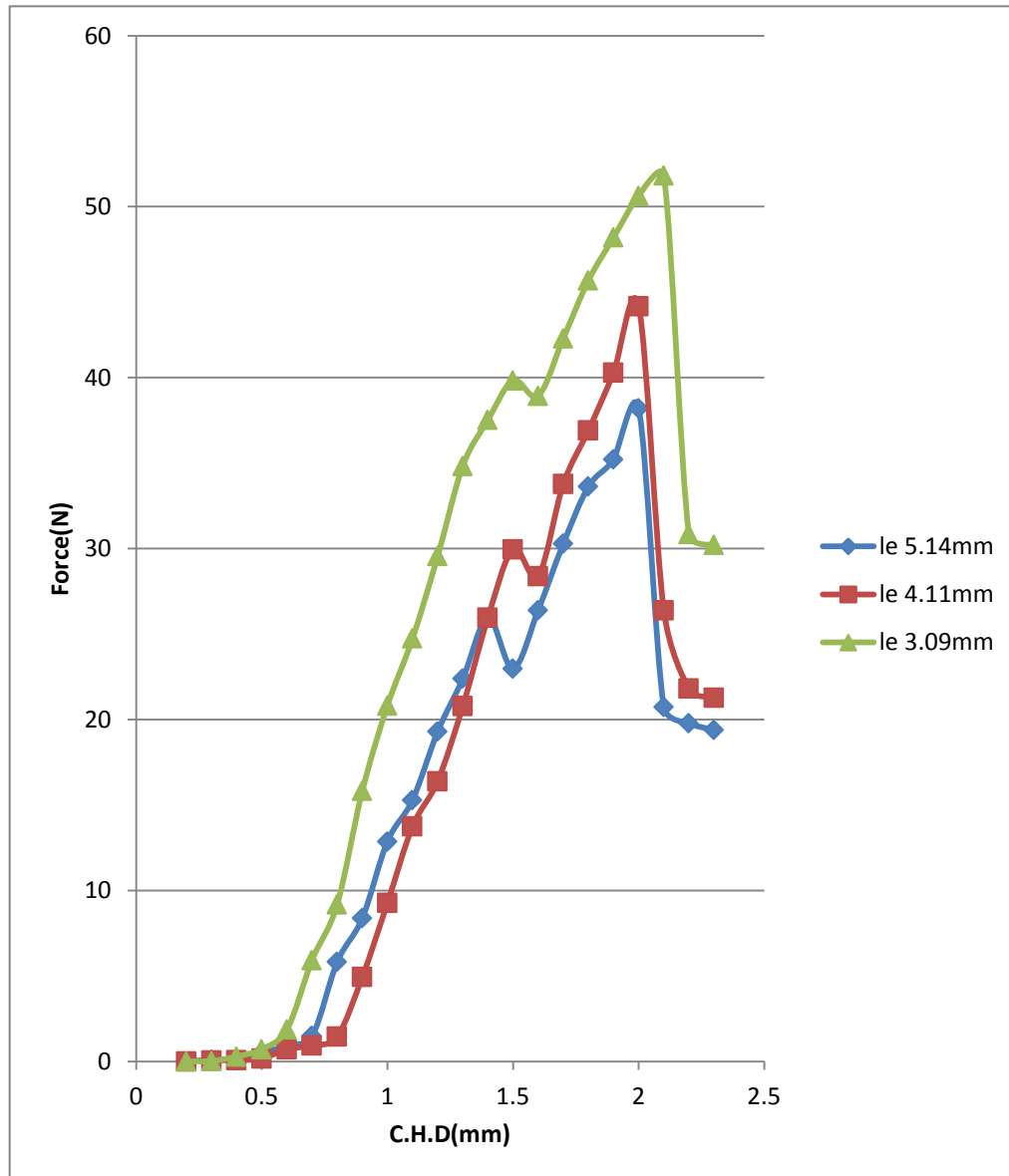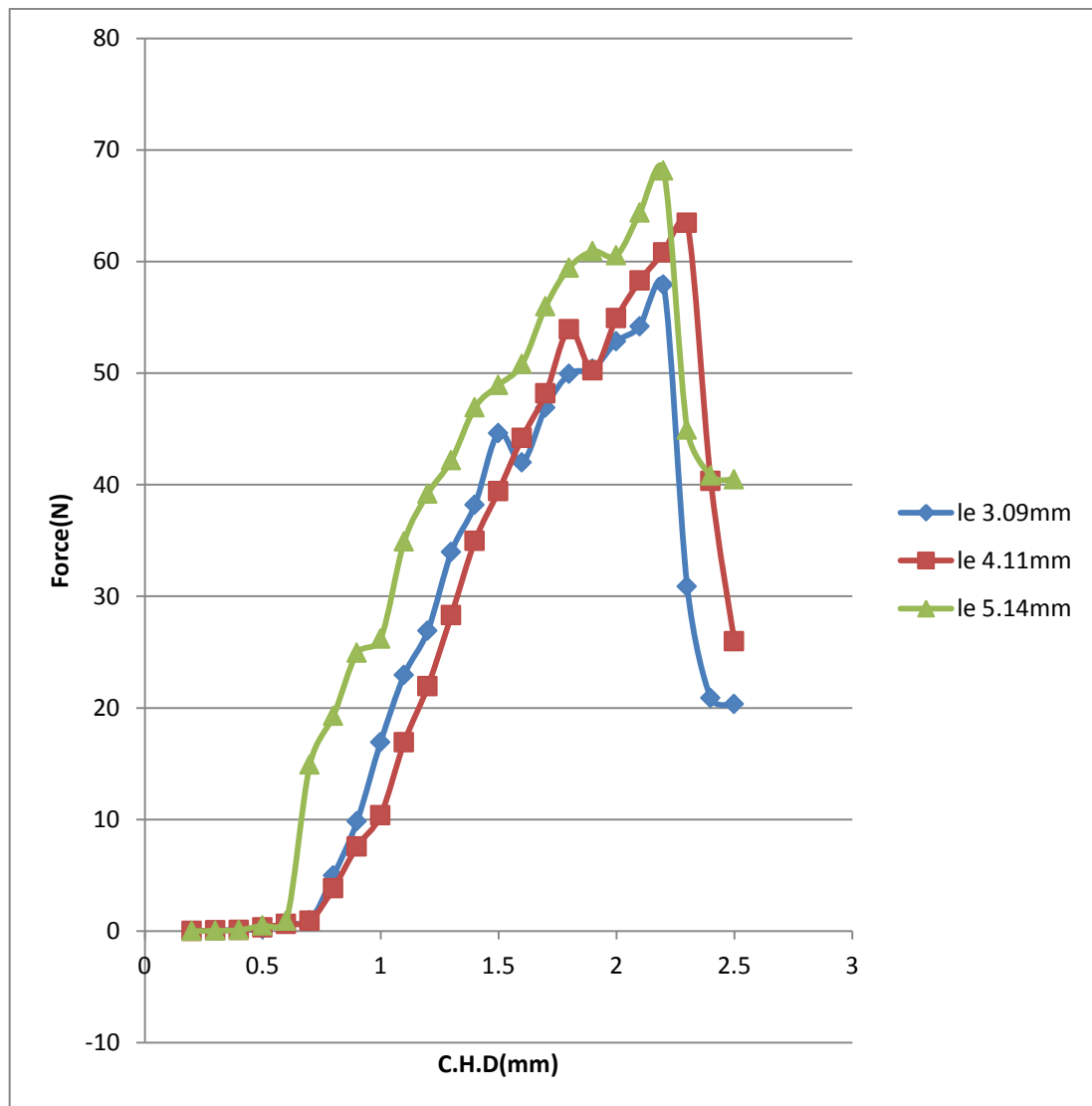

Fig (4-6) the drag-out force vs. cross head displacement curves for epoxy-carbon fiber post cure at 25°C of diameter (0.43mm).

The results from equation (2-1), (2-40) and (2-56) are listed in table (4-6)

Table (4-6): the results from interfacial shear strength, shear-lag and energy release rate equations for epoxy-carbon fiber post cure at 25°C of diameter 0.43mm

Embedded length le(mm)	3.09	4.11	5.14
Drag-out deboned force at peak(N)	57.923	63.476	68.137
Drag-out friction force (N)	20.354	25.978	40.491
Pull-out debond force at peak(N)	77.936	89.634	97.834
Pull-out friction force (N)	38.845	57.614	72.172
IFSS at peak debond point (MPa)	27.834	29.726	30.854
Shear-lag parameter $\beta(\mu m)^{-1}$	0.00037	0.00037	0.00037
$G_{\infty}(l_e)J/m^2$	253.863	365.715	386.867
$G_{\infty}(l_e)$ at K=0 J/m^2	286.615	384.835	398.265

4-2-3 Epoxy-Kevlar Fiber Post cure at25^{o}C

Fig (4-7) Shown the results from drag-out test for epoxy-kevlar fiber post cure at 25°C of diameter 0.22mm.

Fig (4-7) the drag-out force vs. cross head displacement curves for epoxy-kevlar fiber post cure at 25°C of diameter (0.22mm).

The results from equation (2-1), (2-40) and (2-53) are listed in table (4-7)

Table (4-7): the results from interfacial shear strength, shear-lag and energy release rate equations for epoxy-kevlar fiber post cure at 25°C of diameter 0.22mm

Embedded length le(mm)	3.09	4.11	5.14
Drag-out deboned force at peak(N)	40.397	55.163	61.285
Drag-out friction force (N)	24.845	39.734	33.945
Pull-out debond force at peak(N)	68.723	74.913	81.526
Pull-out friction force (N)	34.714	|45.292	62.623
IFSS at peak debond point (MPa)	20.671	23.823	26.681
Shear-lag parameter $\beta(\mu m)^{-1}$	0.00052	0.00052	0.00052
$G_\infty(l_e)J/m^2$	187.834	286.365	291.121
$G_\infty(l_e)$ at K=0 J/m^2	214.845	297.309	316.276

Fig (4-8) Shown the results from drag-out test for epoxy-kevlar fiber post cure at 25°C of diameter 0.34mm.
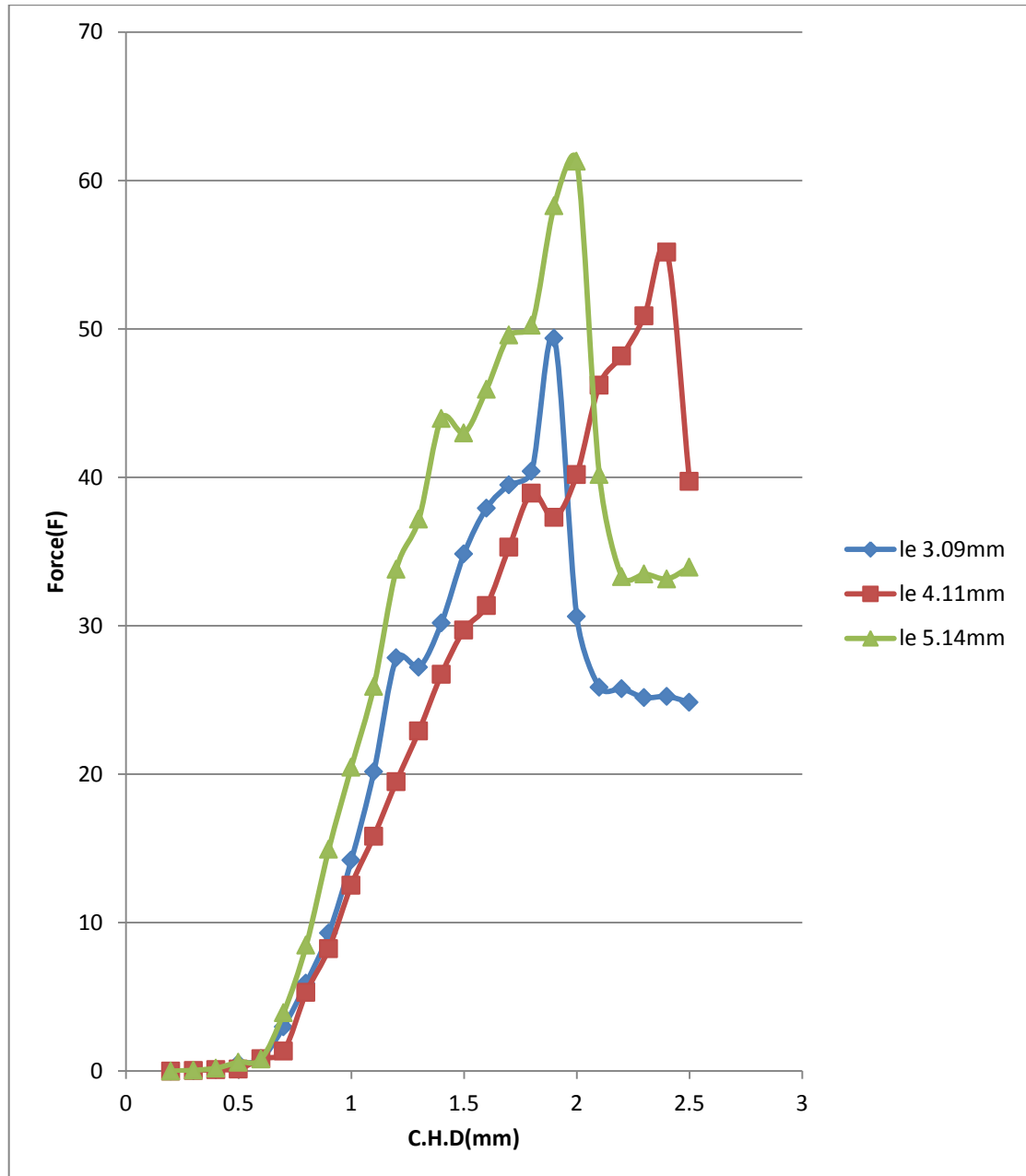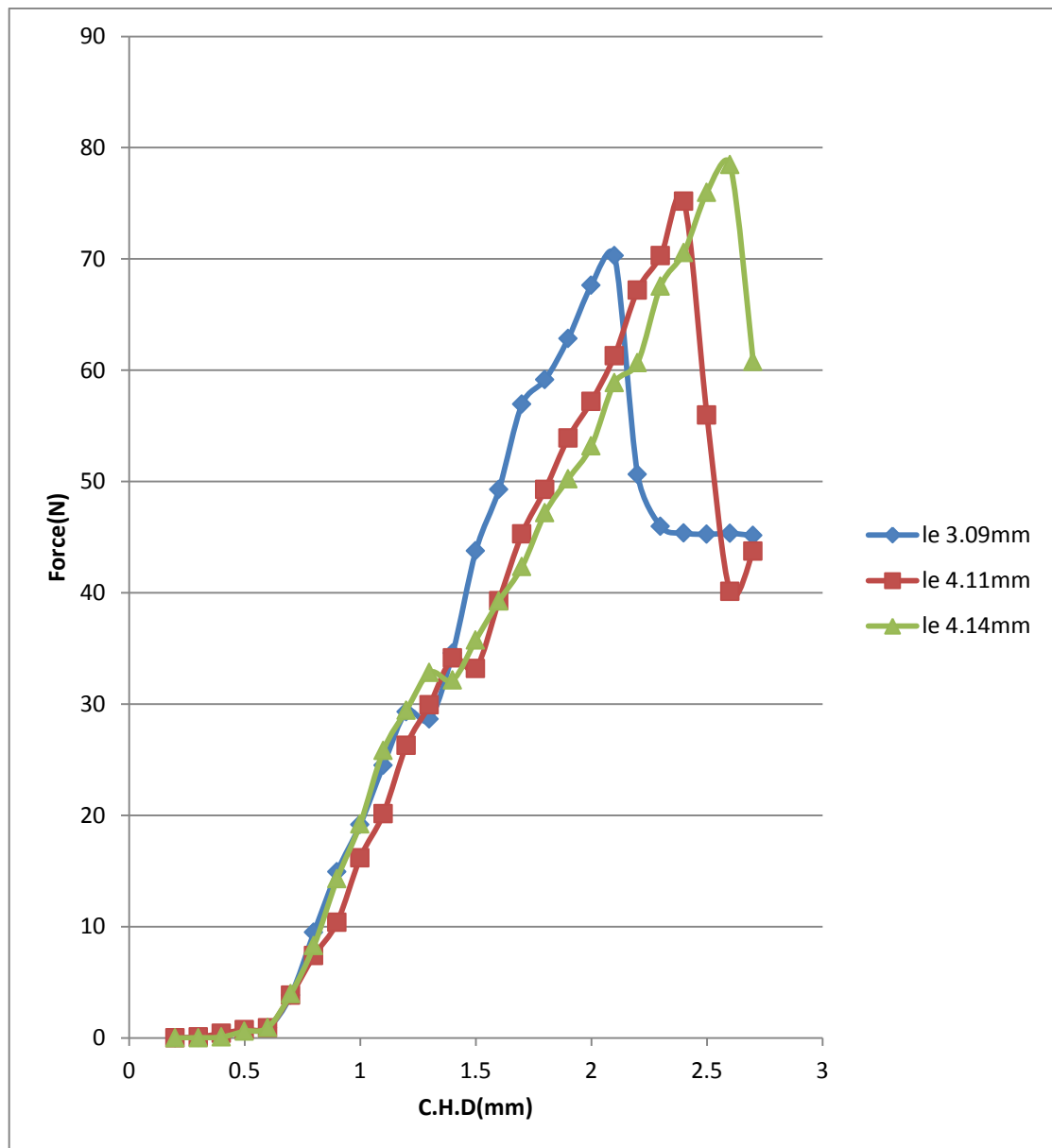

Fig (4-8) The drag-out force vs. cross head displacement curves for epoxy- kevlar fiber post cure at 25ºC of diameter (0.34mm).

The results from equation (2-1), (2-40) and (2-53) are listed in Table (4-8)

Table (4-8): The results from interfacial shear strength, shear-lag and energy release rate equations for epoxy-kevlar fiber post cure at 25°C of diameter 0.34mm

Embedded length le(mm)	3.09	4.11	5.14
Drag-out deboned force at peak(N)	70.298	75.192	78.476
Drag-out friction force (N)	45.143	43.745	60.453
Pull-out debond force at peak(N)	108.619	164.834	182.716
Pull-out friction force (N)	95.362	135.528	147.528
IFSS at peak debond point (MPa)	33.734	37.623	36.624
Shear-lag parameter $\beta(\mu m)^{-1}$	0.00032	0.00032	0.00032
$G_\infty(l_e)J/m^2 \Delta T = 0$	298.915	342.63	391.816
$G_\infty(l_e)$ at K=0 J/m^2	323.803	358.387	436.482

Fig (4-9) Shown the results from drag-out test for epoxy-kevlar fiber post cure at 25°C of diameter 0.43mm.
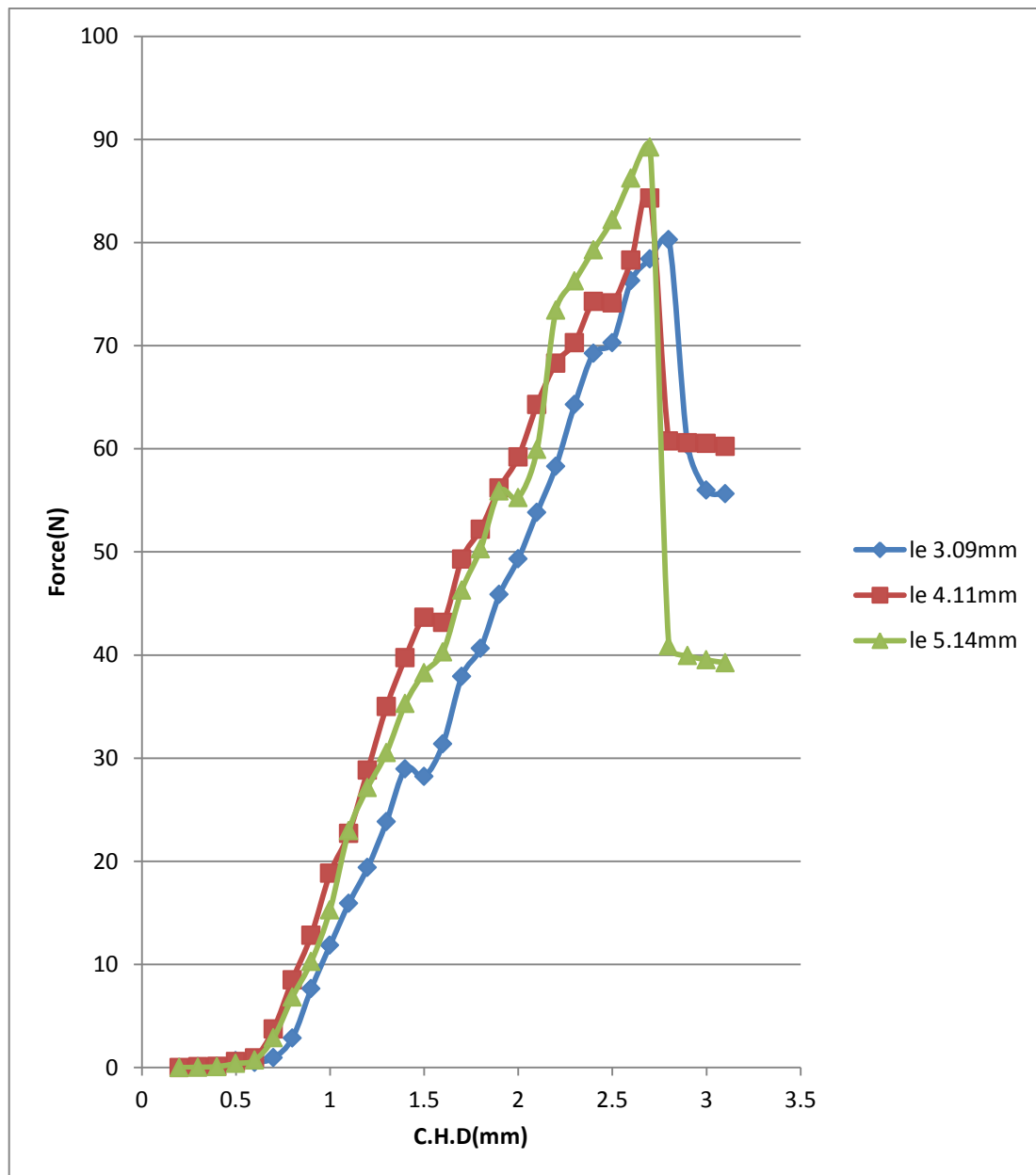

Fig (4-9) the drag-out force vs. cross head displacement curves for epoxy- kevlar fiber post cure at 25°C of diameter (0.43mm).

The results from equation (2-1), (2-40) and (2-53) are listed in Table (4-9).

Table (4-9): the results from interfacial shear strength, shear-lag and energy release rate equations for epoxy-kevlar fiber post cure at 25°C of diameter 0.43mm

Embedded length le(mm)	3.09	4.11	5.14
Drag-out deboned force at peak(N)	80.287	84.298	89.245
Drag-out friction force (N)	55.634	60.235	39.254
Pull-out debond force at peak(N)	112.292	167.823	174.464
Pull-out debond force at peak(N)	88.723	126.916	147.091
IFSS at peak debond point (MPa)	37.182	38.179	38.422
Shear-lag parameter $\beta(\mu m)^{-1}$	0.00025	0.00025	0.00025
$G_\infty(l_e)J/m^2$ at $\Delta T = 0$	476.903	482.145	583.925
$G_\infty(l_e)$ at K=0 J/m^2	483.293	496.723	596.926

4-2-4 Epoxy-Polyethylene post cure at 25°C

Fig (4-10) Shown the results from drag-out test for epoxy-polyethylene fiber post cure at 25°C of diameter 0.45mm.
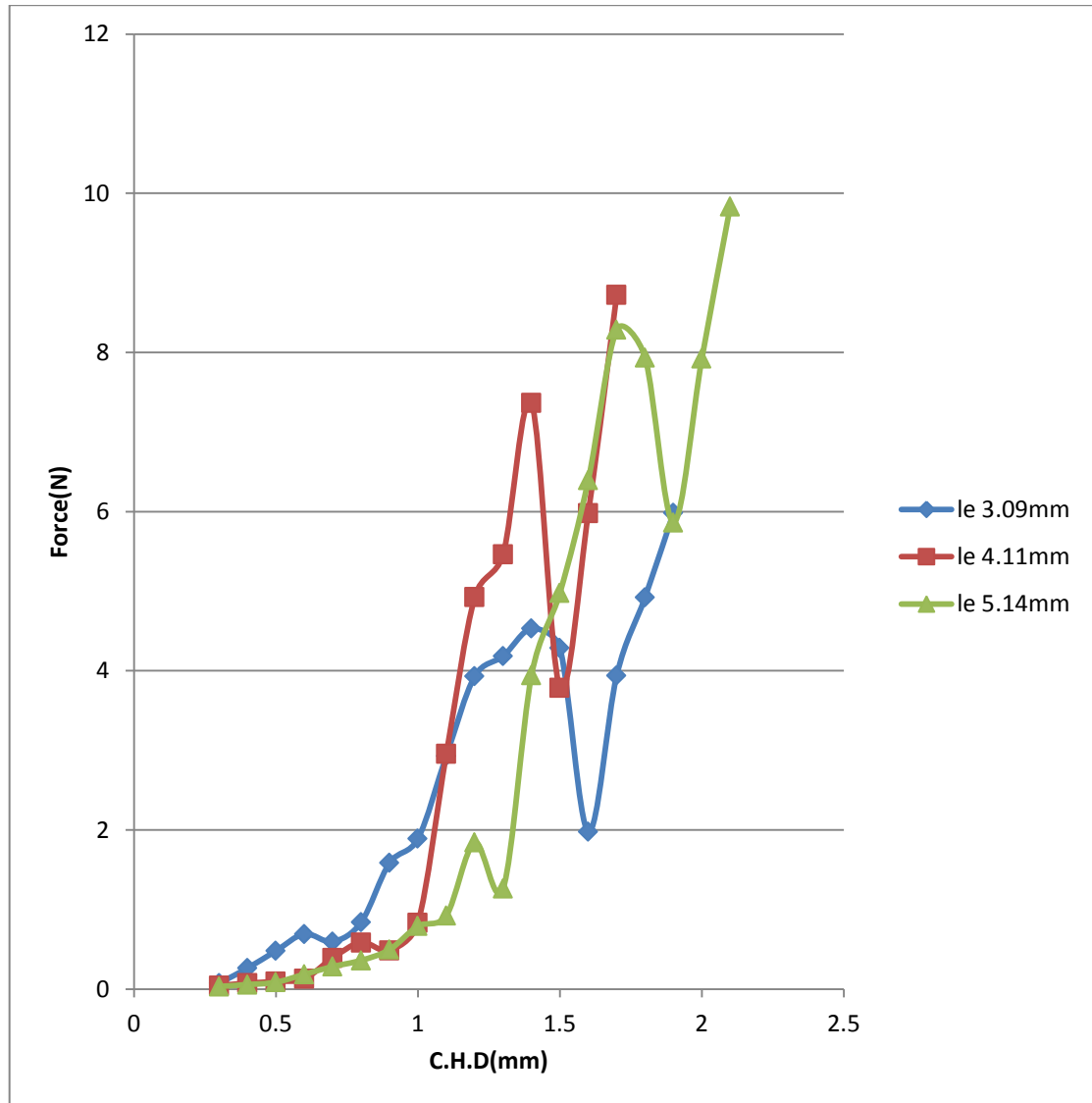

Fig (4-10) the drag-out force vs. cross head displacement curves for epoxy-polyethylene fiber post cure at 25°C of diameter (0.45mm).

The results from equation (2-1), (2-40) and (2-53) are listed in Table (4-10).

Table (4-10): the results from interfacial shear strength, shear-lag and energy release rate equations for epoxy-polyethylene fiber post cure at 25°C of diameter 0.45mm

Embedded length le(mm)	3.09	4.11	5.14
Drag-out deboned force at peak(N)	4.287	7.365	8.287
Drag-out friction force (N)	6.521	9.213	10.243
Pull-out debond force at peak(N)	9.462	15.723	19.412
Pull-out friction force at peak(N)	14.723	21.148	26.712
IFSS at peak debond point (MPa)	2.167	4.281	5.108
Shear-lag parameter $\beta(\mu m)^{-1}$	0.00023	0.00023	0.00023
$G_{\infty}(l_e)J/m^2$	33.171	38.182	45.153
$G_{\infty}(l_e)$ at K=0 J/m^2	24.826	27.813	33.725

4-2-5 Epoxy-Glass fiber post cure at 50ᵒC

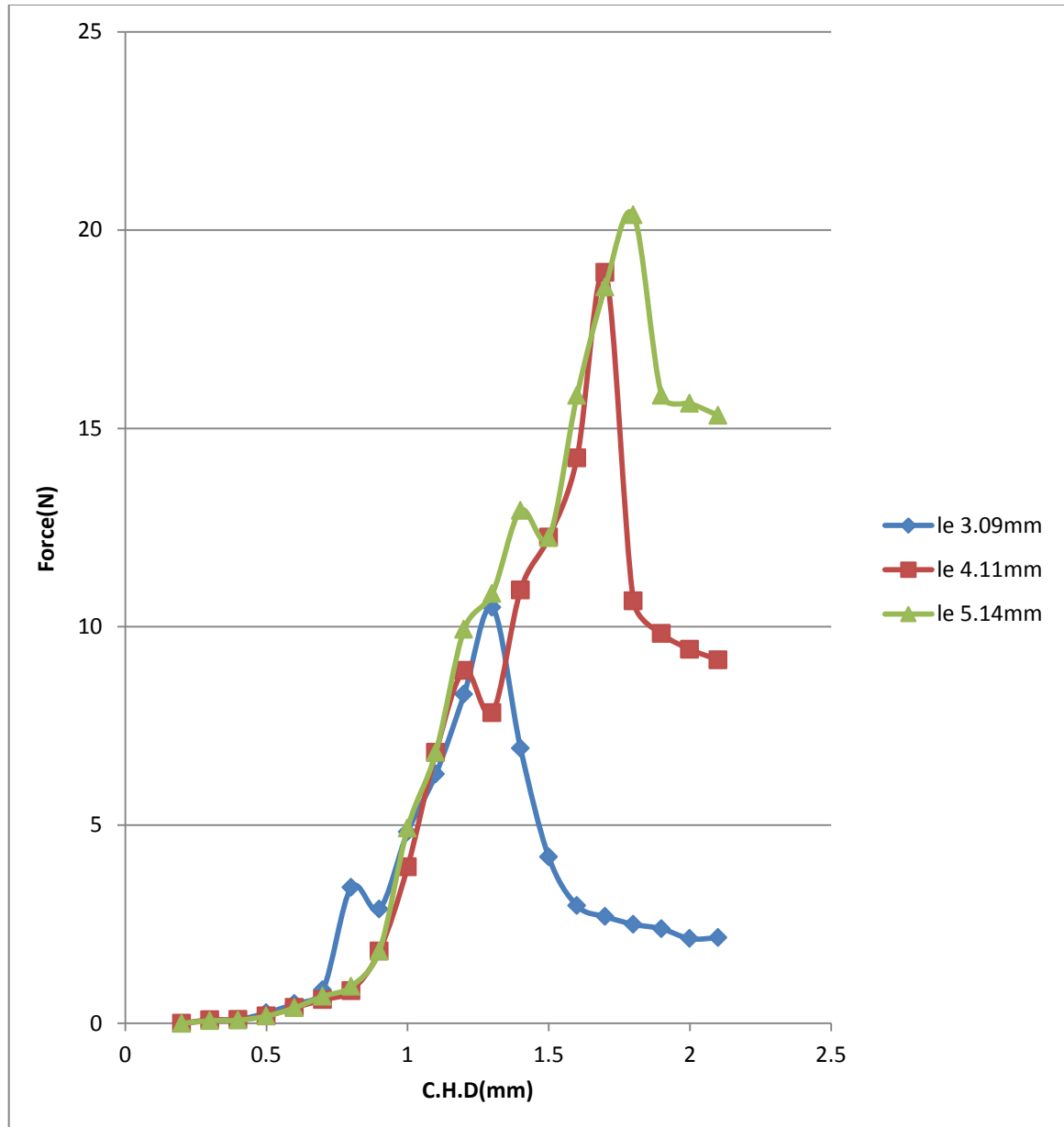Fig (4-11) Shown the results from drag-out test for epoxy-glass fiber post cure at 50ºC of diameter 0.22mm.

Fig (4-11) the drag-out force vs.cross head displacement curves for epoxy-glass fiber post cure at 50C⁰ of diameter (0.22mm).

The results from equation (2-1), (2-40) and (2-53) are listed in Table (4-11).

Table (4-11): the results from interfacial shear strength, shear-lag and energy release rate equations for epoxy-glass fiber post cure at 50ᵒC of diameter 0.22mm

Embedded length l_e(mm)	3.09	4.11	5.14
Drag-out deboned force at peak(N)	10.487	18.934	20.383
Drag-out friction force (N)	2.158	9.165	15.329
Pull-out debond force at peak(N)	24.926	35.182	39.172
Pull-out friction force (N)	5.129	8.172	14.109
IFSS at peak debond point (MPa)	10.168	13.834	16.914
Shear-lag parameter $\beta(\mu m)^{-1}$	0.00094	0.00094	0.00094
$G_\infty(l_e)J/m^2$ at $\Delta T = -25$	636.912	648.117	886.712
$G_\infty(l_e)$ at K=0 J/m^2	673.352	682.734	894.382

Fig (4-12) Shown the results from drag-out test for epoxy-glass fiber post cure at 50°C of diameter 0.34mm.
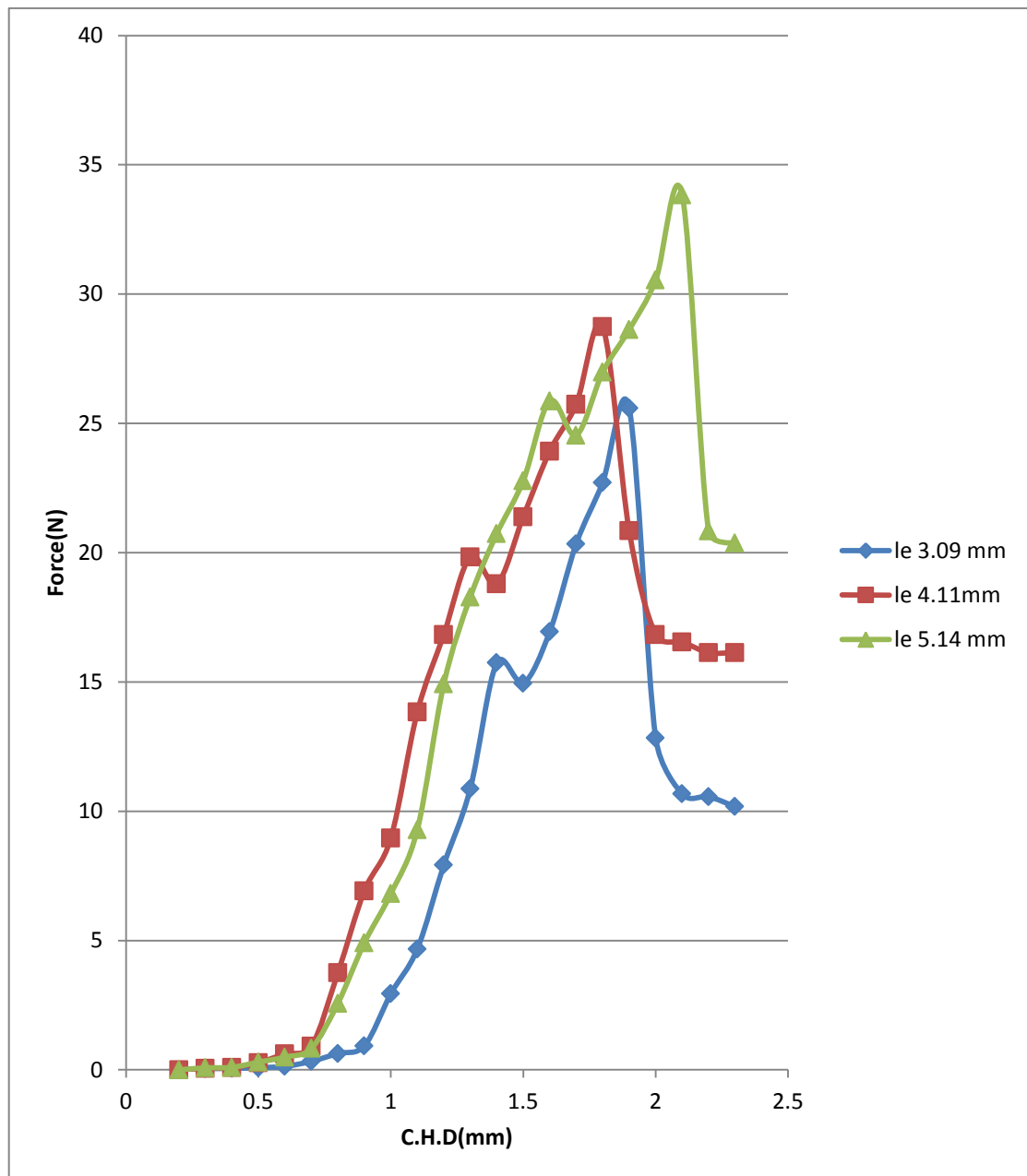

Fig (4-12) the drag-out force vs. cross head displacement curves for epoxy-glass fiber post cure at 50°C of diameter (0.34mm).

The results from equation (2-1), (2-40) and (2-53) are listed in Table (4-12)

Table (4-12): The results from interfacial shear strength, shear-lag and energy release rate equations for epoxy-glass fiber post cure at 50°C of diameter 0.34mm

Embedded length l$_e$(mm)	3.09	4.11	5.14
Drag-out deboned force at peak(N)	25.856	28.576	33.386
Drag-out friction force (N)	10.182	16.138	20.365
Pull-out debond force at peak(N)	44.386	72.904	78.001
Pull-out friction force (N)	13.109	17.612	19.831
IFSS at peak debond point (MPa)	15.845	17.618	18.281
Shear-lag parameter $\beta(\mu m)^{-1}$	0.00072	0.00072	0.00072
$G_\infty(l_e)J/m^2$ at $\Delta T = -25$	889.823	891.812	895.782
$G_\infty(l_e)$ at K=0 J/m^2	897.287	923.542	934.623

Fig (4-13) Shown the results from drag-out test for epoxy-glass fiber post cure at 50°C of diameter 0.43mm.

Fig (4-13) the drag-out force vs. cross head displacement curves for epoxy-glass fiber at post cure 50°C of diameter (0.43mm).

The results from equation (2-1), (2-40) and (2-53) are listed in Table (4-13).

Table (4-13): The results from interfacial shear strength, shear-lag and energy release rate equations for epoxy-glass fiber at post cure 50°C of diameter 0.43mm

Embedded length l$_e$(mm)	3.09	4.11	5.14
Drag-out deboned force at peak(N)	40.834	49.634	55.945
Drag-out friction force (N)	19.241	29.243	34.124
Pull-out debond force at peak(N)	63.088	78.194	86.182
Pull-out friction force (N)	25.849	31.726	46.612
IFSS at peak debond point (MPa)	15.823	17.812	18.101
Shear-lag parameter $\beta(\mu m)^{-1}$	0.00069	0.00069	0.00069
$G_\infty(l_e) J/m^2$ at $\Delta T = -25$	915.182	925.173	963.292
$G_\infty(l_e)$ at K=0 J/m^2	925.847	936.287	978.723

4-2-6 Epoxy-Carbon Post Cure at 50°C

Fig (4-14) Shown the results from drag-out test for epoxy-carbon fiber post cure at 50°C of diameter 0.22mm.
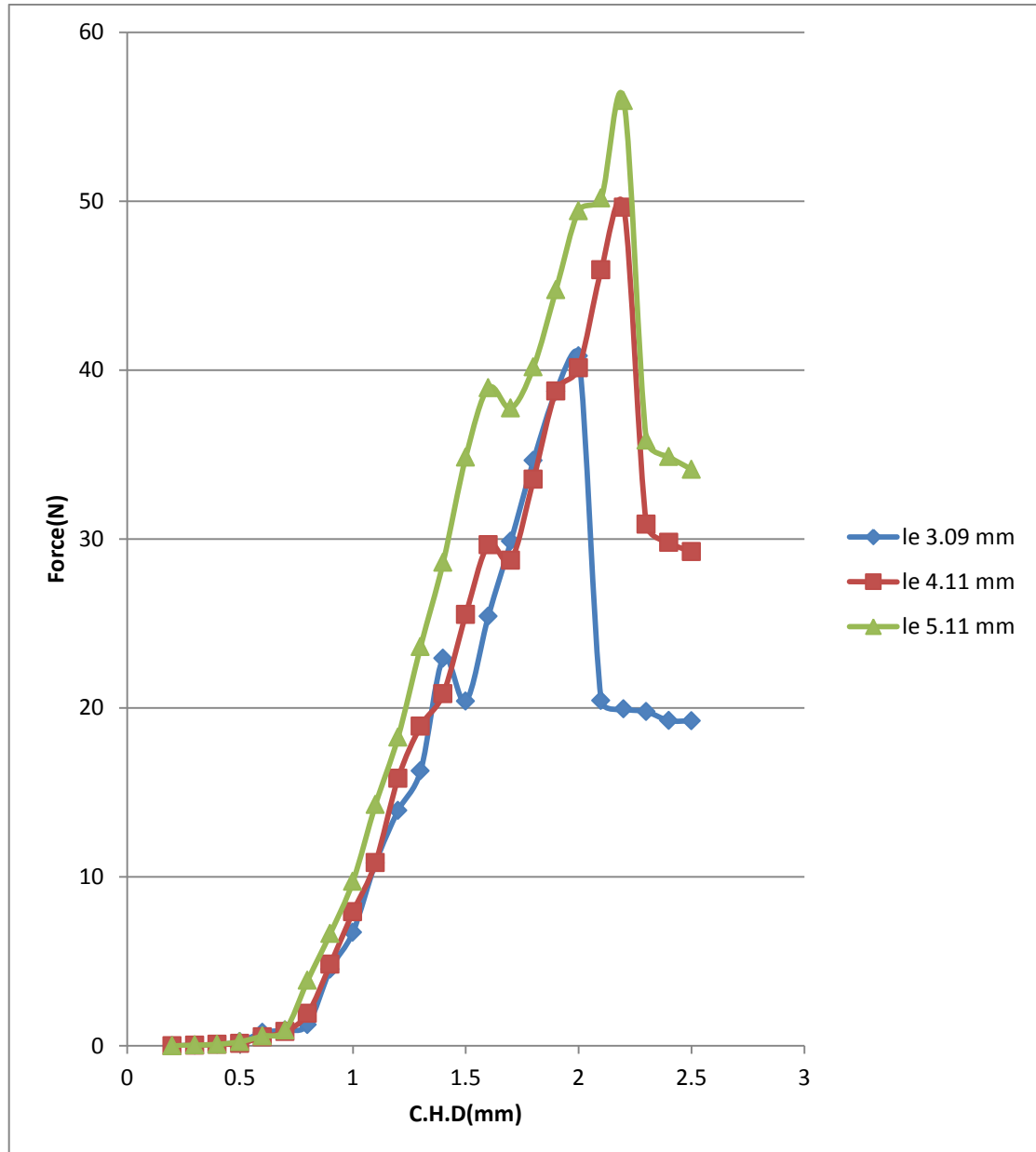

Fig (4-14) the drag-out force vs. cross head displacement curves for epoxy-carbon fiber post cure at 50°C of diameter (0.22mm).

The results from equation (2-1), (2-40) and (2-53) are listed in table (4-14).

Table (4-14): The results from interfacial shear strength, shear-lag and energy release rate equations for epoxy-carbon fiber post cure at 50°C of diameter 0.22mm

Embedded length l$_e$(mm)	3.09	4.11	5.14
Drag-out deboned force at peak(N)	20.745	28.734	35.548
Drag-out friction force (N)	8.254	14.143	19.283
Pull-out debond force at peak(N)	37.707	45.164	59.121
Pull-out friction force (N)	10.627	17.925	26.812
IFSS at peak debond point (MPa)	19.669	21.701	24.172
Shear-lag parameter $\beta(\mu m)^{-1}$	0.00057	0.00057	0.00057
$G_\infty(l_e)J/m^2$ at $\Delta T = -25$	792.846	797.182	812.714
$G_\infty(l_e)$ at K=0 J/m^2	816.618	827.736	838.819

Fig (4-15) Shown the results from drag-out test for epoxy-carbon fiber at post cure 50°C of diameter 0.34mm.
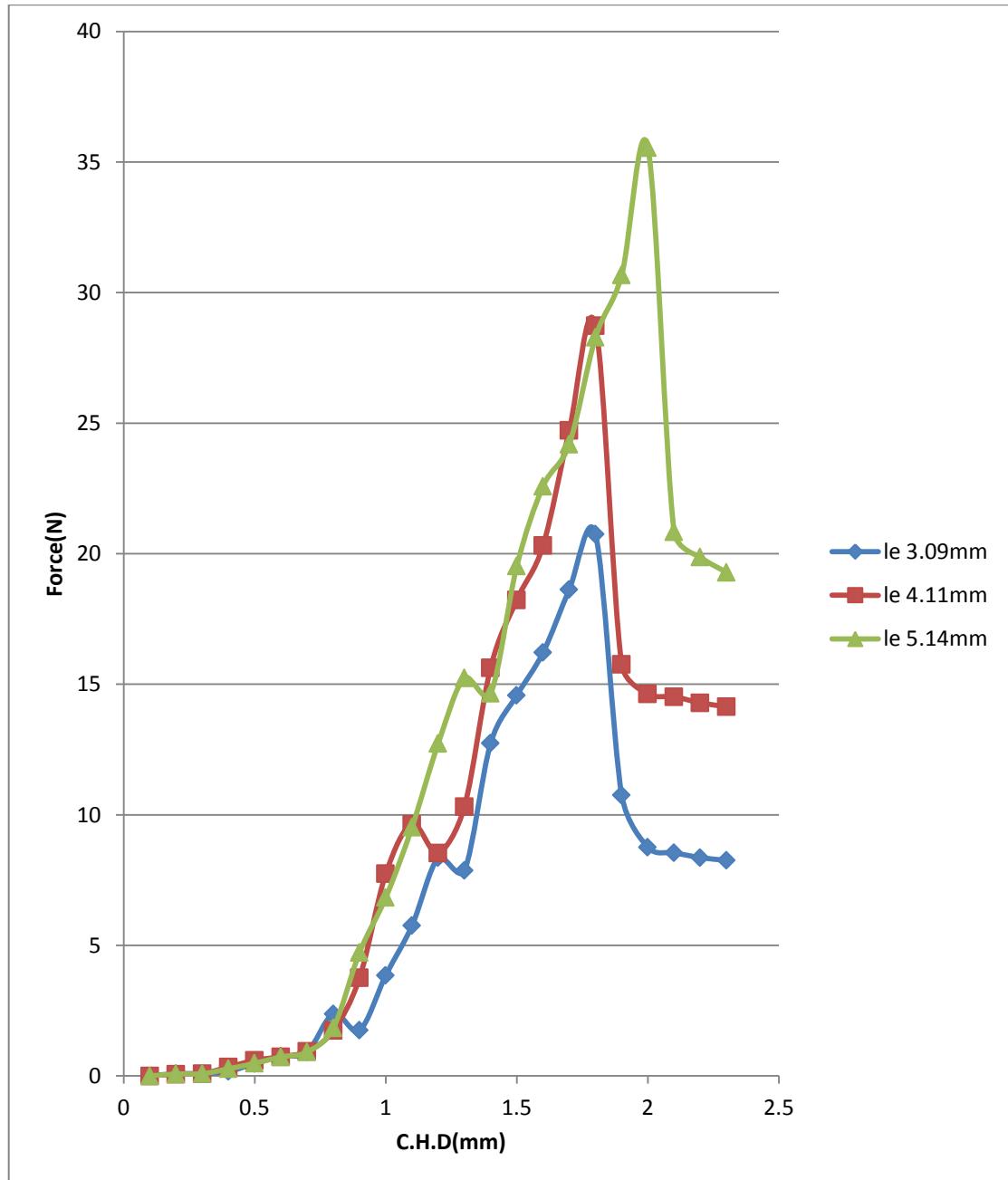

Fig (4-15) The drag-out force vs. cross head displacement curves for epoxy-carbon fiber post cure at 50°C of diameter (0.34mm).

The results from eqs (2-1), (2-40) and (2-53) are listed in Table (4-15).

Table (4-15): The results from interfacial shear strength, shear-lag and energy release rate equations for epoxy-carbon fiber at post cure 50°C of　diameter 0.34mm

Embedded length l$_e$(mm)	3.09	4.11	5.14
Drag-out deboned force at peak(N)	39.412	44.849	49.932
Drag-out friction force (N)	19.542	24.634	27.739
Pull-out debond force at peak(N)	57.991	64.714	71.726
Pull-out friction force (N)	23.745	29.634	35.623
IFSS at peak debond point (MPa)	26.835	28.623	28.834
Shear-lag parameter $\beta(\mu m)^{-1}$	0.00043	0.00043	0.00043
$G_\infty(l_e)J/m^2$ at $\Delta T = -25$	734.283	787.912	865.172
$G_\infty(l_e)$ at K=0 J/m^2	748.623	795.453	881.265

Fig (4-16) Shown the results from drag-out test for epoxy-carbon fiber post cure at 50°C of diameter 0.43mm.
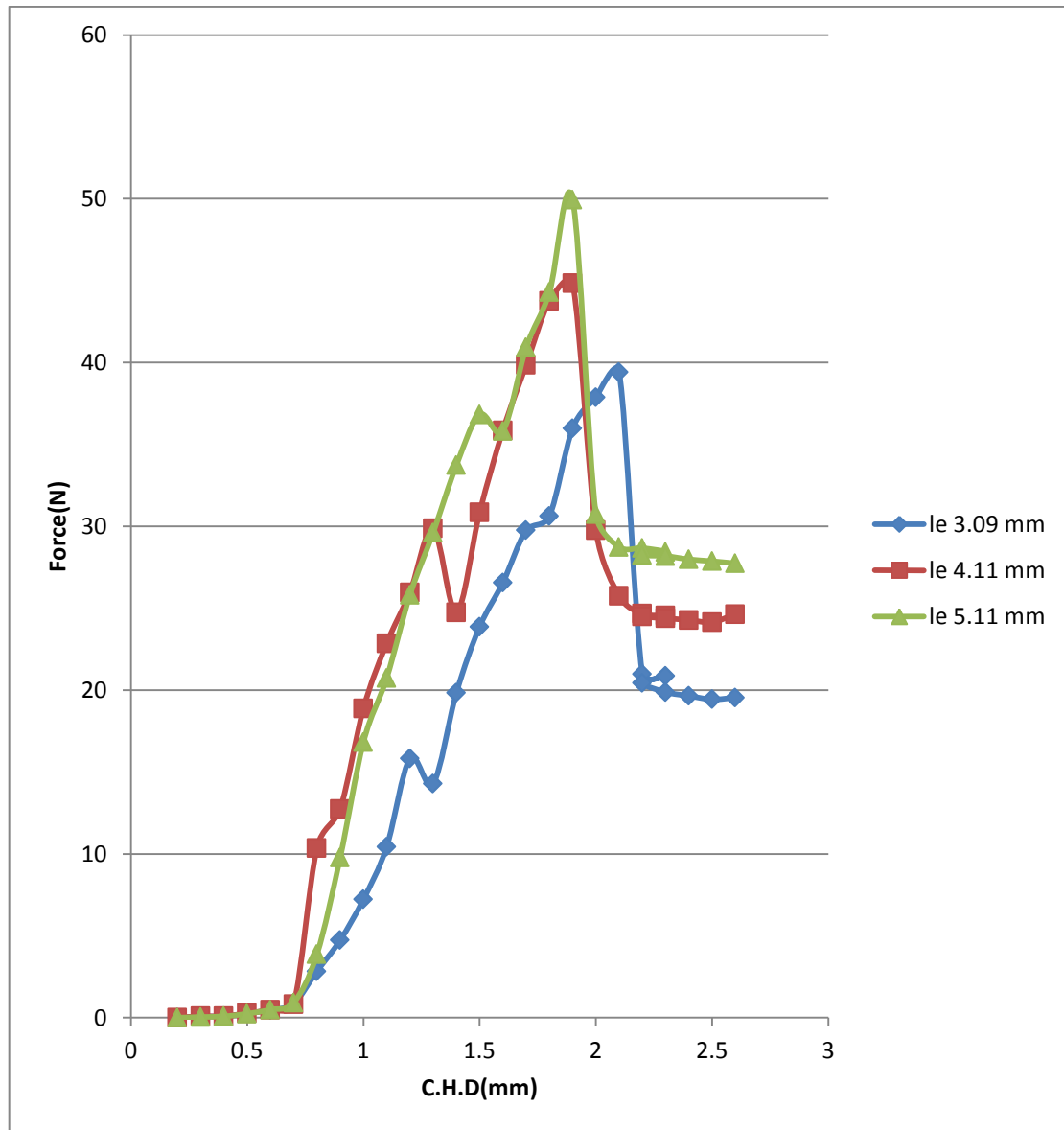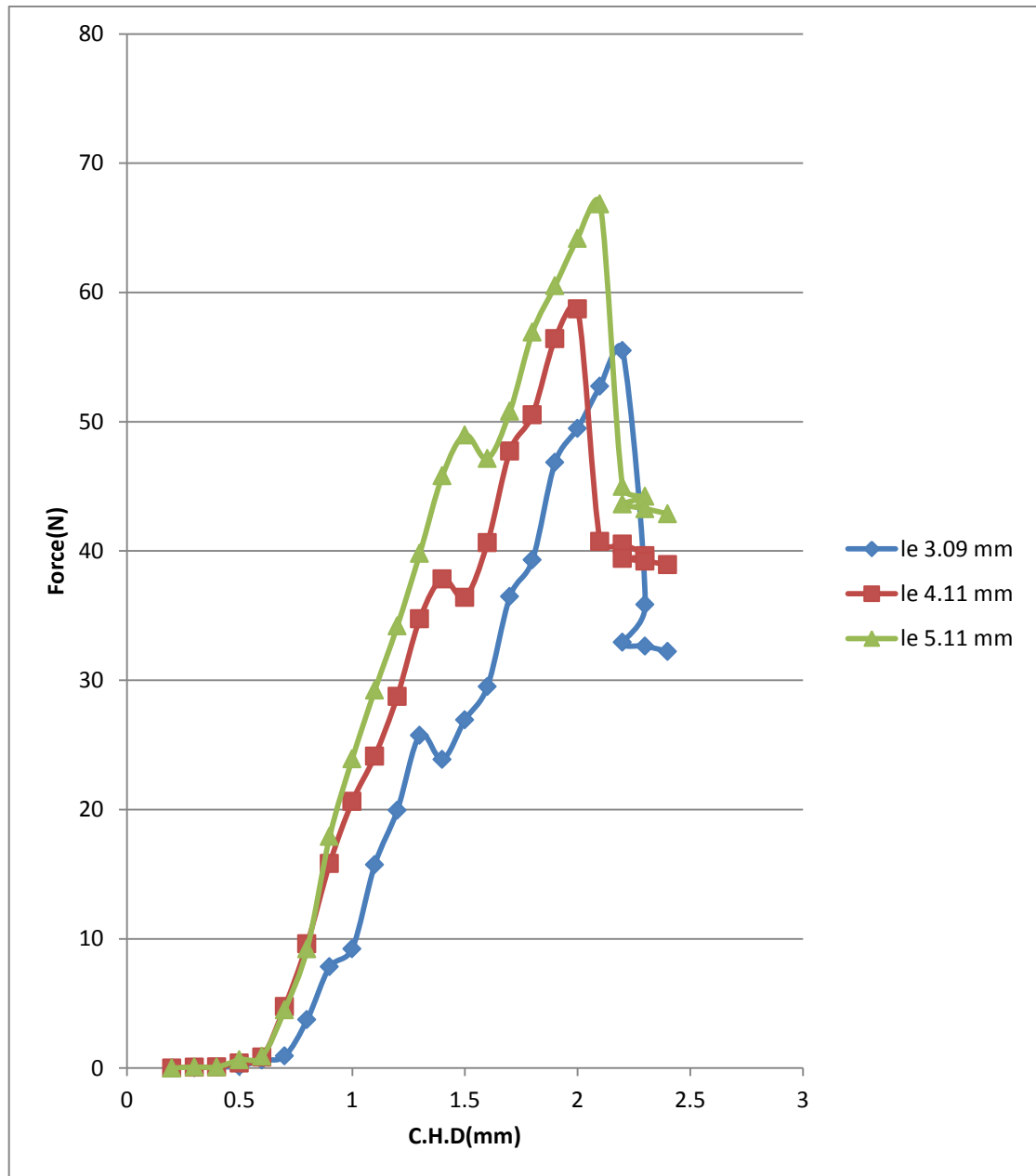

Fig (4-16) The drag-out force vs. cross head displacement curves for epoxy-carbon fiber at 50°C of diameter (0.43mm).

The results from eqs (2-1), (2-40) and (2-53) are listed in Table (4-16).

Table (4-16): The results from interfacial shear strength, shear-lag and energy release rate equations for epoxy-carbon fiber post cure at 50ºC of diameter 0.43mm

Embedded length l_e(mm)	3.09	4.11	5.14
Drag-out deboned force at peak(N)	55.512	58.723	66.834
Drag-out friction force (N)	32.231	38.934	42.873
Pull-out debond force at peak(N)	74.579	83.713	90.813
Pull-out friction force (N)	41.497	48.836	54.834
IFSS at peak debond point (MPa)	25.981	32.813	37.926
Shear-lag parameter $\beta(\mu m)^{-1}$	0.00037	0.00037	0.00037
$G_\infty(l_e)J/m^2$ at $\Delta T = -25$	935.165	947.377	956.109
$G_\infty(l_e)$ at K=0 J/m^2	947.827	962.532	973.191

4-2-7 Epoxy-Kevlar post cure at 50°C

Fig (4-17) Shown the results from drag-out test for epoxy-kevlar fiber post cure at 50°C of diameter 0.22mm.

Fig (4-17) The drag-out force vs. cross head displacement curves for epoxy-kevlar fiber post cure at 50°C of diameter (0.22mm).

The results from equs (2-1), (2-40) and (2-53) are listed in table (4-17).

Table (4-17): The results from interfacial shear strength, shear-lag and energy release rate equations for epoxy-kevlar fiber post cure at 50°C of   diameter 0.22mm

Embedded length l$_e$(mm)	3.09	4.11	5.14
Drag-out deboned force at peak(N)	60.172	68.354	75.512
Drag-out friction force (N)	39.231	47.243	50.343
Pull-out debond force at peak(N)	97.858	133.778	161.721
Pull-out friction force (N)	46.835	95.587	112.832
IFSS at peak debond point (MPa)	45.856	47.612	48.735
Shear-lag parameter $\beta(\mu m)^{-1}$	0.00052	0.00052	0.00052
$G_\infty(l_e) J/m^2$ at $\Delta T = -25$	824.712	867.292	912.723
$G_\infty(l_e)$ at K=0 J/m^2	843.716	877.809	926.357

Fig (4-18) Shown the results from drag-out test for epoxy-kevlar fiber post cure at 50°C of diameter 0.34mm.
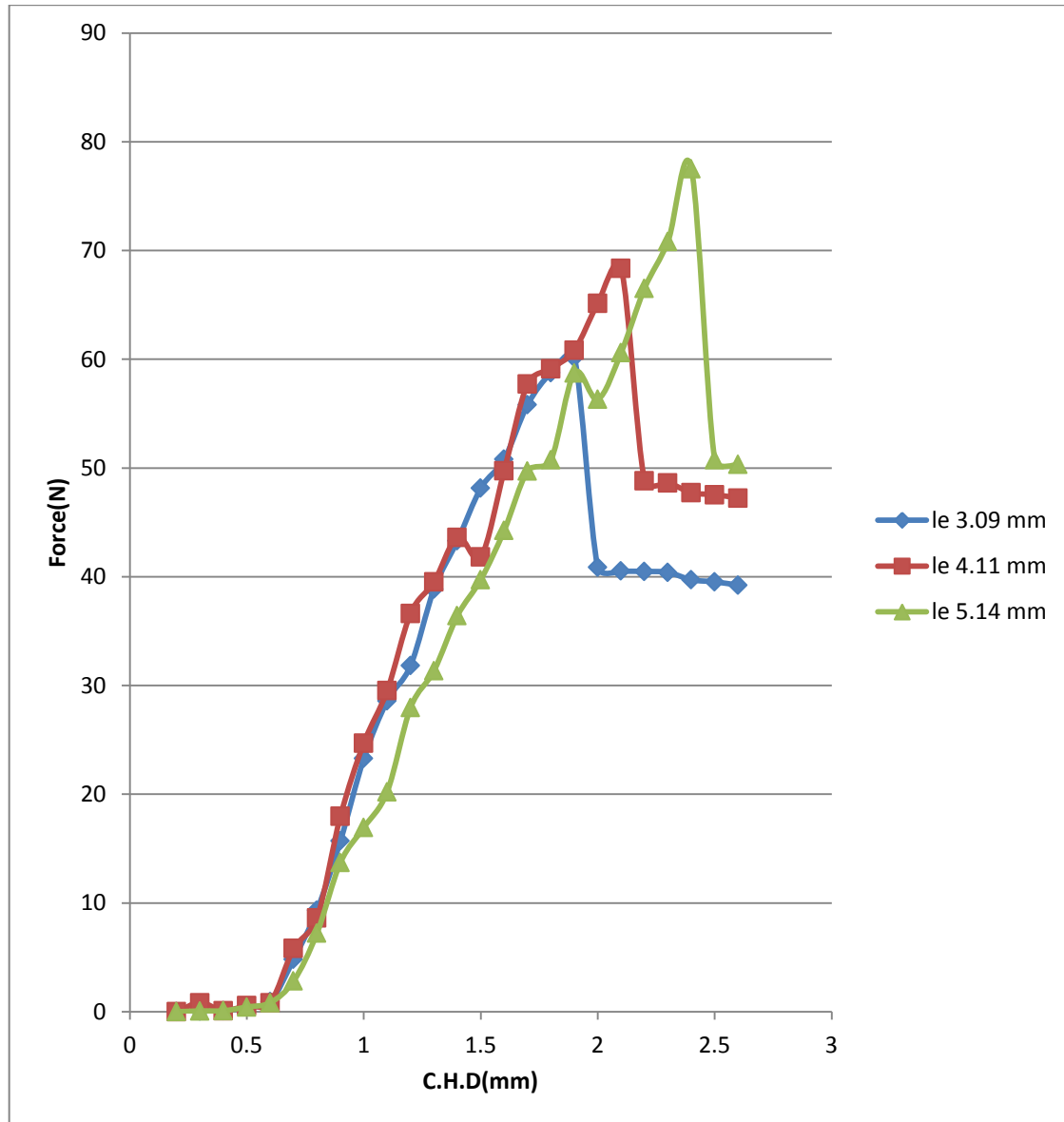

Fig (4-18) The drag-out force vs. cross head displacement curves for epoxy-kevlar fiber post cure at 50°C of diameter (0.34mm).

The results from eqs (2-1), (2-40) and (2-53) are listed in Table (4-18).

Table (4-18): The results from interfacial shear strength, shear-lag and energy release rate equations for epoxy-kevlar fiber post cure at 50°C of diameter 0.34mm

Embedded length l_e(mm)	3.09	4.11	5.14
Drag-out deboned force at peak(N)	79.357	88.573	92.341
Drag-out friction force (N)	30.634	50.412	60.431
Pull-out debond force at peak(N)	106.614	121.528	137.182
Pull-out friction force (N)	35.058	38.723	49.283
IFSS at peak debond point (MPa)	48.381	53.726	57.916
Shear-lag parameter $\beta(\mu m)^{-1}$	0.00032	0.00032	0.00032
$G_\infty(l_e)J/m^2$ at $\Delta T = -25$	978.283	983.102	1105.719
$G_\infty(l_e)$ at K=0 J/m^2	984.671	995.365	1125.713

Fig (4-19) Shown the results from drag-out test for epoxy-kevlar fiber post cure at 50°C of diameter 0.43mm.
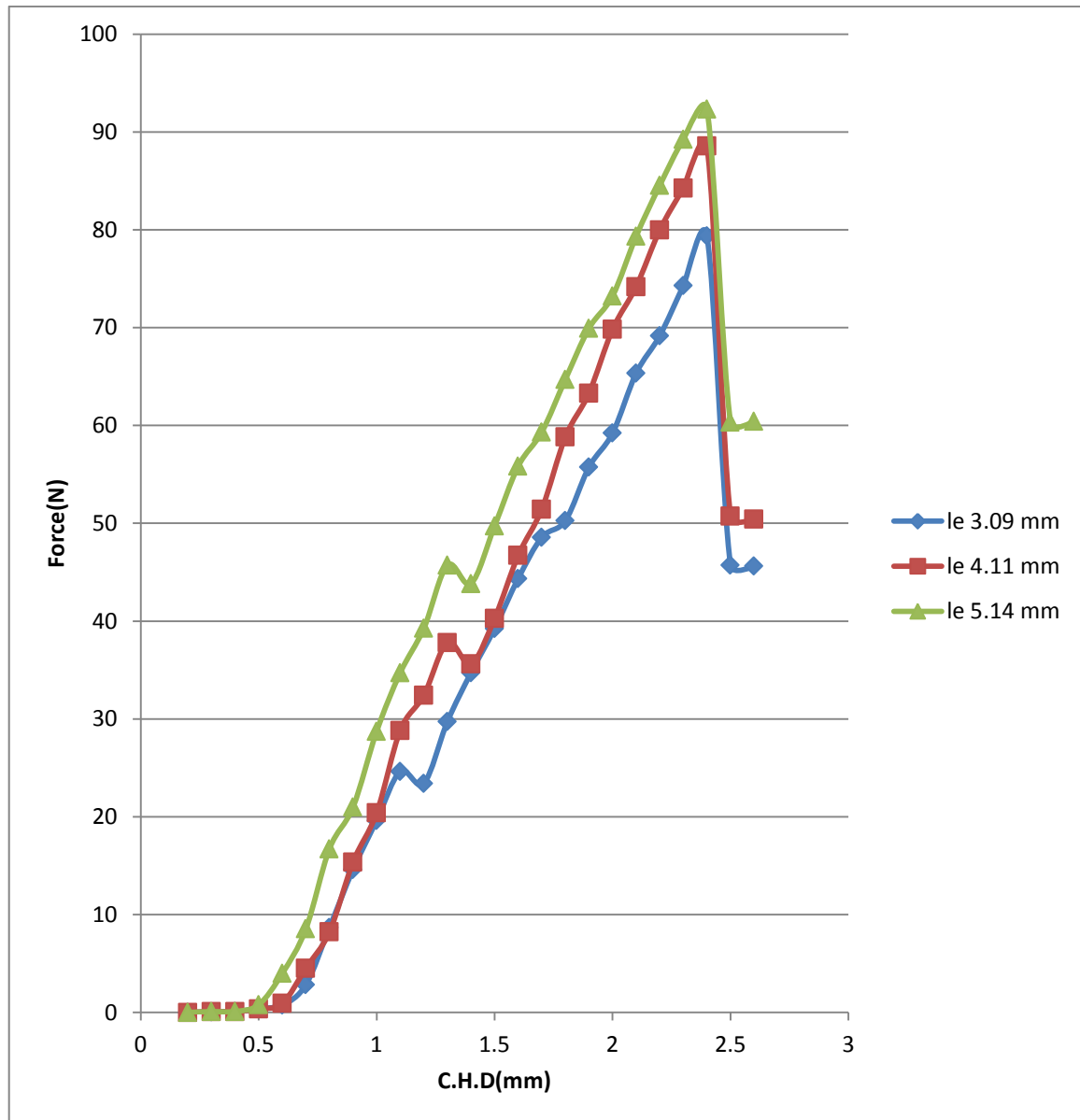

Fig (4-19) The drag-out force vs. cross head displacement curves for epoxy-kevlar fiber post cure at 50°C of diameter (0.43mm).

The results from eqs (2-1), (2-40) and (2-53) are listed in table (4-19)

Table (4-19): The results from interfacial shear strength, shear-lag and energy release rate equations for epoxy-kevlar fiber post cure at 50°C of diameter 0.43m

Embedded length l$_e$(mm)	3.09	4.11	5.14
Drag-out deboned force at peak(N)	95.384	100.642	106.823
Drag-out friction force (N)	50.453	69.253	85.267
Pull-out debond force at peak(N)	140.352	162.815	185.812
Pull-out friction force (N)	65.201	69.128	76.283
IFSS at peak debond point (MPa)	54.735	56.423	57.825
Shear-lag parameter $\beta(\mu m)^{-1}$	0.00025	0.00025	0.00025
$G_\infty(l_e)J/m^2$ at $\Delta T = -25$	912.265	945.715	967.72
$G_\infty(l_e)$ at K=0 J/m^2	934.836	965.339	984.523

4-2-8 Epoxy Polyethylene Fiber post cure at 50°C

Fig (4-20) Shown the results from drag-out test for epoxy-polyethylene fiber post cure at 50°C of diameter 0.45mm.
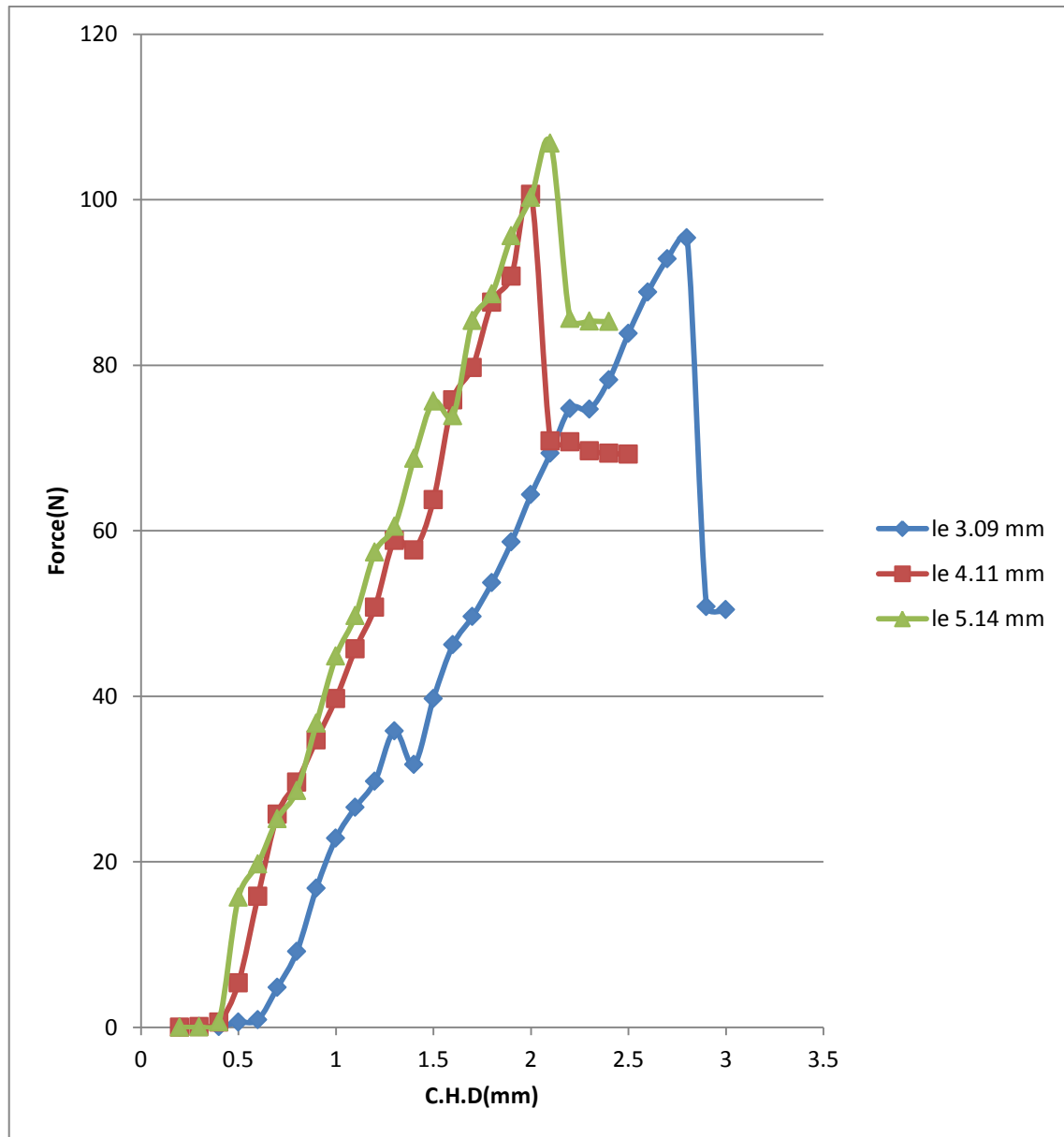

Fig (4-20) The drag-out force vs. cross head displacement curves for epoxy-polyethylene fiber post cure at 50°C of diameter (0.45mm).

The results from eqs (2-1), (2-40) and (2-53) are listed in table (4-20).

Table (4-20): The results from interfacial shear strength, shear-lag and energy release rate equations for epoxy-polyethylene fiber post cure at 50°C of diameter 0.45mm

Embedded length l_e(mm)	3.09	4.11	5.14
Drag-out deboned force at peak(N)	8.421	10.231	12.834
Drag-out friction force (N)	14.132	12.362	16.867
Pull-out debond force at peak(N)	14.961	28.032	41.229
Pull-out friction force (N)	7.515	9.912	12.273
IFSS at peak debond point (MPa)	10.592	16.811	19.437
Shear-lag parameter $\beta(\mu m)^{-1}$	0.00023	0.00023	0.00023
$G_\infty(l_e) J/m^2$ at $\Delta T = -25$	79.832	86.273	95.283
$G_\infty(l_e)$ at K=0 J/m^2	56.734	63.873	73.523

4-2-9 Epoxy-Glass fiber post cure at 75°C

Fig (4-21) Shown the results from drag-out test for epoxy-glass fiber post cure at 75°C of diameter 0.22mm.
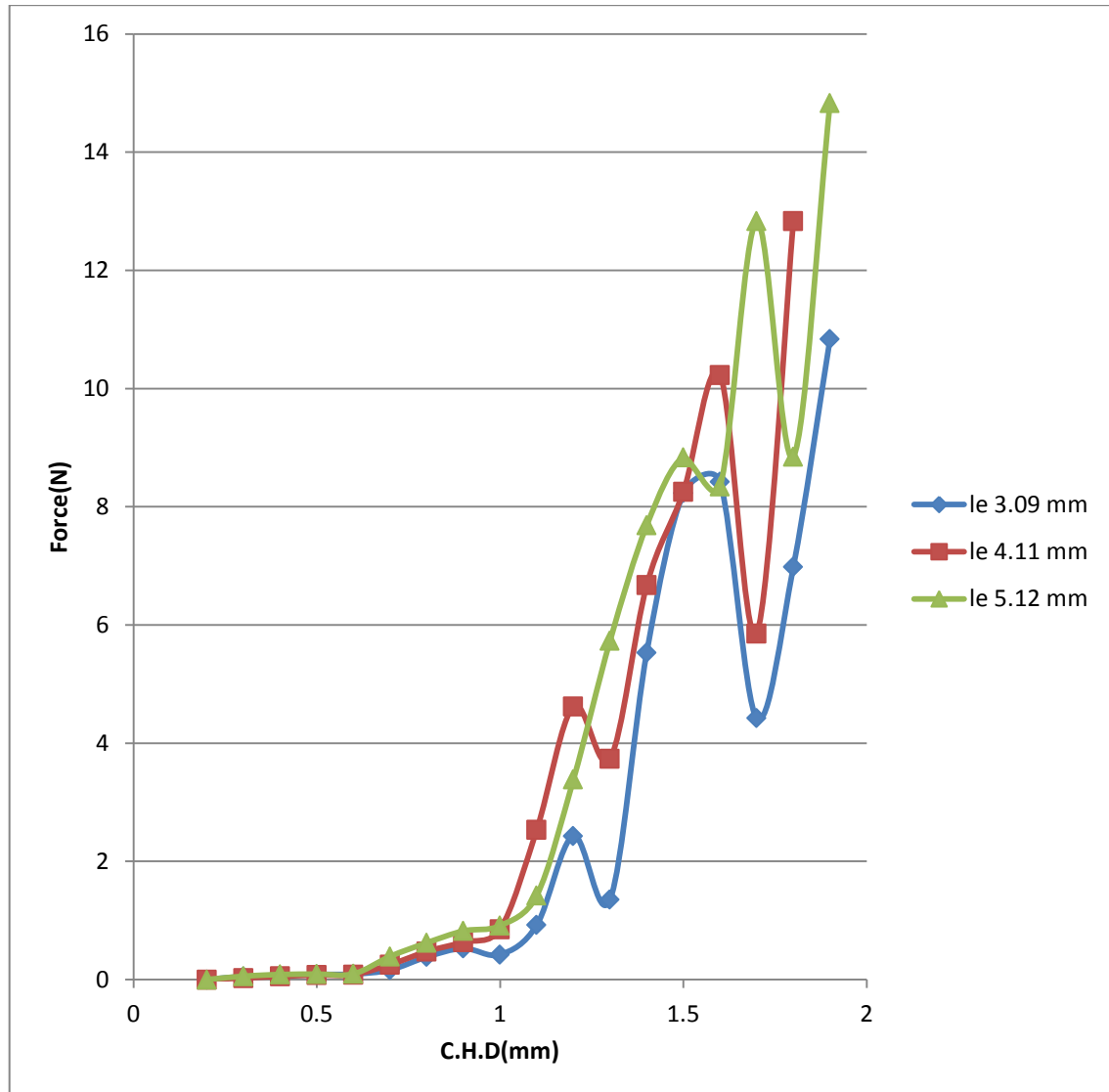

Fig (4-21) The drag-out force vs. cross head displacement curves for epoxy-glass fiber post cure at 75°C of diameter (0.22mm).

The results from eqs (2-1), (2-40) and (2-5۳) are listed in table (4-21).

Table (4-21): The results from interfacial shear strength, shear-lag and energy release rate equations for epoxy-glass fiber post cure at 75°C of diameter 0.22mm

Embedded length l$_e$(mm)	3.09	4.11	5.14
Drag-out deboned force at peak(N)	15.756	20.823	27.721
Drag-out friction force (N)	7.452	15.263	20.128
Pull-out debond force at peak(N)	30.428	38.532	48.109
Pull-out friction force (N)	12.119	19.192	27.172
IFSS at peak debond point (MPa)	14.258	13.572	16.551
Shear-lag parameter $\beta(\mu m)^{-1}$	0.00094	0.00094	0.00094
$G_\infty(l_e)J/m^2$ at $\Delta T = -50^o C$	1128.617	1146.501	1179.512
$G_\infty(l_e)$ at K=0 J/m^2	1134.098	1178.361	1195.232

Fig (4-22) Shown the results from drag-out test for epoxy-glass fiber post cure at 75°C of diameter 0.34mm.
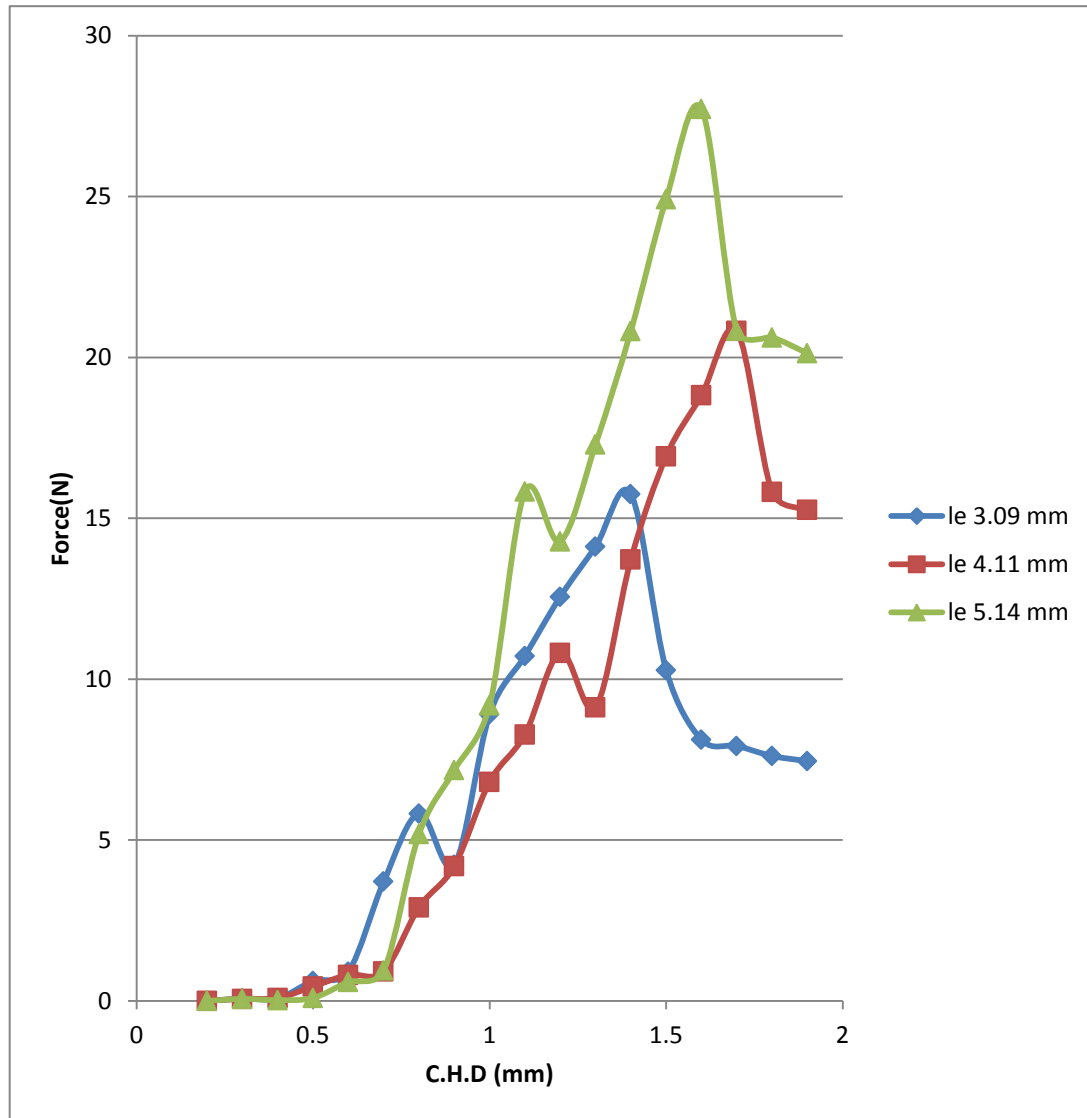

Fig (4-22) The drag-out force vs. cross head displacement curves for epoxy-glass fiber post cure at 75°C of diameter (0.34mm).

The results from eqs (2-1), (2-40) and (2-53) are listed in table (4-22).

Table (4-22): The results from interfacial shear strength, shear-lag and energy release rate equations for epoxy-glass fiber post cure at 75ᵒC of diameter 0.34mm

Embedded length l_e(mm)	3.09	4.11	5.14
Drag-out deboned force at peak(N)	34.982	39.867	45.823
Drag-out friction force (N)	19.412	25.311	30.135
Pull-out debond force at peak(N)	67.558	74.845	87.481
Pull-out friction force (N)	28.563	36.162	52.562
IFSS at peak debond point (MPa)	20.484	21.826	22.591
Shear-lag parameter $\beta(\mu m)^{-1}$	0.00072	0.00072	0.00072
$G_\infty(l_e)J/m^2$ at $\Delta T = -50\,^oC$	1168.293	1187.937	1196.523
$G_\infty(l_e)$ at K=0 J/m^2	1182.719	1195.612	1224.716

Fig (4-23) Shown the results from drag-out test for epoxy-glass fiber post cure at 75°C of diameter 0.43mm.
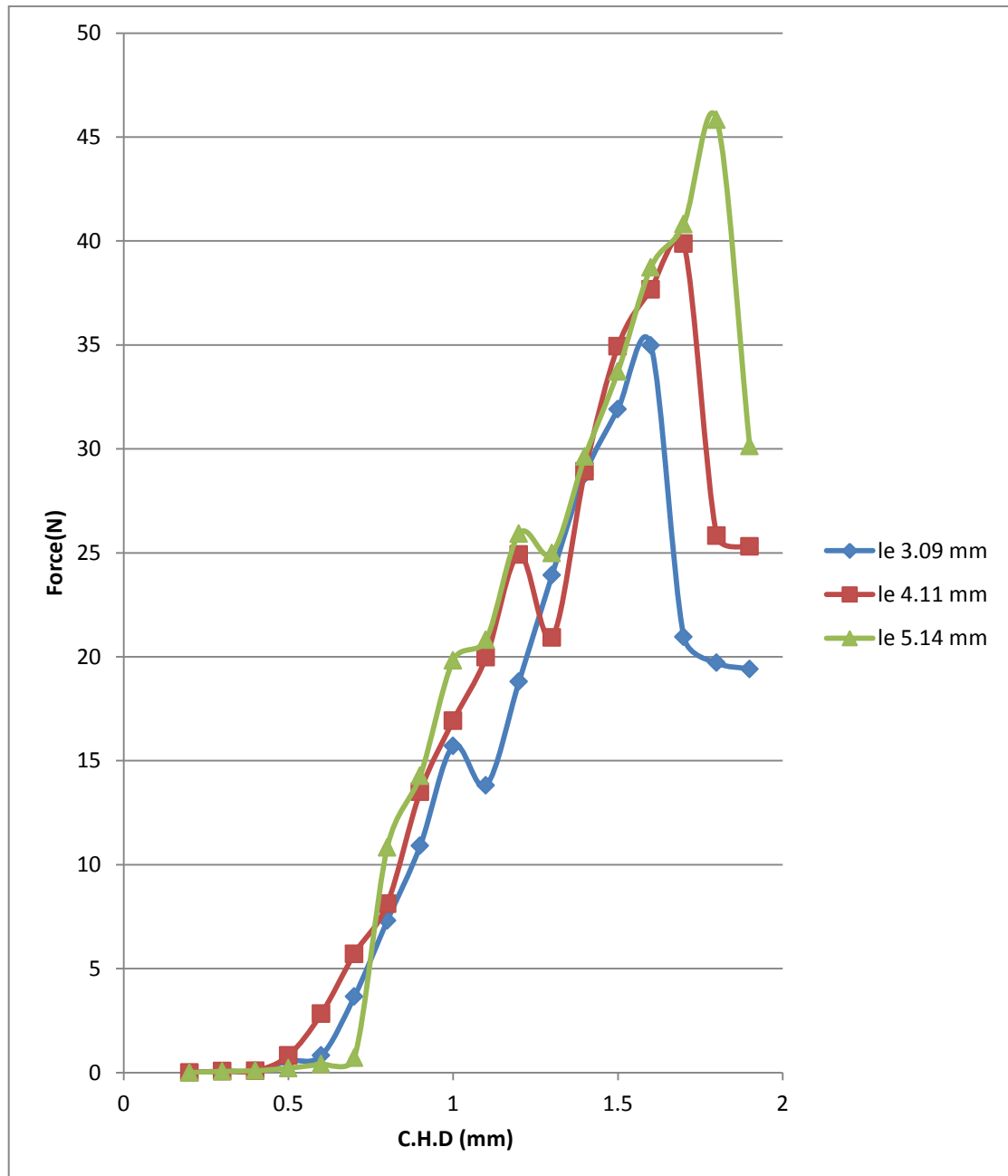

Fig (4-23) The drag-out force vs. cross head displacement curves for epoxy-glass fiber post cure at 75°C of diameter (0.43mm).

The results from eq (2-1), (2-40) and (2-53) are listed in table (4-23).

Table (4-23): The results from interfacial shear strength, shear-lag and energy release rate equations for epoxy-glass fiber post cure at 75°C of diameter 0.43mm

Embedded length l_e(mm)	3.09	4.11	5.14
Drag-out deboned force at peak(N)	48.523	50.823	58.765
Drag-out friction force (N)	20.217	30.365	35.475
Pull-out debond force at peak(N)	99.957	127.681	135.823
Pull-out friction force (N)	36.747	57.821	78.231
IFSS at peak debond point (MPa)	23.959	24.684	22.845
Shear-lag parameter $\beta(\mu m)^{-1}$	0.00069	0.00069	0.00069
$G_\infty(l_e)J/m^2$ at $\Delta T = -50\,^{\mathrm{o}}\mathrm{C}$	1196.523	1692.264	1843.365
$G_\infty(l_e)$ at K=0 J/m^2	1241.734	1712.723	1932.274

4-2-10- Epoxy-Carbon fiber post cure at 75°C

Fig (4-24) Shown the results from drag-out test for epoxy-carbon fiber post cure at 75°C of diameter 0.22mm.
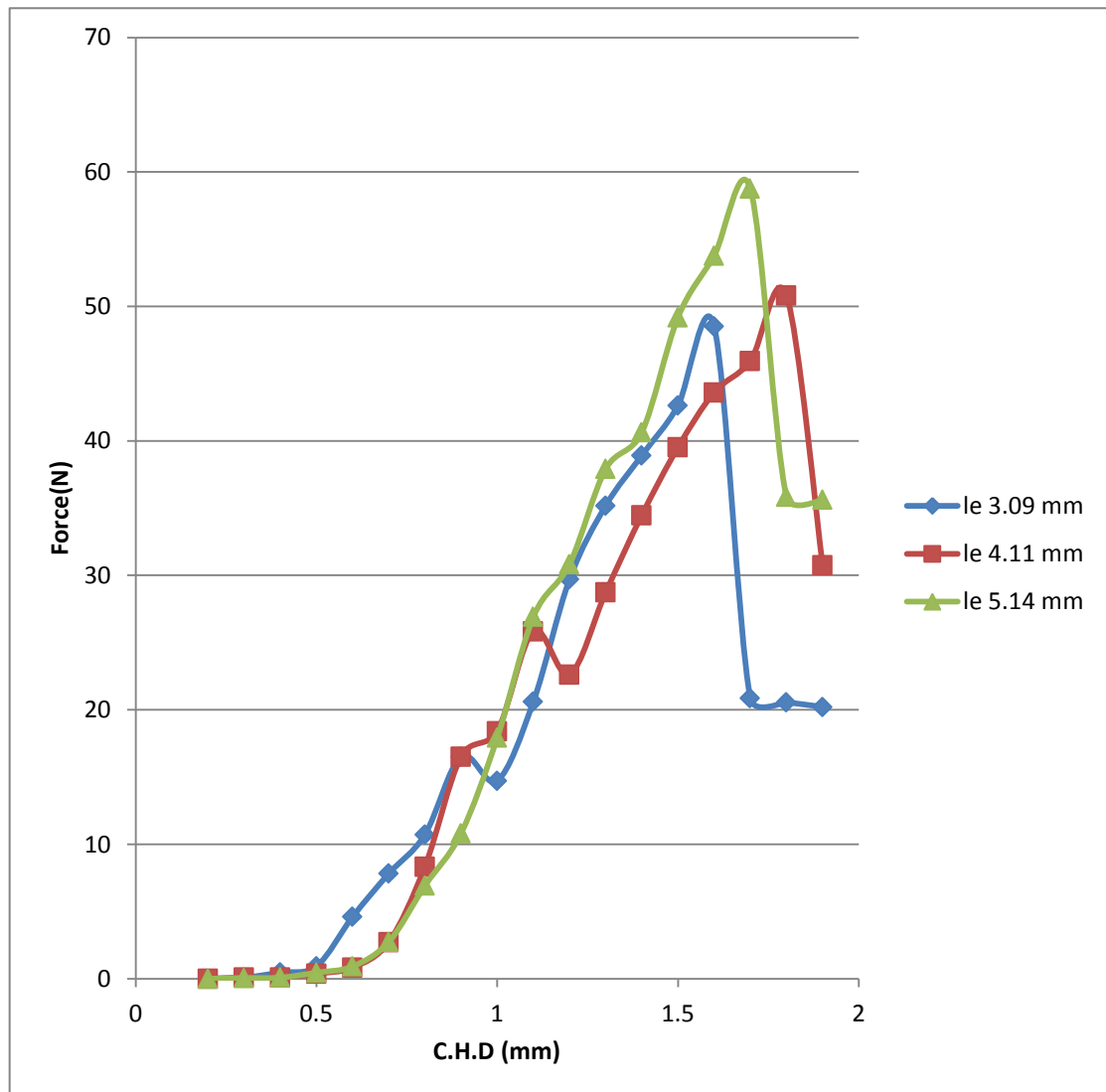

Fig (4-24) the drag-out force vs. cross head displacement curves for epoxy-carbon fiber post cure at 75°C of diameter (0.22mm).

The results from eq. (2-1), (2-40) and (2-53) are listed in table (4-24)

Table (4-24): The results from interfacial shear strength, shear-lag and energy release rate equations for epoxy-glass fiber post cure at 75$^{\text{o}}$C of diameter 0.22mm

Embedded length l$_e$(mm)	3.09	4.11	5.14
Drag-out deboned force at peak(N)	30.728	38.643	40.724
Drag-out friction force (N)	15.243	25.287	30.265
Pull-out debond force at peak(N)	55.852	88.282	123.134
Pull-out friction force (N)	24.715	47.923	85.375
IFSS at peak debond point (MPa)	26.172	27.294	28.306
Shear-lag parameter $\beta(\mu m)^{-1}$	0.00075	0.00075	0.00075
$G_\infty(l_e)J/m^2$ at $\Delta T = -50 \ ^{\text{o}}C$	1482.734	1667.091	1898.162
$G_\infty(l_e)$ at K=0 J/m^2	1496.306	1732.372	1972.231

Fig (4-25) Shown the results from drag-out test for epoxy-carbon fiber post cure at 75°C of diameter 0.34mm.
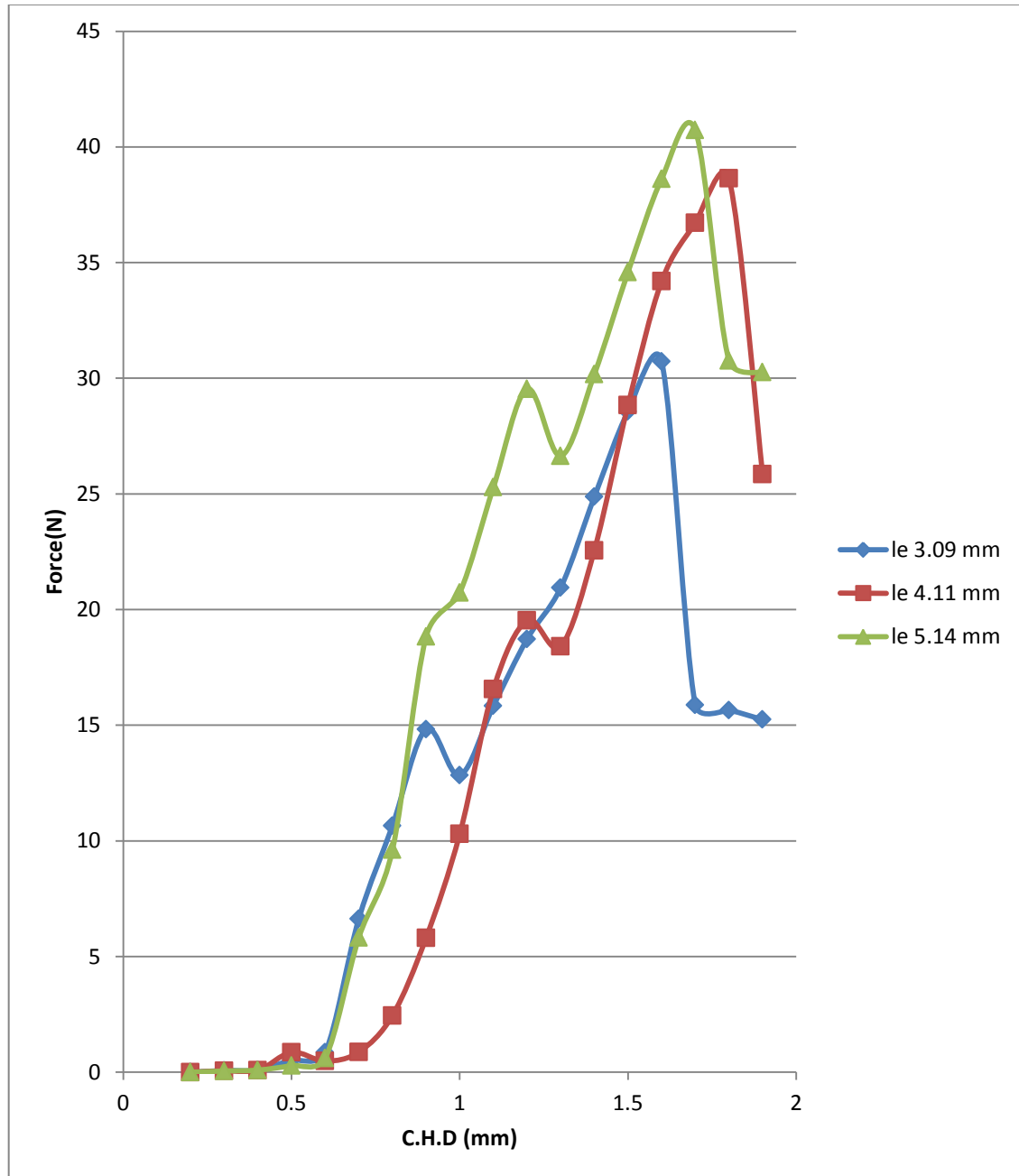

Fig (4-25) The drag-out force vs. cross head displacement curves for epoxy-carbon fiber post cure at 75°C of diameter (0.34mm).

The results from eqs. (2-1), (2-40) and (2-53) are listed in table (4-25).

Table (4-25): The results from interfacial shear strength, shear-lag and energy release rate equations for epoxy-carbon fiber post cure at 75°C of diameter 0.34mm

Embedded length l_e(mm)	3.09	4.11	5.14
Drag-out deboned force at peak(N)	49.342	58.973	65.834
Drag-out friction force (N)	33.172	40.823	45.143
Pull-out debond force at peak(N)	80.245	115.418	161.136
Pull-out friction force (N)	46.565	91.672	125.821
IFSS at peak debond point (MPa)	29.534	23.845	39.366
Shear-lag parameter $\beta(\mu m)^{-1}$	0.00043	0.00043	0.00043
$G_{\infty}(l_e)J/m^2$ at $\Delta T = -50\,^{o}C$	1865.862	1916.809	1973.712
$G_{\infty}(l_e)$ at K=0 J/m^2	1882.614	1946.154	1987.132

Fig (4-26) Shown the results from drag-out test for epoxy-carbon fiber post cure at 75°C of diameter 0.43mm.
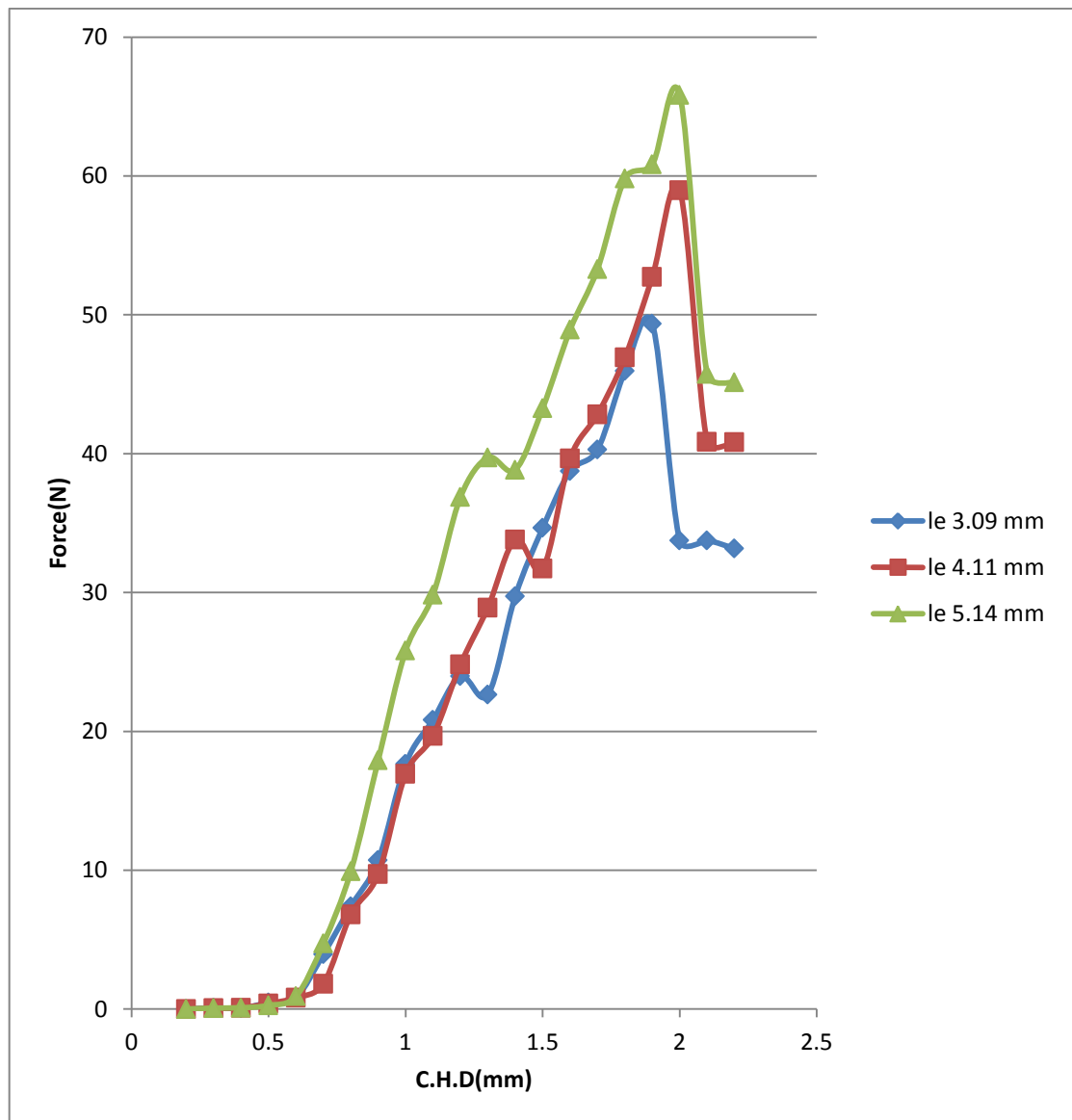

Fig (4-26) The drag-out force vs. cross head displacement curves for epoxy-carbon fiber post cure at 75°C of diameter (0.43mm).

The results from eqs. (2-1), (2-40) and (2-53) are listed in table (4-26).

Table (4-26): the results from interfacial shear strength, shear-lag and energy release rate equations for epoxy-carbon fiber post cure at 75°C of diameter 0.43mm.

Embedded length l$_e$(mm)	3.09	4.11	5.14
Drag-out deboned force at peak(N)	73.812	75.878	79.243
Drag-out friction force (N)	50.243	60.132	65.249
Pull-out debond force at peak(N)	120.041	173.254	214.373
Pull-out friction force (N)	64.687	95.723	165.208
IFSS at peak debond point (MPa)	28.773	27.183	29.624
Shear-lag parameter $\beta(\mu m)^{-1}$	0.00037	0.00037	0.00037
$G_\infty(l_e)J/m^2$ at $\Delta T = -50$ ^{o}C	2183.712	2954.351	3197.834
$G_\infty(l_e)$ at K=0 J/m^2	2232.517	3152.312	3256.103

4-2-11 Epoxy-Kevlar post cure at 75°C

Fig (4-27) Shown the results from drag-out test for epoxy-kevlar fiber post cure at 75°C of diameter 0.22mm.
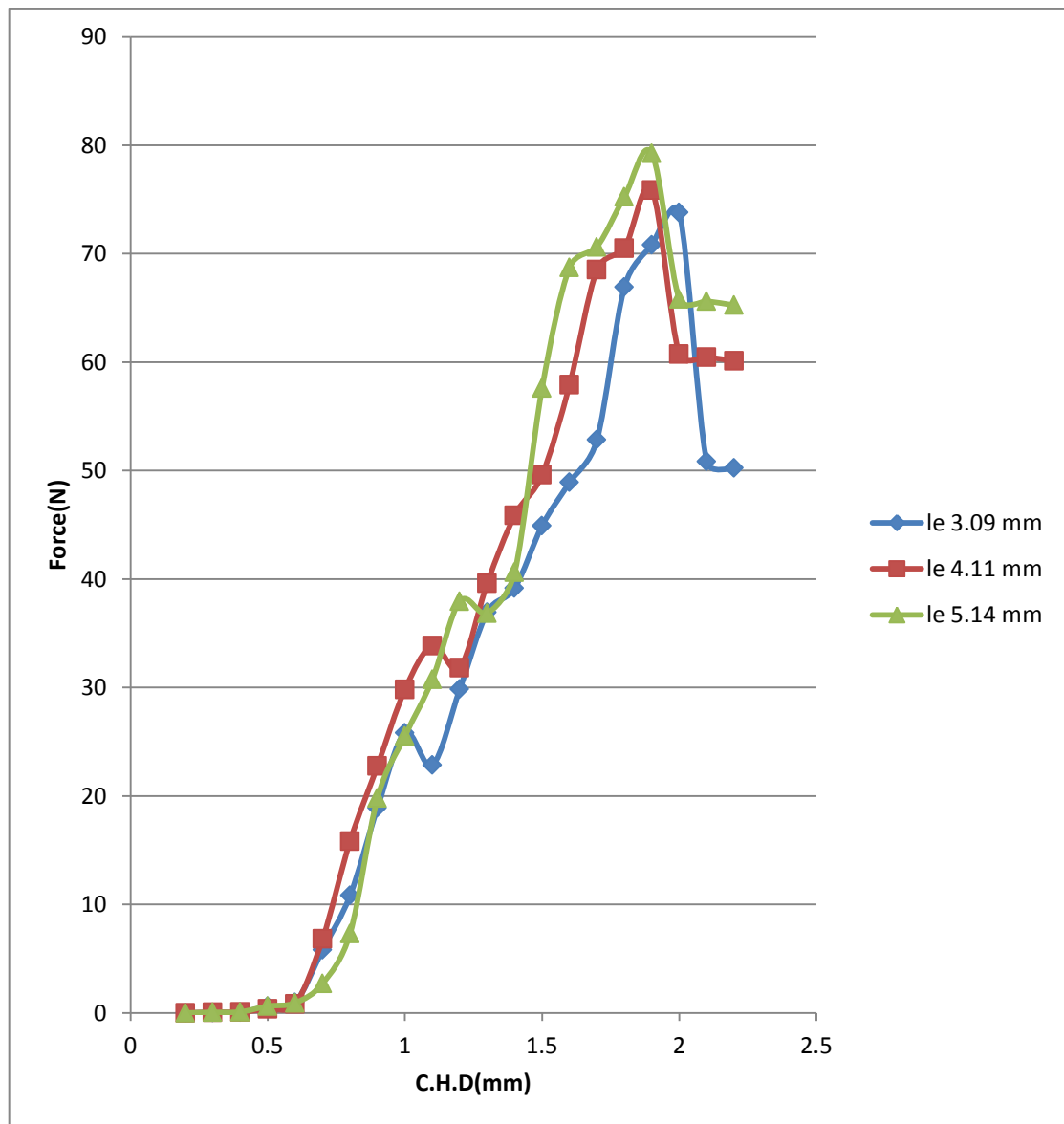

Fig (4-27) The drag-out force vs. cross head displacement curves for epoxy-kevlar fiber post cure at 75°C of diameter (0.22mm).

The results from eqs. (2-1), (2-40) and (2-53) are listed in table (4-27).

Table (4-27): The results from interfacial shear strength, shear-lag and energy release rate equations for epoxy-kevlar fiber post cure at 75°C of diameter 0.22mm

Embedded length l$_e$(mm)	3.09	4.11	5.14
Drag-out deboned force at peak(N)	75.234	79.723	83.723
Drag-out friction force (N)	30.187	40.261	50.132
Pull-out debond force at peak(N)	136.748	172.453	204.922
Pull-out friction force (N)	42.136	71.944	122.704
IFSS at peak debond point (MPa)	58.812	62.108	64.512
Shear-lag parameter $\beta(\mu m)^{-1}$	0.00052	0.00052	0.00052
$G_\infty(l_e)J/m^2$ at $\Delta T = 50\ ^{o}$C	3254.823	3402.627	4968.198
$G_\infty(l_e)$ at K=0 J/m^2	3387.365	3531.734	5164.827

Fig (4-28) Shown the results from drag-out test for epoxy-kevlar fiber post cure at 75°C of diameter 0.34mm.
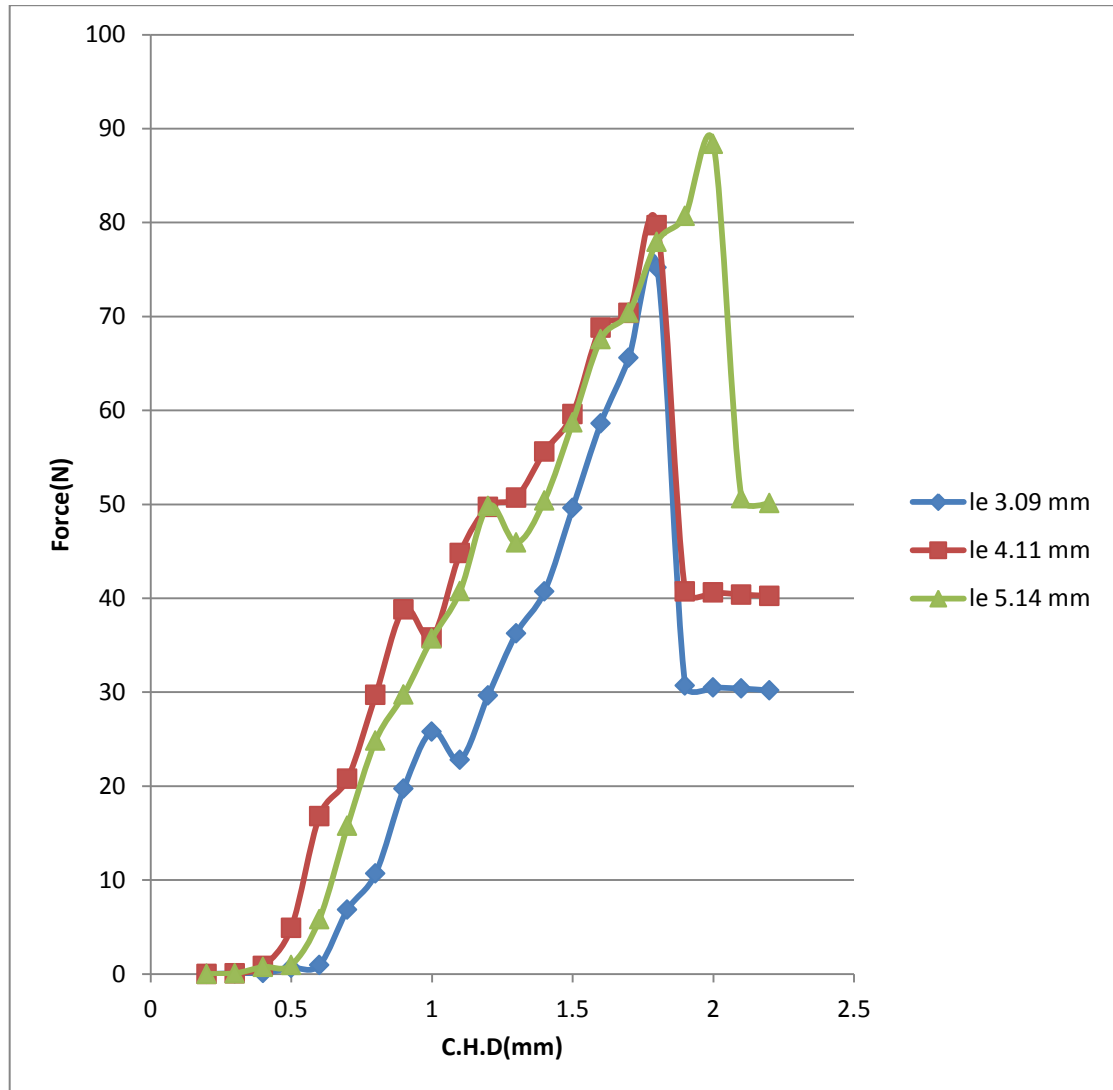

Fig (4-28) The drag-out force vs. cross head displacement curves for epoxy-kevlar fiber post cure at 75°C of diameter (0.34mm).

The results from eqs (2-1), (2-40) and (2-53) are listed in table (4-28).

Table (4-28): The results from interfacial shear strength, shear-lag and energy release rate equations for epoxy-kevlar fiber post cure at 75°C of diameter 0.34mm.

Embedded length l$_e$(mm)	3.09	4.11	5.14
Drag-out deboned force at peak(N)	85.283	92.482	112.742
Drag-out friction force (N)	43.745	65.132	73.143
Pull-out debond force at peak(N)	125.934	172.773	241.455
Pull-out friction force (N)	58.834	118.923	156.647
IFSS at peak debond point (MPa)	43.635	66.831	68.728
Shear-lag parameter $\beta(\mu m)^{-1}$	0.00032	0.00032	0.00032
$G_\infty(l_e)J/m^2$ at $\Delta T = 50\ ^oC$	5297.712	5671.812	6835.971
$G_\infty(l_e)$ at K=0 J/m^2	5482.213	5692.273	7173.203

Fig (4-29) Shown the results from drag-out test for epoxy-kevlar fiber post cure at 75°C of diameter 0.43mm.
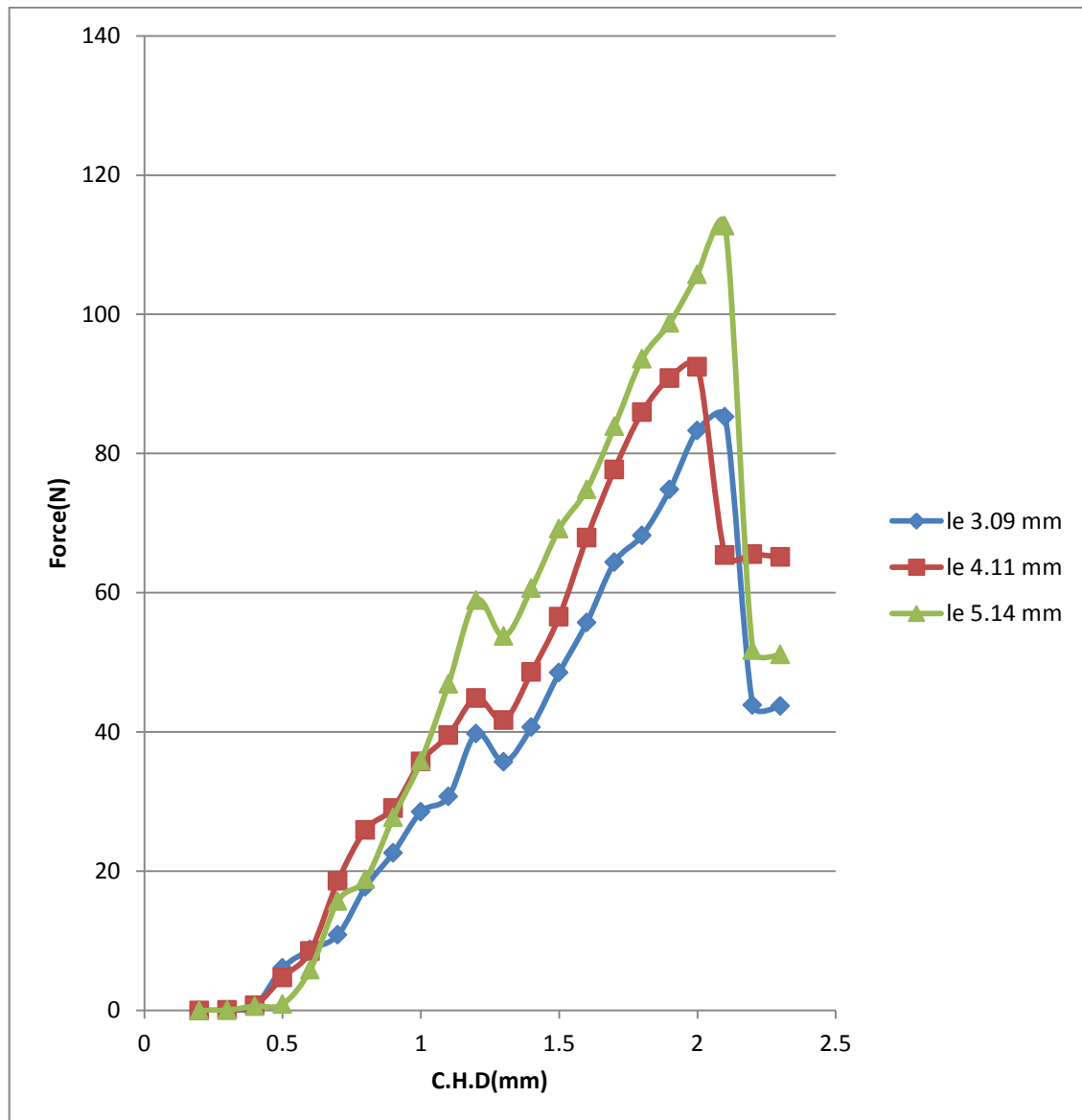

Fig (4-29) the drag-out force vs. cross head displacement curves for epoxy-kevlar fiber post cure at 75°C of diameter (0.43mm).

The results from eqs (2-1), (2-40) and (2-53) are listed in table (4-29).

Table (4-29): The results from interfacial shear strength, shear-lag and energy release rate equations for epoxy-kevlar fiber post cure at 75°C of diameter 0.43mm

Embedded length l$_e$(mm)	3.09	4.11	5.14
Drag-out deboned force at peak(N)	120.634	136.273	140.312
Drag-out friction force (N)	70.152	94.283	110.139
Pull-out debond force at peak(N)	162.069	243.513	343.433
Pull-out friction force (N)	83.372	184.531	246.136
IFSS at peak debond point (MPa)	61.671	64.681	69.823
Shear-lag parameter $\beta(\mu m)^{-1}$	0.00025	0.00025	0.00025
$G_\infty(l_e)J/m^2$ at $\Delta T = 50 \ ^oC$	6112.412	6361.835	6512.245
$G_\infty(l_e)$ at K=0 J/m^2	6264.162	6471.276	6926.821

4-2-12- Epoxy-polyethylene fiber post cure 75°C

Fig (4-30) Shown the results from drag-out test for epoxy-polyethylene fiber post cure at 75°C of diameter 0.43mm.
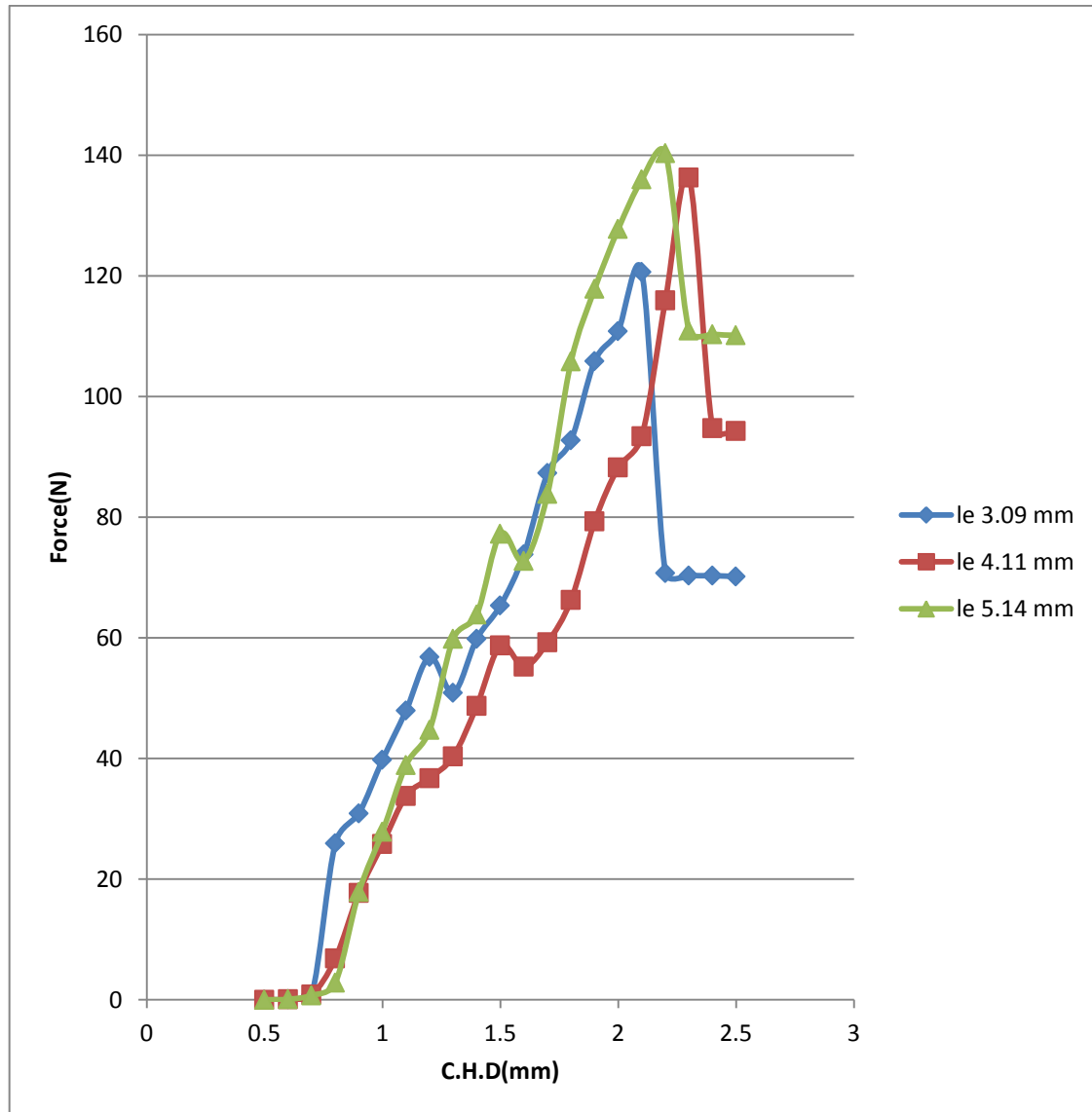

Fig (4-30) The drag-out force vs. cross head displacement curves for epoxy-polyethylene fiber post cure at 75°C of diameter (0.45mm).

The results from eqs (2-1), (2-40) and (2-53) are listed in Table (4-30)

Table (4-30): The results from interfacial shear strength, shear-lag and energy release rate equations for epoxy-polyethylene fiber post cure at 75°C of diameter 0.45mm

Embedded length l_e(mm)	3.09	4.11	5.14
Drag-out deboned force at peak(N)	14.825	17.878	19.752
Drag-out friction force (N)	16.287	20.261	22.864
Pull-out debond force at peak(N)	38.174	56.521	63.453
Pull-out friction force (N)	44.866	61.994	72.905
IFSS at peak debond point (MPa)	17.884	17.672	18.723
Shear-lag parameter $\beta(\mu m)^{-1}$	0.00023	0.00023	0.00023
$G_\infty(l_e)J/m^2$ at $\Delta T = -50\ ^oC$	113.734	126.961	146.823
$G_\infty(l_e)$ at K=0 J/m^2	87.167	96.182	124.514

4-2-13 Polyester- Glass fiber post cure at 25°C

Fig (4-31) Shown the results from drag-out test for polyester -glass fiber post cure at 25°C of diameter 0.22mm.
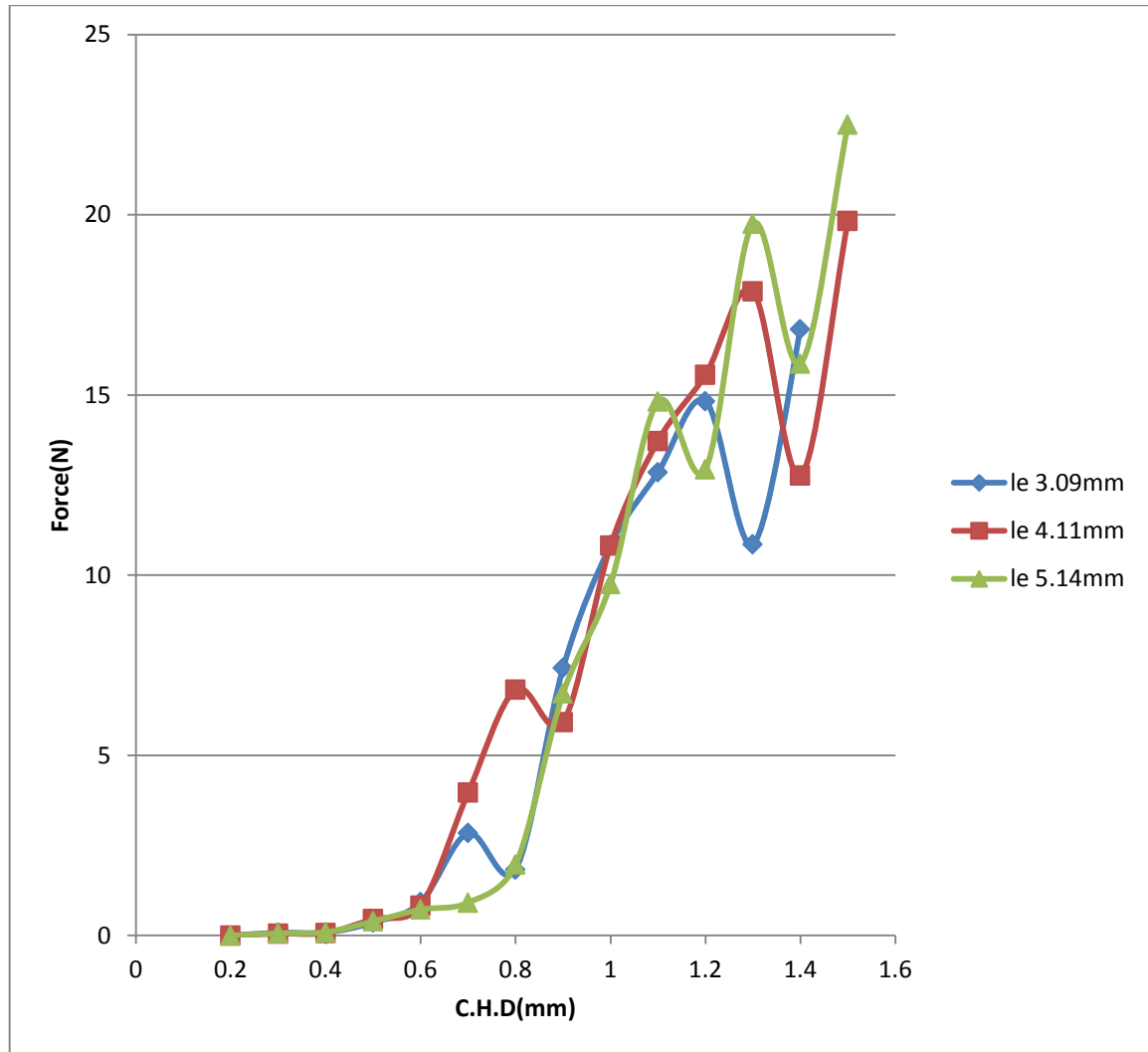

Fig (4-31) the drag-out force vs. cross head displacement curves for polyester-glass fiber post cure at 25°C of diameter (0.22mm).

The results from eqs (2-1), (2-40) and (2-56) are listed in Table (4-31)

Table (4-31): The results from interfacial shear strength, shear-lag and energy release rate equations for polyester-glass fiber post cure at 25$^{\text{o}}$C of diameter 0.22mm

Embedded length l$_e$(mm)	3.09	4.11	5.14
Drag-out deboned force at peak(N)	3.252	6.328	10.918
Drag-out friction force (N)	0.985	2.983	5.823
Pull-out debond force at peak(N)	15.728	19.154	27.824
Pull-out friction force (N)	8.525	10.827	17.391
IFSS at peak debond point (MPa)	11.834	12.821	13.981
Shear-lag parameter $\beta(\mu m)^{-1}$	0.00104	0.00104	0.00104
$G_{\infty}(l_e)J/m^2$ at $\Delta T = 0$	74.812	83.725	88.101
$G_{\infty}(l_e)$ at K=0 J/m^2	86.292	98.283	117.187

Fig (4-32) Shown the results from drag-out test for polyester -glass fiber post cure at 25°C of diameter 0.34mm.
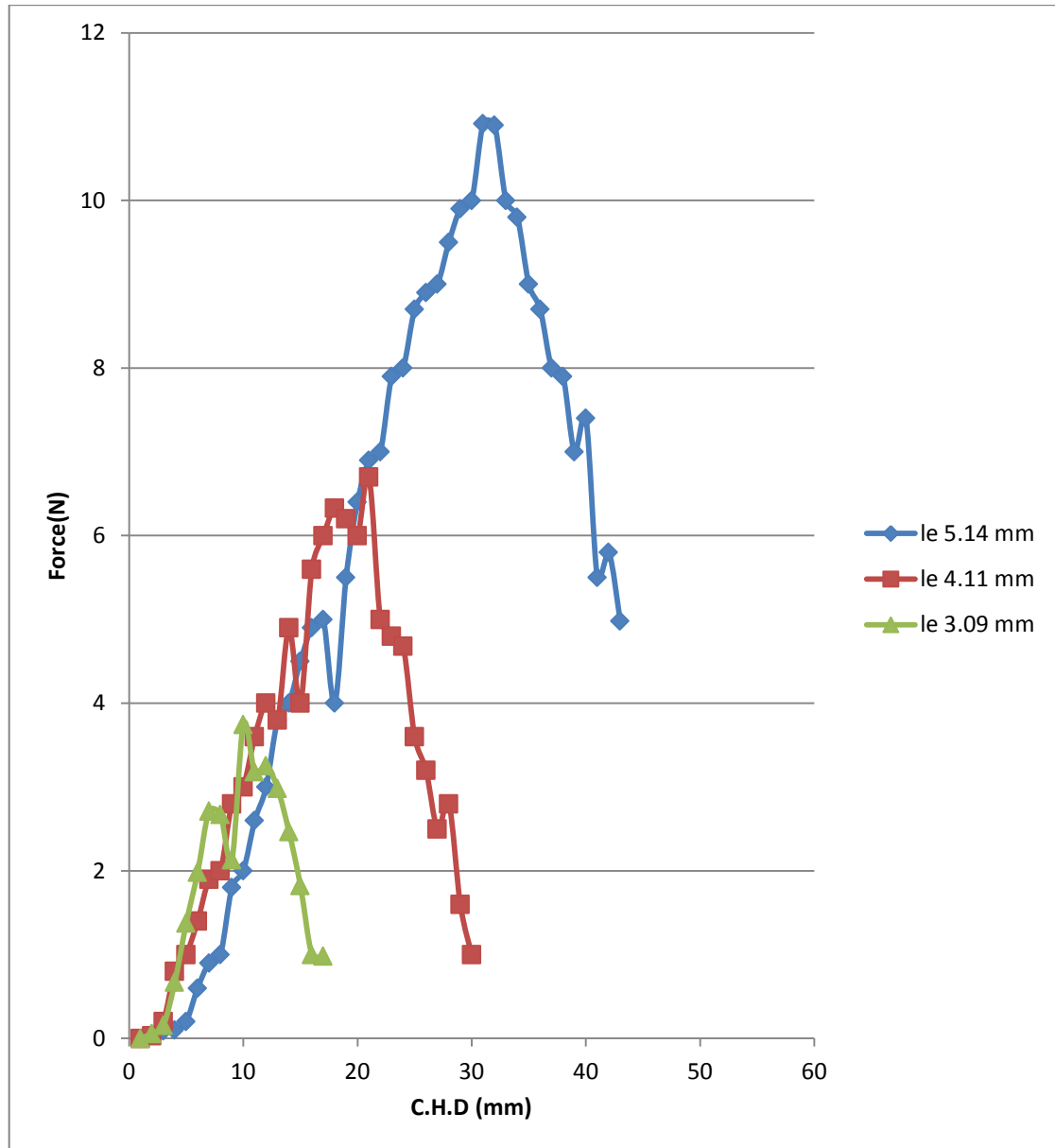

Fig (4-32) the drag-out force vs. cross head displacement curves for polyester-glass fiber post cure at 25°C of diameter (0.34mm).

The results from eqs (2-1), (2-40) and (2-53) are listed in table (4-32)

Table (4-32): The results from interfacial shear strength, shear-lag and energy release rate equations for polyester-glass fiber post cure at 25°C of diameter 0.34mm

Embedded length le(mm)	3.09	4.11	5.14
Drag-out deboned force at peak(N)	14.431	19.722	20.315
Drag-out friction force (N)	7.235	12.634	15.937
Pull-out debond force at peak(N)	28.671	38.812	56.284
Pull-out friction force (N)	14.721	21.821	34.824
IFSS at peak debond point (MPa)	13.824	14.927	15.528
Shear-lag parameter $\beta(\mu m)^{-1}$	0.00108	0.00108	0.00108
$G_\infty(l_e)J/m^2$ at $\Delta T = 0$	67.845	87.714	91.481
$G_\infty(l_e)$ at K=0 J/m^2	89.834	136.724	143.712

Fig (4-33) Shown the results from drag-out test for polyester -glass fiber post cure at 25°C of diameter 0.43mm.
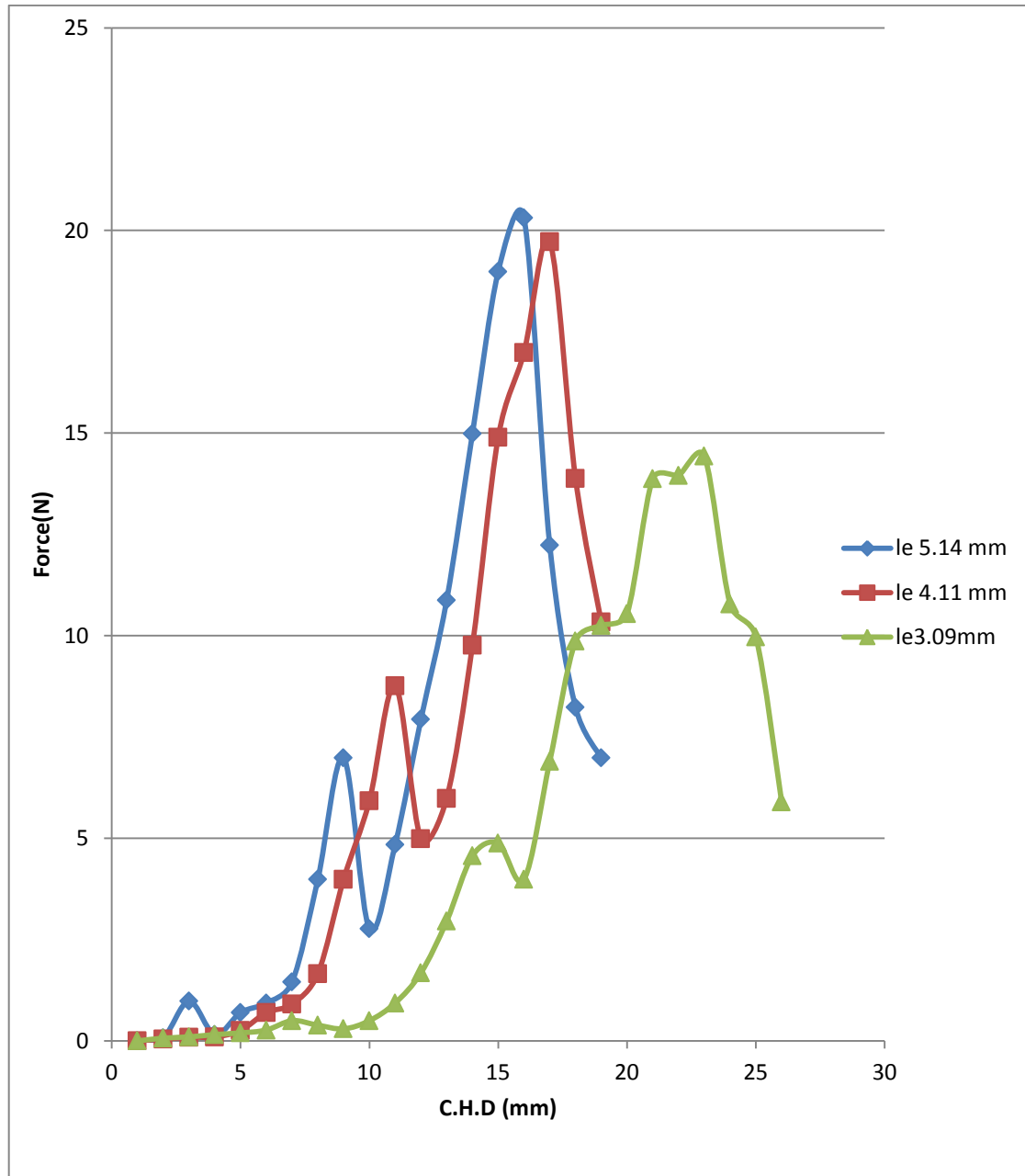

Fig (4-33) The drag-out force vs. cross head displacement curves for polyester-glass fiber post cure at 25°C of diameter (0.43mm).

The results from eqs (2-1), (2-40) and (2-56) are listed in Table (4-33).

Table (4-33): The results from interfacial shear strength, shear-lag and energy release rate equations for polyester-glass fiber post cure at 25°C of diameter 0.43mm

Embedded length le(mm)	3.09	4.11	5.14
Drag-out deboned force at peak(N)	40.346	68.657	70.213
Drag-out friction force (N)	21.823	39.529	42.815
Pull-out debond force at peak(N)	73.908	89.824	96.265
Pull-out friction force (N)	45.812	54.381	61.626
IFSS at peak debond point (MPa)	16.956	17.823	17.956
Shear-lag parameter $\beta(\mu m)^{-1}$	0.00016	0.00016	0.0016
$G_{\infty}(l_e) J/m^2$ at $\Delta T = 0$	84.926	87.712	95.183
$G_{\infty}(l_e)$ at K=0 J/m^2	96.671	104.561	110.613

4-2-14- Polyester-carbon post cure at 25°C

Fig (4-34) Shown the results from drag-out test for polyester - carbon fiber post cure at 25°C of diameter 0.22mm.
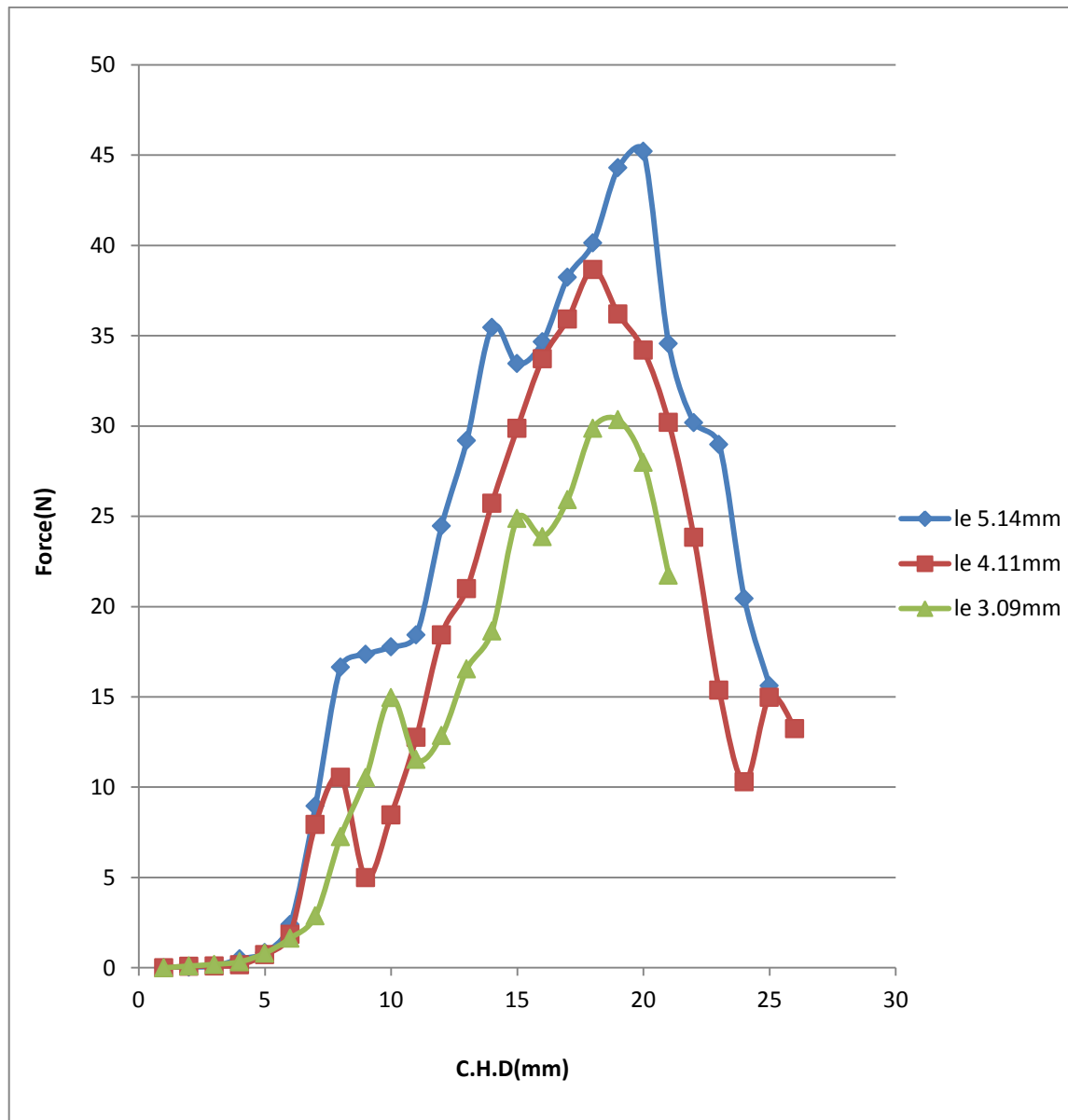

Fig (4-34) The drag-out force vs. cross head displacement curves for polyester-carbon fiber post cure at 25°C of diameter (0.22mm).

The results from equation (2-1), (2-40) and (2-53) are listed in Table (4-34)

Table (4-34): The results from interfacial shear strength, shear-lag and energy release rate equations for polyester-carbon fiber post cure at 25°C of diameter 0.22mm

Embedded length le(mm)	3.09	4.11	5.14
Drag-out deboned force at peak(N)	8.598	10.768	12.634
Drag-out friction force (N)	3.873	4.784	6.723
Pull-out debond force at peak(N)	27.264	35.365	38.512
Pull-out friction force (N)	18.814	26.561	31.712
IFSS at peak debond point (MPa)	8.826	9.972	11.561
Shear-lag parameter $\beta(\mu m)^{-1}$	0.00033	0.00033	0.00032
$G_{\infty}(l_e)J/m^2$ at $\Delta T = 0$	63.812	72.271	76.871
$G_{\infty}(l_e)$ at K=0 J/m^2	84.731	96.519	122.741

Fig (4-35) Shown the results from drag-out test for polyester - carbon fiber post cure at 25°C of diameter 0.34mm.
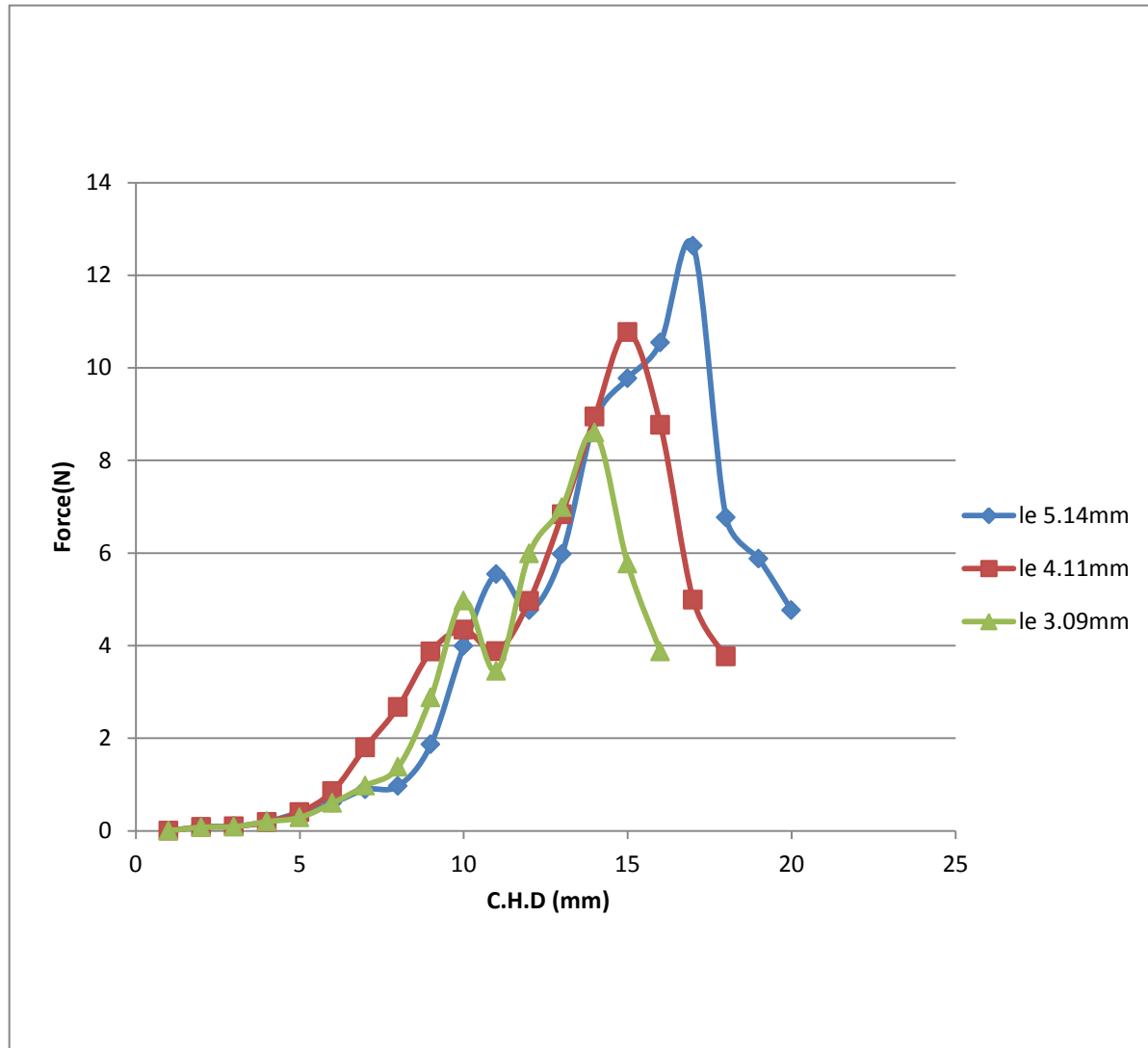

Fig (4-35) The drag-out force vs. cross head displacement curves for polyester-carbon fiber post cure at 25°C of diameter (0.34mm).

The results from eqS (2-1), (2-40) and (2-53) are listed in Table (4-35)

Table (4-35): The results from interfacial shear strength, shear-lag and energy release rate equations for polyester-carbon fiber post cure at 25°C of diameter 0.34mm

Embedded length le(mm)	3.09	4.11	5.14
Drag-out deboned force at peak(N)	20.874	25.979	35.879
Drag-out friction force (N)	13.982	15.682	22.745
Pull-out debond force at peak(N)	47.631	52.612	64.596
Pull-out friction force (N)	33.172	38.275	47.523
IFSS at peak debond point (MPa)	11.752	16.452	17.384
Shear-lag parameter $\beta(\mu m)^{-1}$	0.00031	0.00031	0.00031
$G_{\infty}(l_e) J/m^2$ at $\Delta T = 0$	65.825	69.276	93.476
$G_{\infty}(l_e)$ at K=0 J/m^2	78.823	84.613	`153.826

Fig (4-36) Shown the results from drag-out test for polyester - carbon fiber post cure at 25°C of diameter 0.43mm.
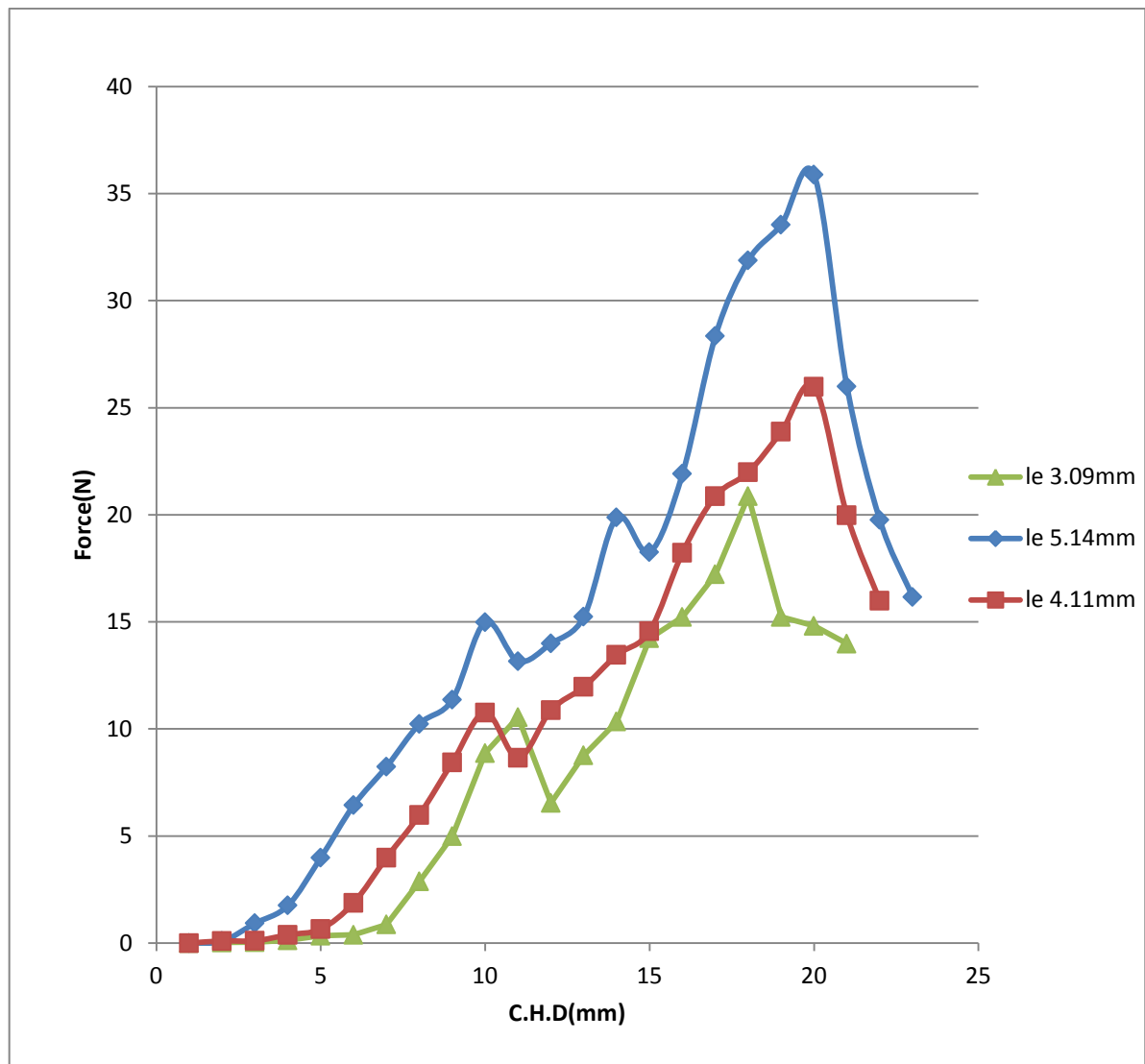

Fig (4-36) The drag-out force vs. cross head displacement curves for polyester-carbon fiber post cure at 25°C of diameter (0.43mm).

The results from eqs (2-1), (2-40) and (2-53) are listed in Table (4-36)

Table (4-36): The results from interfacial shear strength, shear-lag and energy release rate equations for polyester-carbon fiber post cure at 25°C of diameter 0.43mm

Embedded length le(mm)	3.09	4.11	5.14
Drag-out deboned force at peak(N)	68.454	70.547	92.342
Drag-out friction force (N)	45.232	50.625	70.781
Pull-out debond force at peak(N)	82.692	89.691	118.823
Pull-out friction force (N)	64.131	72.225	84.562
IFSS at peak debond point (MPa)	15.152	19.912	21.314
Shear-lag parameter $\beta(\mu m)^{-1}$	0.00024	0.00024	0.00024
$G_\infty(l_e) J/m^2$ at $\Delta T = 0$	85.172	92.166	98.562
$G_\infty(l_e)$ at K=0 J/m^2	97.472	128.716	135.104

4-2-15 Polyester-Kevlar post cure at 25°C

Fig (4-37) Shown the results from drag-out test for polyester – kevlar fiber post cure at 25°C of diameter 0.22mm.
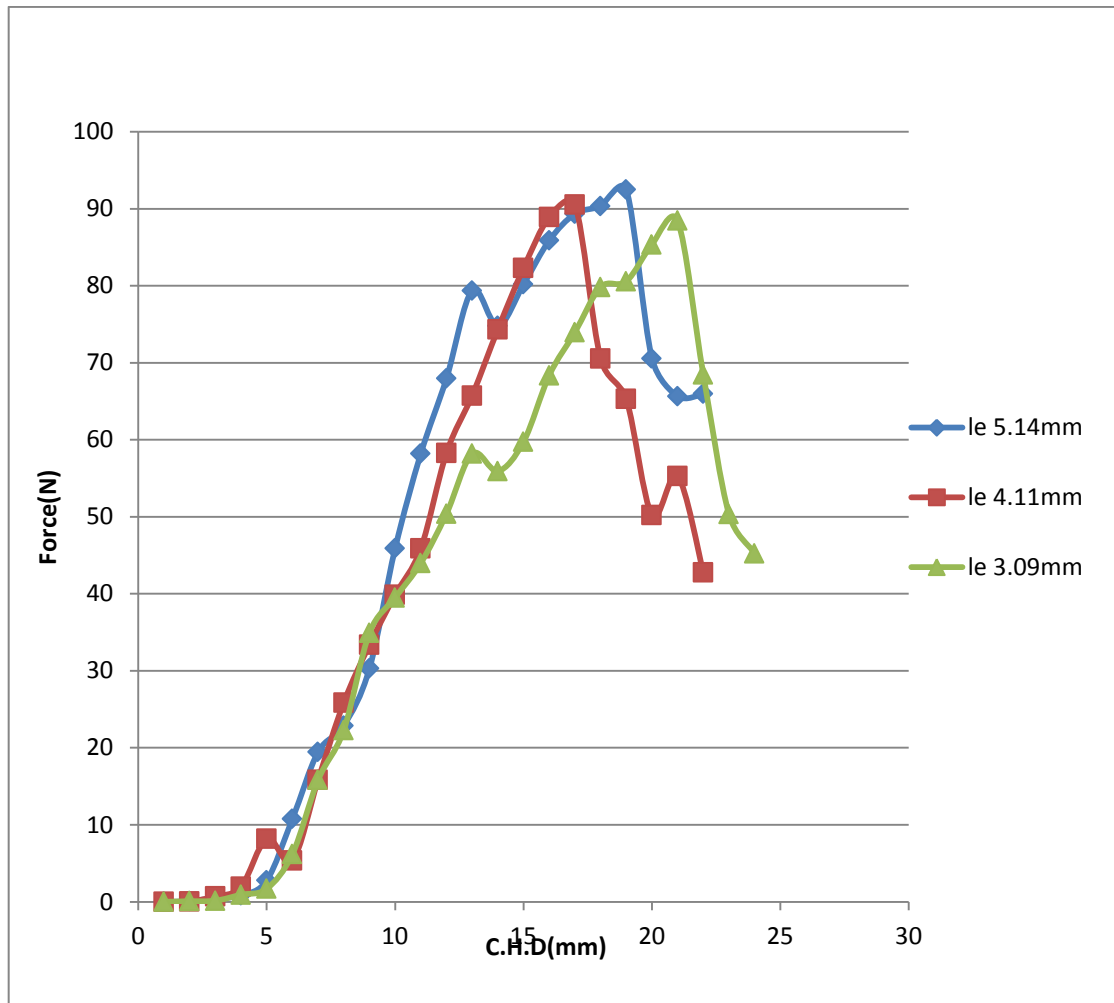

Fig (4-37) the drag-out force vs. cross head displacement curves for polyester-kevlar fiber post cure at 25°C of diameter (0.22mm).

The results from eqs (2-1), (2-40) and (2-53) are listed in Table (4-37)

Table (4-37): The results from interfacial shear strength, shear-lag and energy release rate equations for polyester-kevlar fiber post cure at 25°C of diameter 0.22mm

Embedded length le(mm)	3.09	4.11	5.14
Drag-out deboned force at peak(N)	32.341	35.876	42.463
Drag-out friction force (N)	21.614	25.712	31.512
Pull-out debond force at peak(N)	76.351	83.318	92.163
Pull-out friction force (N)	46.412	53.461	79.513
IFSS at peak debond point (MPa)	18.723	19.412	22.451
Shear-lag parameter $\beta(\mu m)^{-1}$	0.00042	0.00042	0.00042
$G_\infty(l_e)J/m^2$ at $\Delta T = 0$	120.916	128.743	136.142
$G_\infty(l_e)$ at K=0 J/m^2	142.692	168.173	182.673

Fig (4-38) Shown the results from drag-out test for polyester – kevlar fiber post cure at 25°C of diameter 0.34mm in.
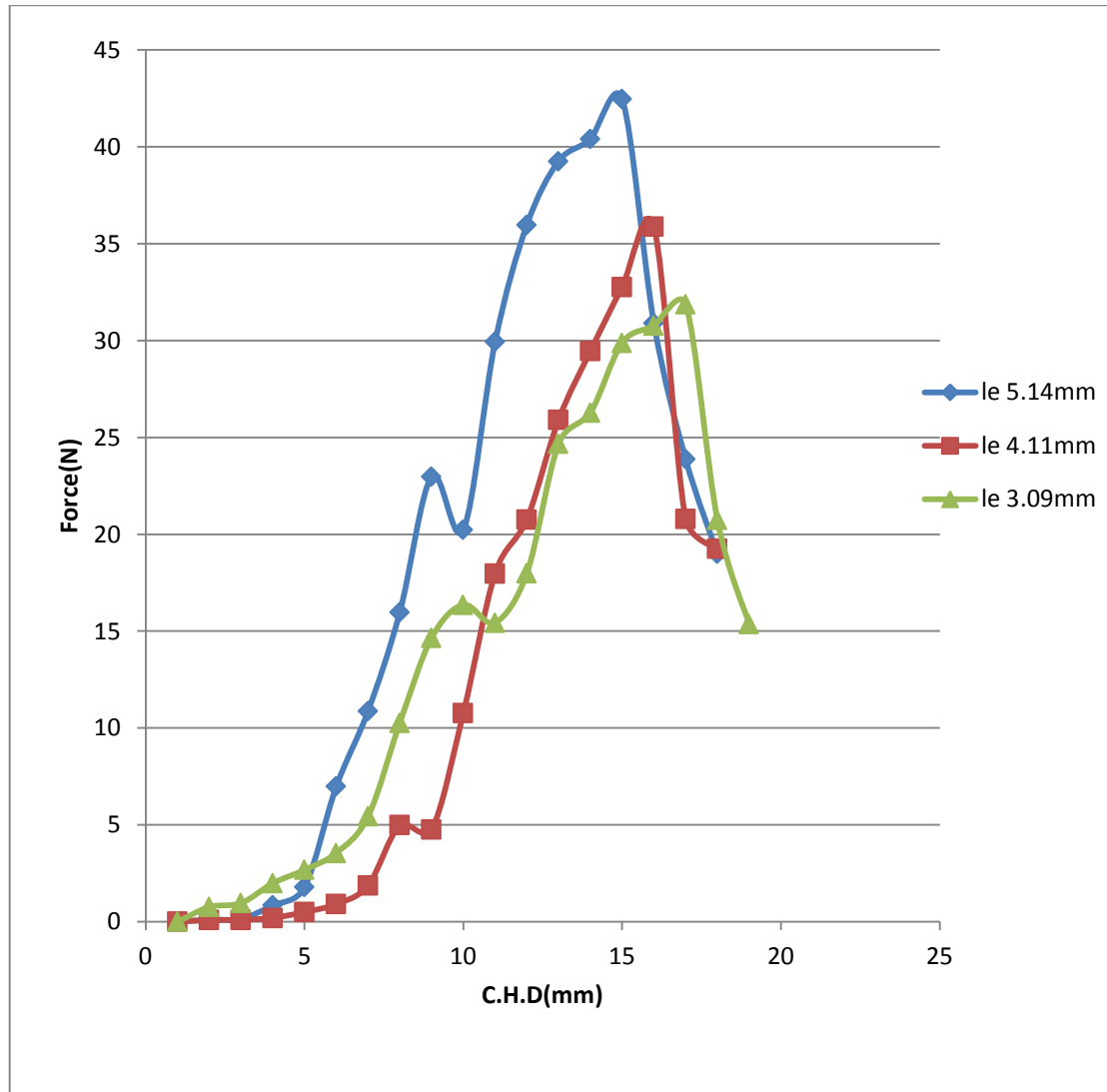

Fig (4-38) The drag-out force vs. cross head displacement curves for polyester-kevlar fiber post cure at 25°C of diameter (0.34mm).

The results from eqs (2-1), (2-40) and (2-53) are listed in Table (4-38).

Table (4-38): فhe results from interfacial shear strength, shear-lag and energy release rate equations for polyester-kevlar fiber post cure at 25°C of diameter 0.34mm.

Embedded length le(mm)	3.09	4.11	5.14
Drag-out deboned force at peak(N)	50.212	78.319	85.621
Drag-out friction force (N)	30.612	41.102	56.182
Pull-out debond force at peak(N)	73.173	92.716	107.412
Pull-out friction force (N)	57.412	72.217	87.518
IFSS at peak debond point (MPa)	18.712	18.925	20.561
Shear-lag parameter $\beta(\mu m)^{-1}$	0.00051	0.00051	0.00051
$G_\infty(l_e)J/m^2$ at $\Delta T = 0$	115.571	126.51	137.401
$G_\infty(l_e)$ at K=0 J/m^2	131.734	143.867	165.741

Fig (4-39) Shown the results from drag-out test for polyester – kevlar fiber post cure at 25°C of diameter 0.43mm.
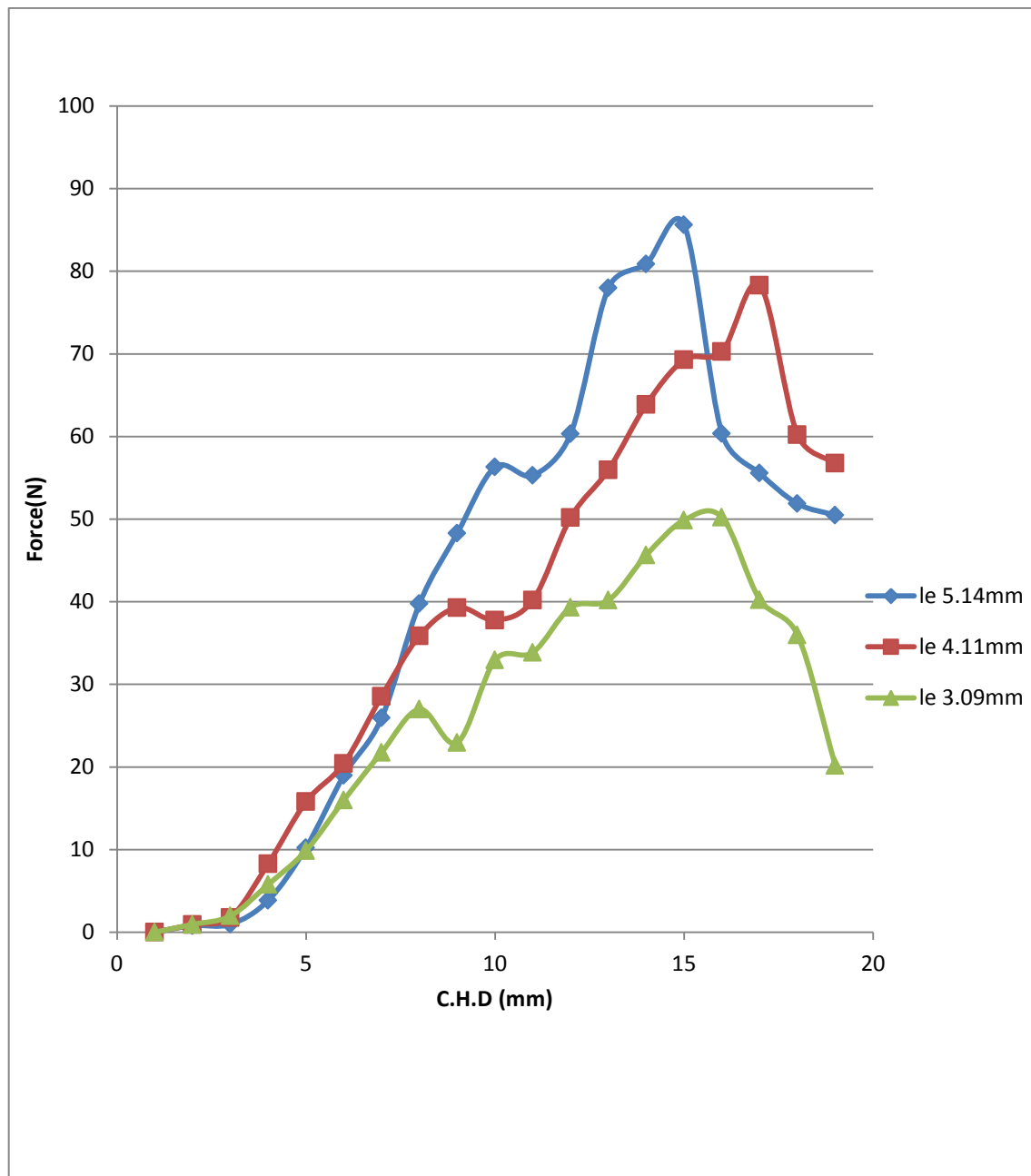

Fig (4-39) The drag-out force vs. cross head displacement curves for polyester-kevlar fiber post cure at 25°C of diameter (0.43mm).

The results from eqs (2-1), (2-40) and (2-53) are listed in Table (4-39)

Table (4-39): The results from interfacial shear strength, shear-lag and energy release rate equations for polyester-kevlar fiber post cure at 25°C of diameter 0.43mm.

Embedded length le(mm)	3.09	4.11	5.14
Drag-out deboned force at peak(N)	88.453	90.563	92.478
Drag-out friction force (N)	45.162	56.814	63.706
Pull-out debond force at peak(N)	125.615	137.812	143.175
Pull-out friction force (N)	94.512	114.714	127.171
IFSS at peak debond point (MPa)	23.512	24.719	27.801
Shear-lag parameter $\beta(\mu m)^{-1}$	0.00063	0.00036	0.00063
$G_\infty(l_e) J/m^2$ at $\Delta T = 0$	110.616	125.817	139.718
$G_\infty(l_e)$ at K=0 J/m^2	128.641	141.834	156.848

4-2-16 Polyester-Polyethylene fiber post cure at 25°C

Fig (4-40) Shown the results from drag-out test for polyester – polyethylene fiber post cure at 25°C of diameter 0.45mm.
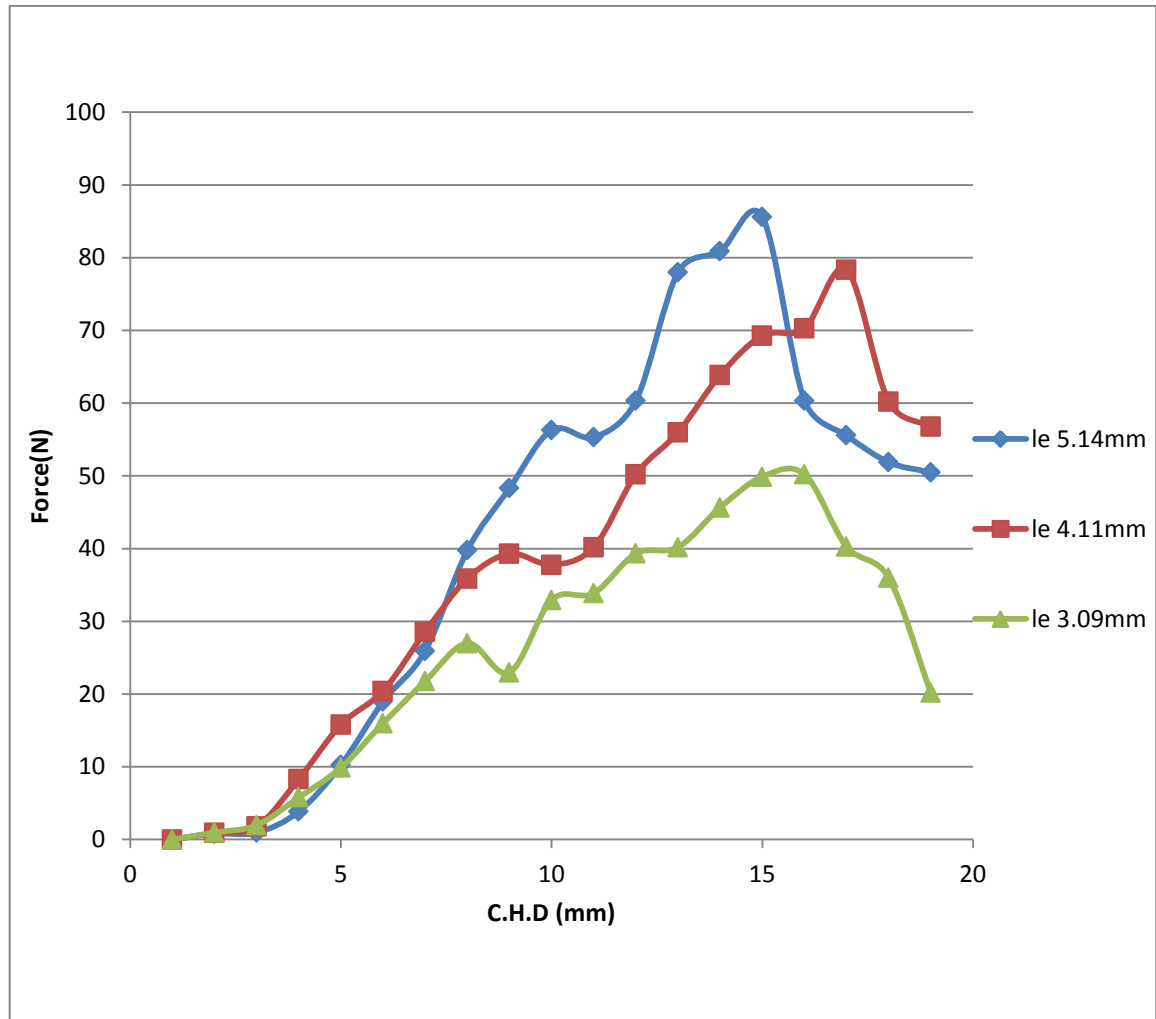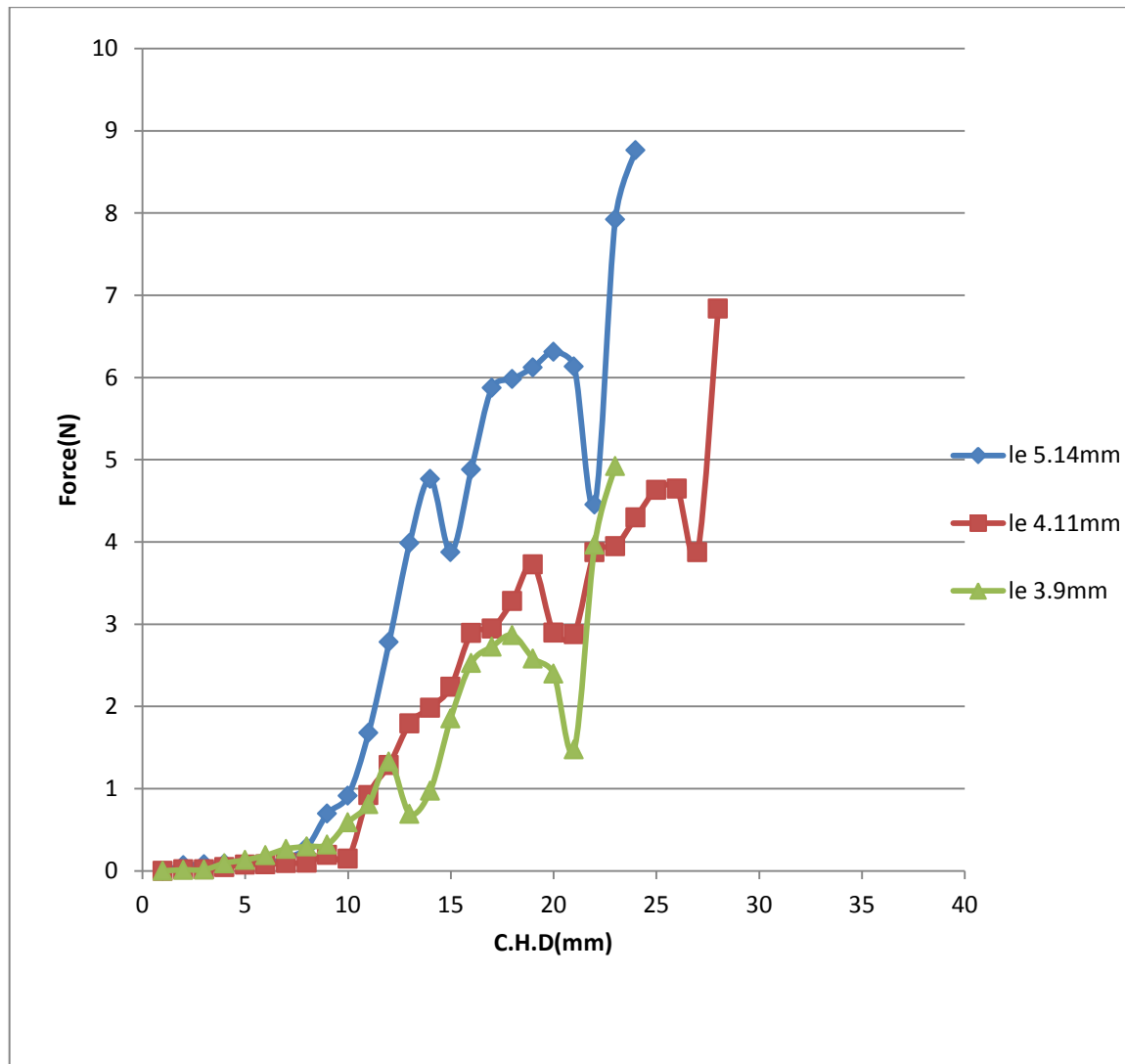

Fig (4-40) The drag-out force vs. cross head displacement curves for polyester-polyethylene fiber post cure at 25°C of diameter (0.45mm).

The results from eqs(2-1), (2-40) and (2-56) are listed in

Table (4-40).

Table (4-40): The results from interfacial shear strength, shear-lag and energy release rate equations for polyester-polyethylene fiber post cure at 25°C of diameter 0.45mm.

Embedded length le(mm)	3.09	4.11	5.14
Drag-out deboned force at peak(N)	2.867	4.647	6.312
Drag-out friction force (N)	5.583	6.937	8.853
Pull-out debond force at peak(N)	10.823	14.953	18.163
Pull-out friction force (N)	17.573	19.492	22.271
IFSS at peak debond point (MPa)	0.836	1.871	2.143
Shear-lag parameter $\beta(\mu m)^{-1}$	0.00023	0.00023	0.00023
$G_{\infty}(l_e) J/m^2$ at $\Delta T = 0$	3.541	5.523	8.173
$G_{\infty}(l_e)$ at K=0 J/m^2	0.961	1.734	3.934

In Fig (4-41) AB represents the elastic behavior of matrix-fiber composite where the induced shear stresses along the fiber. The stiffness of fiber-matrix system depends on such parameters as Young modulus of fiber and matrix respectively, the fiber-matrix volume fraction, the shear modulus of matrix and the pours layer as well as the load condition. As the load increased a crack initiation began at knick point (B), curve BC represent the difference in elastic behavior between the fiber and the matrix induces a shear stress at the interface.

The curve CD and as the load increased the crack would propagate until reach the peak point D or the full debond, the non linearity in line CD due to matrix yielding. The sudden dropped in line DE due to the resistance to farther movement of the fiber which is mainly for fraction and surface roughness. In pull-out test the pull-out force (line EF) dropped to zero while in microbond or drag-out test EF would be approximately at constant load due to continuous movement.
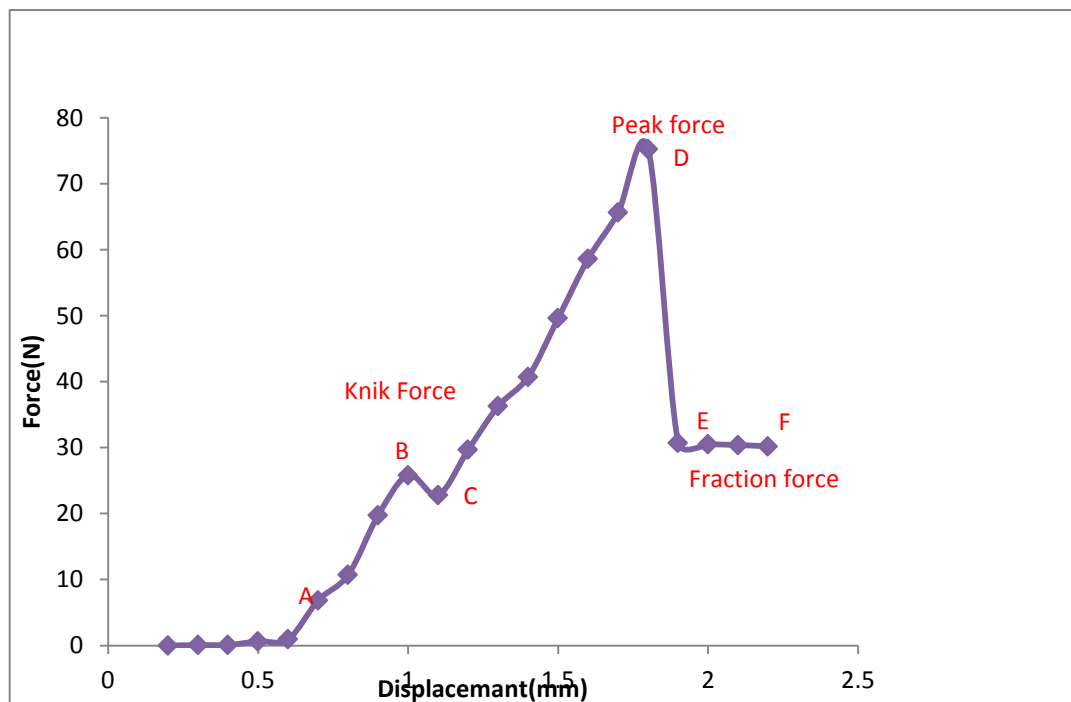

Fig (4-41) typical drag-out force-cross head displacement for epoxy-kevlar fiber diameter 0.22mm at 70°C

4-3 Effect of Embedded Length and Radius of Fiber:

The energy release rate $G_{\infty(l_e)}$ is always increasing as the embedded length increase (l_e) for each fiber diameter. The critical energy release rat $G_{\infty(l_e)}$ in Eqs. (2-53) is calculated as the crack length (a) equal to the embedded fiber length (l_e). And at the peak force in force-displacement curve so when the embedded length increases the adhesion area increase and the pull-out deboned force increase, in other word. The increased of fiber- matrix interface area is associated with debonding and as the peak force increased the energy consumed during fiber pull-out or the area under the load-displacement curve would increase. To discuss the effect of fiber radius on the energy release for same embedded length is in Table (4-42).

Table (4-41) Energy release rate of different embedded length and different fiber radius

Matrix-Fiber Materials	Embedded Length(mm)	Energy release rate J/m^2			Temperature
		Fiber Diameter(mm)			
Epoxy-Glass Fiber		0.22	0.34	0.43	25°C
	3.09	48.845	127.971	297.284	
	4.11	89.856	136.829	312.735	
	5.14	124.972	232.384	318.295	
Epoxy-Glass Fiber	3.09	636.912	889.823J	915.182	50°C
	4.11	648.117	891.812	925.173	
	5.14	886.712J	895.782	963.292	
Epoxy-Glass Fiber	3.09	1128.617	1168.293	1199.561	75°C
	4.11	1146.501	1187.937	1692.264	
	5.14	1179.512	1196.523	1843.365	
Epoxy-	3.09	178.723	317.856	374.863	

Carbon Fiber	4.11	279.932	338.623	397.715	25°C
	5.14	298.165	368.836	414.867	
Epoxy-Carbon Fiber	3.09	792.846	734.283	935.165	50°C
	4.11	797.182	787.912	947.377	
	5.14	812.714	865.172	956.109	
Epoxy-Carbon Fiber	3.09	1482.734	1865.862	2183.712	75°C
	4.11	1667.091	1916.809	2954.351	
	5.14	1898.162	1973.712	3197.834	

Matrix-Fiber Materials	Embedded Length(mm)	Energy release rate J/m^2			Temperature
		Fiber Radius(mm)			
Epoxy-Kevlar Fiber		0.22	0.34	0.43	25°C
	3.09	187.834	298.915	297.284	
	4.11	286.365	342.63	482.145	
	5.14	291.121	391.816	583.925	
Epoxy-Kevlar Fiber	3.09	824.712	978.283	996.265	50°C
	4.11	867.292	983.102	1126.715	
	5.14	912.723	1105.719	1187.72	
Epoxy-Kevlar Fiber	3.09	3254.823	5297.712	6112.412	75°C
	4.11	3402.627	5671.812	6361.835	
	5.14	4968.198	6835.971	6512.245	

Matrix-Fiber Materials	Embedded Length(mm)	Energy release rate J/m^2 Temperature			Fiber Radius(mm)
		25°C	50°C	75°C	
Epoxy-Polyethylene Fiber	3.09	33.171J	79.832	113.734	0.45
	4.11	38.182	86.273	126.961	
	5.14	45.153	95.283	146.823	

Matrix-Fiber Materials	Embedded Length(mm)	Energy release rate J/m^2 Fiber Radius(mm)			Temperature
Polyester-Glass Fiber		0.22	0.34	0.43	25°C
	3.09	74.812	67.845	84.926	
	4.11	83.725	87.714	87.712	
	5.14	88.101	91.481	95.183	
Polyester-Carbon Fiber	3.09	63.812	65.825	85.172	25°C
	4.11	72.271	69.276	92.166	
	5.14	76.871	93.476	98.562	
Polyester-Kevlar Fiber	3.09	120.916	115.571	110.616	25°C
	4.11	128.743	126.51	125.817	
	5.14	136.142	137.401	139.718	

Matrix-Fiber Materials	Embedded Length(mm)	Energy release rateJ/m^2		Fiber Radius(mm)
		Temperature 25°C		
Polyester-Polyethylene Fiber	3.09	3.541		45°C
	4.11	5.523		
	5.14	8.173		

The highest value for energy release rate for epoxy-glass fiber post cure at 25°C for embedded length (5.14mm) and diameter (0.43mm) was (318.295 J/m^2). The highest value of energy release post cure at 50°C for the same embedded length and diameter (0.43mm) was (963.292J/m^2) and at epoxy- glass fiber post cure at 75°C. The highest value energy release rate at embedded length (5.14mm) and fiber diameter (0.43mm) is (1843.365J/m^2).

The highest value for energy release rate for epoxy-carbon fiber post cure at 25°C for larger embedded length (5.14mm) and larger diameter (0.43mm) is (414.867J/m^2). The highest value of energy release post cure at 50°C for the same embedded length and diameter (0.43mm) was (956.109 J/m^2) and at epoxy-carbon fiber post cure at 75°C the highest value energy release rate at embedded length (5.14mm) and fiber diameter (0.43mm) (3197.834 J/m^2).

The highest value for energy release rate for epoxy-kevlar fiber post cure at 25°C for larger embedded length (5.14mm) and larger diameter (0.43mm) was (583.925J/m^2). The highest value of energy release post cure at 50°C for the same embedded length and diameter

(0.43mm) was (1187.72J/m^2). And at epoxy-kevlar fiber post cure at 75°C the highest value energy release rate at embedded length (5.14mm) and fiber diameter (0.43mm) is (6512.245J/m^2).

In polyester-glass fiber the highest value of energy release rate when post cure at 25°C also at the larger embedded length and larger diameter (0.43mm) is (95.183 J/m^2).

In polyester-carbon fiber the highest value of energy release rate when post cure at 25°C also at the larger embedded length and larger diameter (0.43mm) was (98.562J/m^2)

In polyester-kevlar fiber the highest value of energy release rate when post cure at 25°C also at the larger embedded length and larger diameter (0.43mm) is (139.718J/m^2).

Observed the energy release rate always increase when fiber diameter and embedded length increase in epoxy and polyester matrix. Because the energy release rate is increase when the surface area of the fiber increase that is mean the adhesion area between fiber and matrix increase (perfect adhesion). But there are some an normal behavior in samples which showed a decrease in the energy release rate when increasing the diameter can be explained this adhesion between the fiber and the matrix is imperfect adhesion for several reasons due to. The presence of bubbles between fiber and matrix or a fiber containing filaments as the sample epoxy-carbon post cure at 50°C and sample of polyester this agreement with reference [20].

The adhesion force between fiber and matrix depends on many parameters, such as surface roughness, kind of the fiber, thickness of the adhesive and surface area [55]. So The energy release epoxy-polyethylene fiber and polyester-polyethylene fiber is very low because

the surface roughness polyethylene fiber few, low surface energy and structure of fiber this agreement reference [56].

4-4-Friction Effect

Friction is important in microbond and pull-out testes because of the predominantly mode II loading condition, Nairn and Co-worker model [14] assumed that the interfacial friction stress during debond growth is equal to the interfacial friction after complete debonding. The energy release rate without friction effect denoted by $G_\infty(l_e)$ at K=0 in Tables (4-1) to (4-40) in the slippage region Fig (4-42). The fiber is load resisted by frictional force three typical load-displacement curves reported in single fiber pull-out test, slip-hardening, constant friction and slip-softening. Slip-hardening occurs often with soft polymer fiber surface or fibers which are less hard than surrounding matrix surface where the abrasion on soft fiber surface against matrix material caused the fraction force to increase over the peak force while when the surface of fiber is harder than matrix a tension soften behavior is observed and the frictional force would be less than peak force. The slip-hardening effect observed in the soft surface polyethylene fiber reinforced epoxy or polyester matrix were polyethylene fiber poor bond due to party to the chemical inertness and the absence of polar groups, low surface energy and smooth surface. This explained the decreases in the values of frictionless energy release rate at k=0 compared with the energy release rate for epoxy-polyethylene fiber at 25°C, 50°C and 75°C in table (4-10),(4-20) and (4-30) and polyester-polyethylene fiber in table (4-40) in the slippage region for slip-hardening the friction force is higher than peak force in Fig (4-10),(4-20),(4-30), (4-40) and (4-42) than friction effect increased the energy release rate while in epoxy-glass fiber, epoxy-carbon fiber ,epoxy-kevlar, polyester-glass fiber, polyester-carbon fiber

and polyester-kevlar fiber slip-softening observed and. The values of frictionless energy release rate at k=0 is higher than the energy release rate at k=0 that is friction. The friction effect decrease the energy release rate values the effect of friction always increase as embedded length increases. The scattered in the values of frictionless energy release rate were due to babbles and flaws at the surface of matrix at interface this agreement with [57,58].
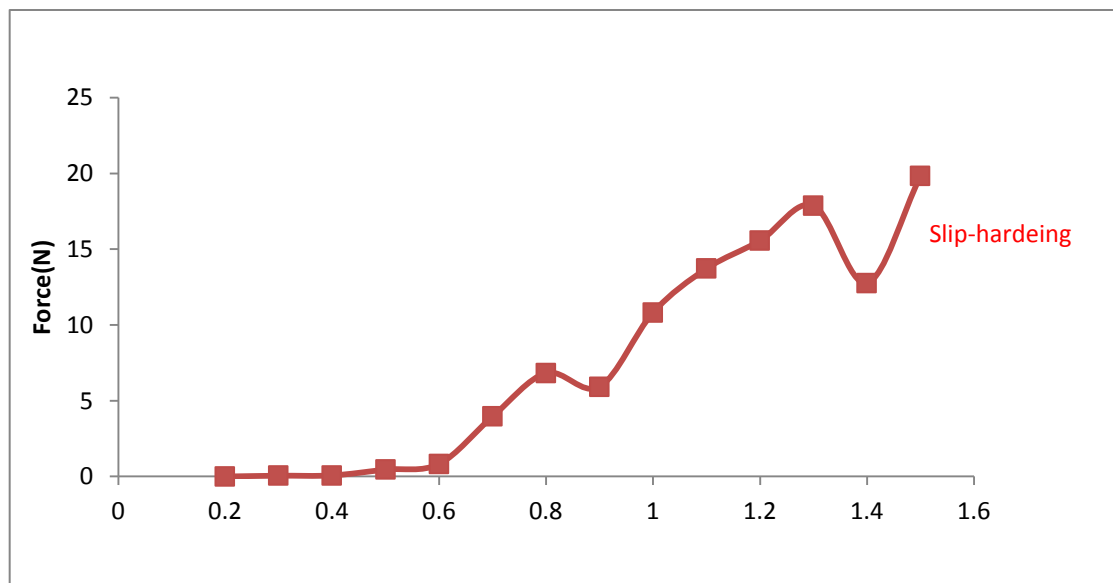

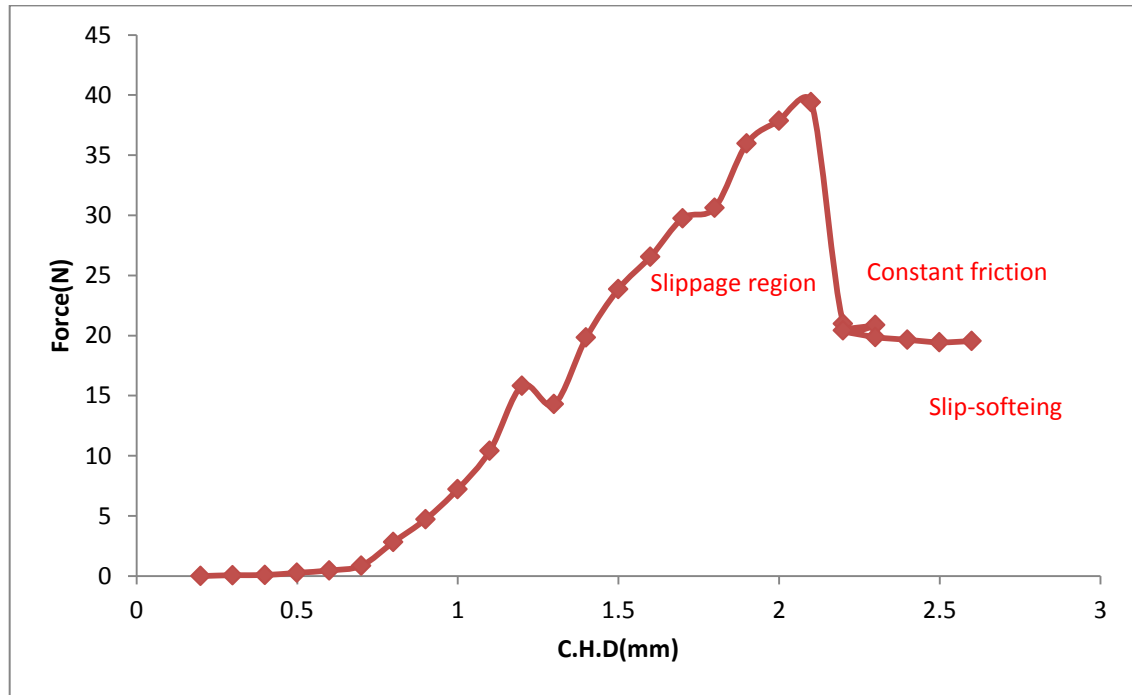**Fig (4-42a): slip-hardening region for epoxy-polyethylene fiber at 25°C**

Fig (4-42 b) slippage region in typical drag-out test for epoxy-glass fiber at 50°C

4-5 Matrix-Fiber Material

The average value for energy release rate $G_\infty(a)$ for matrix–fiber material of different embedded fiber lengths and diameter are listed in Table(4-43)

Table (4-43) Average value for energy release rate for fiber matrix

Matrix-fiber material	Average energy release rate J/m^2		
	25C^0	50C^0	75C^0
Epoxy-glass fiber	243.595	850.312	1304.37
Epoxy-carbon fiber	309.841	847.64	2126.696
Epoxy-kevlar fiber	371.294	944.37	5379.373

Epoxy-polyethylene	38.835	87.129	129.172
Polyester-glass fiber	84.61		
Polyester-carbon fiber	126		
Polyester-cevlar fiber	128.6		
Polyester-polyethylene	5.745		

The physical meaning of energy release rate is the amount of interfacial debonding must be related to the interfacial fracture toughness depends on energy-based criterion energy release rate which is the amount of energy release in the specimens per unit debond interfacial area [59]. The energy release rate is effected by embedded length, residual stresses and fraction. The energy release rate values are calculated for specimen post cure in $25^{o}C$, $50^{o}C$ and $75^{o}C$. Test temperature ($25^{o}C$) so the different between cure temperature and stress temperature (0,-25,-50)

From Table (4-43) that the average energy release rate for epoxy-glass fiber ,epoxy-carbon and epoxy-kevlar post cure at $25^{o}C$ was ($243.595J/m^2$), ($309.841J/m^2$), ($371.294 J/m^2$) respectively and post cure at $50^{o}C$ ($850.312J/m^2$) , ($847.64 J/m^2$), ($944.37 J/m^2$) respectively and post cure at $75^{o}C$ ($1304.37 J/m^2$), ($2126.696 J/m^2$), ($5379.373 J/m^2$) respectively as shown in Fig (4-43)-(4-45) . The highest of energy release rate in all materials use for epoxy-Kevlar in all temperatures and this is because of its high strength to the many inter-chain bonds. These inter-molecular hydrogen bonds form between the carbonyl groups and NH centers. Additional strength is derived from aromatic stacking interactions

between adjacent strands. These interactions have a greater influence on Kevlar this agreement with reference [18].
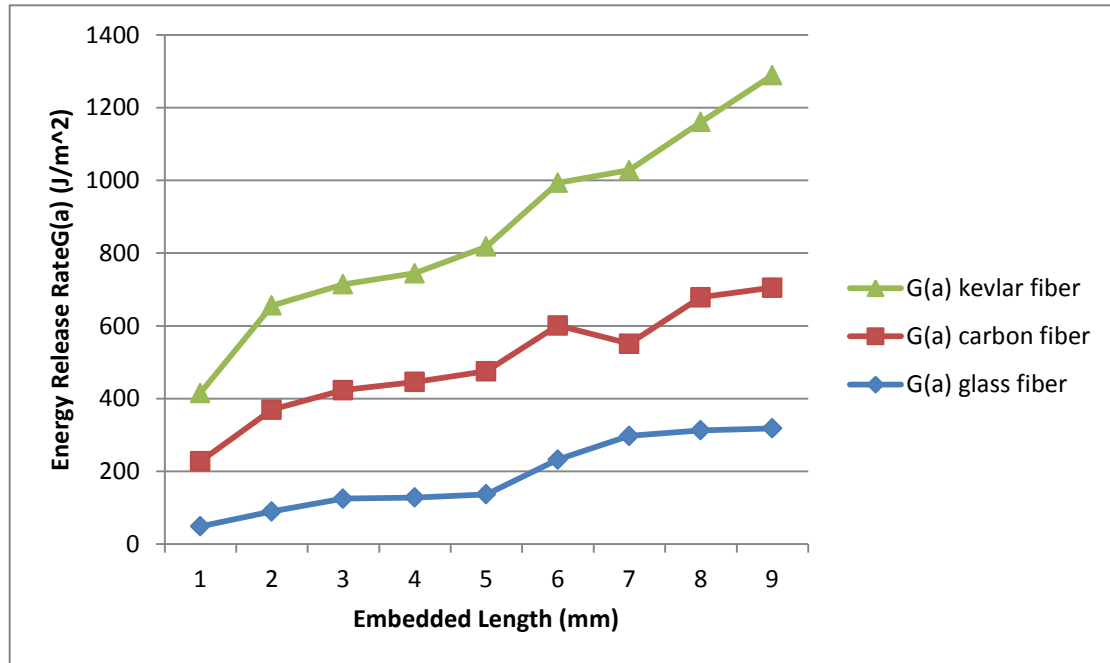

Fig (4-43) energy release rate for epoxy-glass, carbon and Kevlar post cure at 25ºC
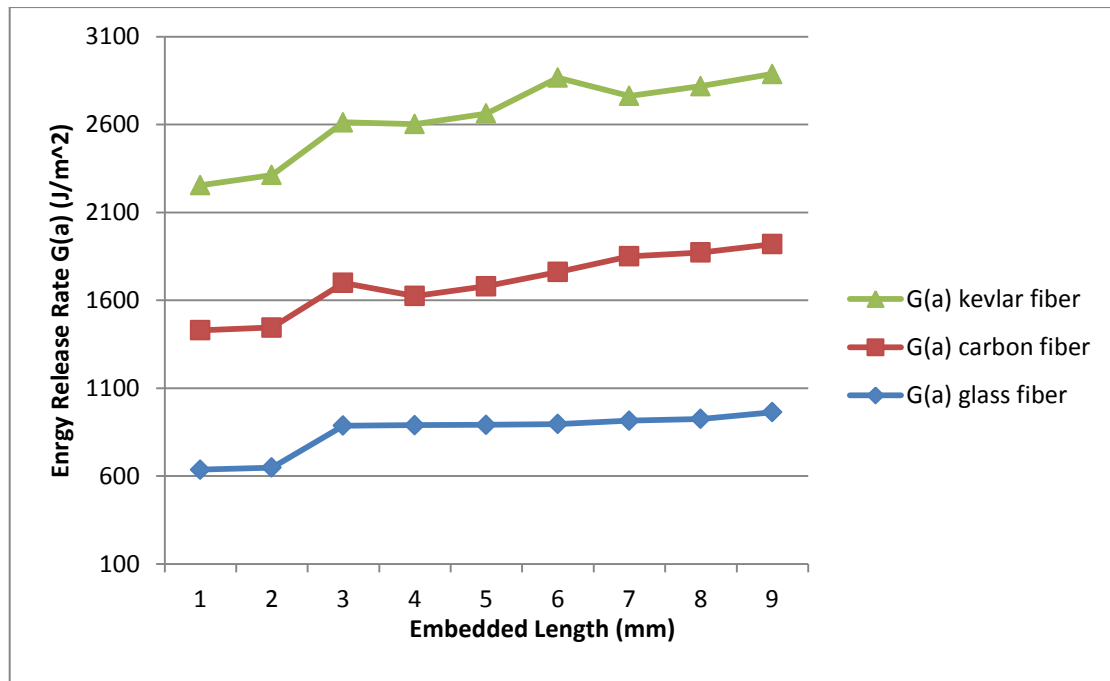

Fig (4-44) energy release rate for epoxy-glass, carbon and Kevlar post cure at 50ºC
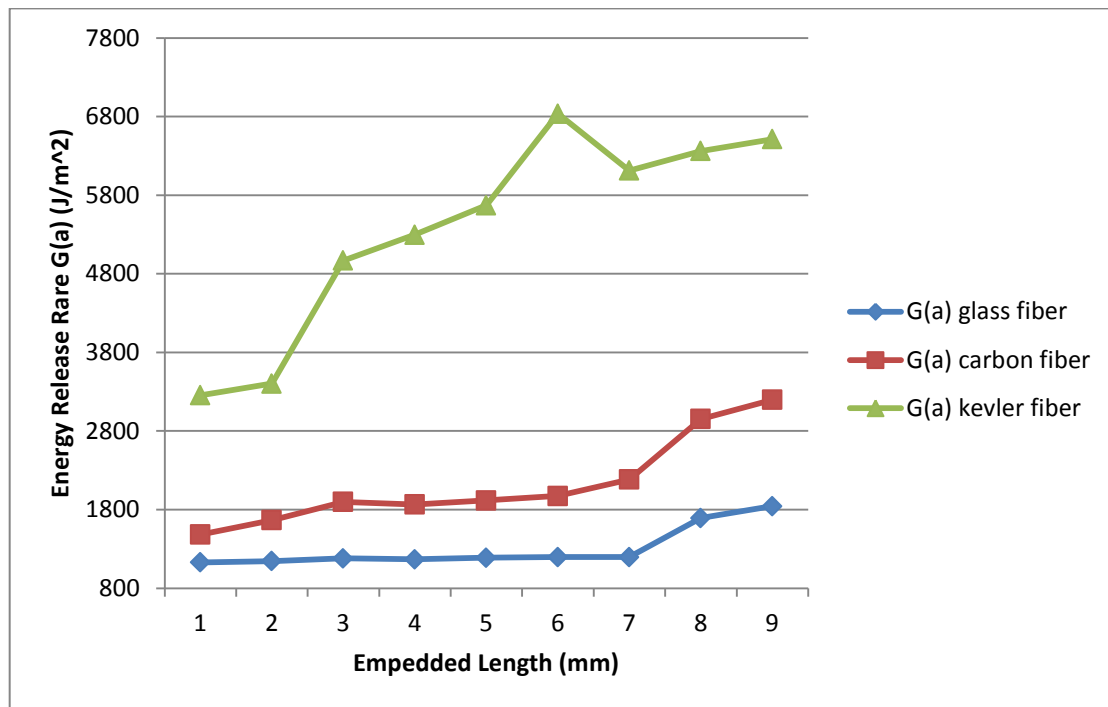
Fig (4-45) energy release rate for epoxy-glass, carbon and Kevlar post cure at 75°C.

The energy release rate for polyester-glass fiber, polyester-carbon fiber and polyester-kevlar fiber was ($84.61 J/m^2$) ($126 J/m^2$) ($128.6 J/m^2$) respectively show in Fig (4-46). The highest energy release rate for polyester-kevlar so the kevlar fiber is the best reinforced fiber for high energy release rate which gave high adhesion between kevalr and matrix due to mechanical and chemical bond.
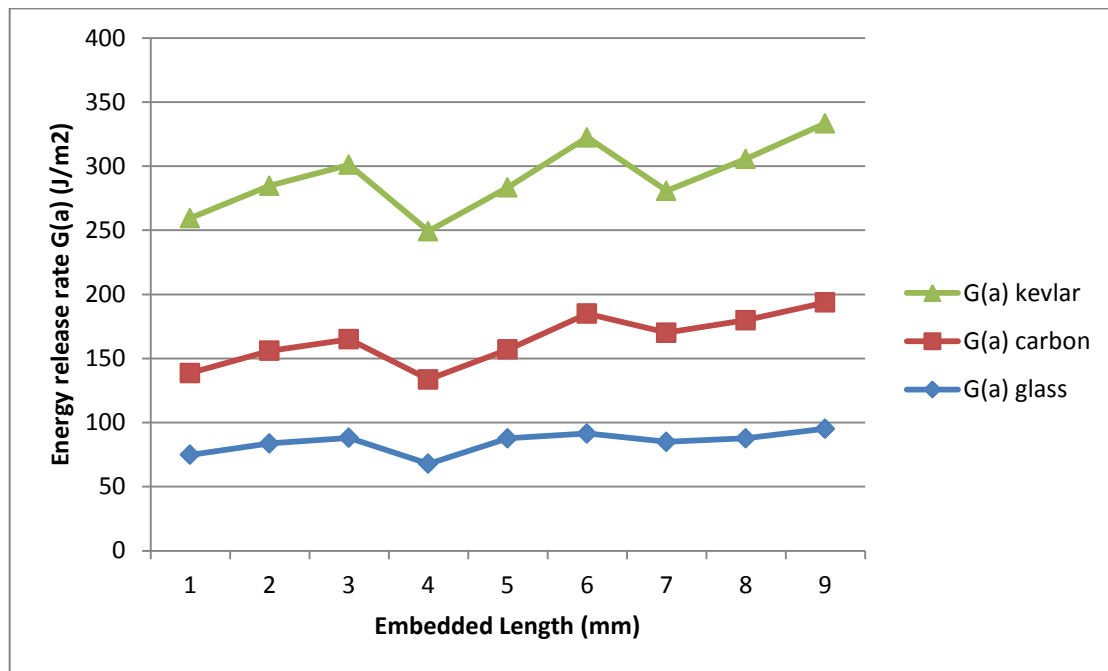
Fig (4-46) energy release rate for polyester-glass, carbon and Kevlar post cure at 25°C.

The energy release rate for epoxy-polyethylene (38.835J/m^2) (87.129J/m^2) (129.172J/m^2) and polyester-polyethylene (5.745J/m^2) are very low in compared with the rest of the material because of the poor adhesion of ultra high polyethylene (UHPE) fiber to epoxy resin due to its surface structure characteristics it have low friction coefficient, highly resistant to corrosive chemicals and has extremely low moisture absorption this agreement with reference [57,58]. In general the energy release rate for epoxy matrix is higher than polyester matrix this is because the force adhesion for epoxy matrix is greater than polyester Matrix this agreement with reference [18].

4-6 Effect of Thermal on Energy Release Rate

The specimens were post cured at three temperatures 25°C, 50°C, and 75°C for two hour so the effect of post cure is clear from Table (4-43) the average energy release rate for glass fiber post cure at room temperature (25°C)is (243.595J/m^2) and at 50°C is (850.312J/m^2) and at 75°C(1304.37J/m^2) as shown in Fig (4-47).
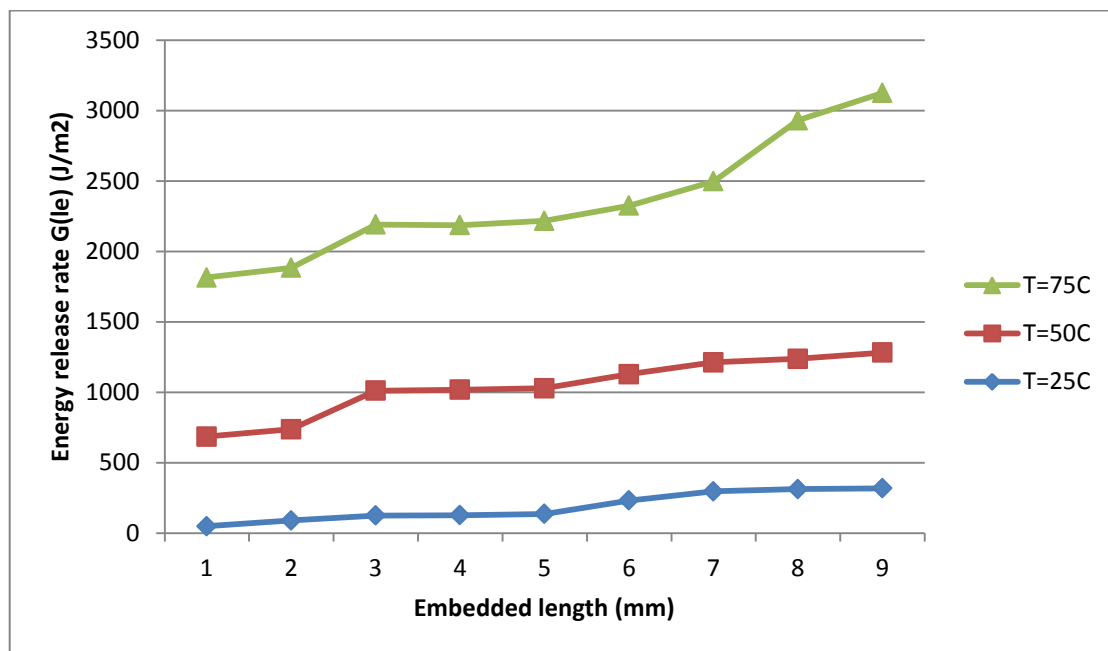

Fig (4-47) Effect of post cure on energy release rate for epoxy-glass fiber.

The energy release rate for epoxy-carbon fiber also post cure at three temperatures 25°C, 50°C, and 75°C for two hour (309.841J/m^2), (847.64J/m^2) and (2126.696J/m^2) as shown in Fig (4-48). The effect of post cure on energy release rate for epoxy-kevlar fiber also post cured at three temperatures 25°C, 50°C, and 75°C for two hour (371.294J/m^2) (944.37J/m^2) and (5379.373J/m^2) respectively as shown in Fig (4-49). The energy release rate for epoxy-polyethylene fiber also cured at three temperatures 25°C, 50°C, and 75°C for two hour (38.835J/m^2), (87.129J/m^2) and (129.172J/m^2) respectively as shown in Fig (4-50).

In general all epoxy specimens, when increased the energy release rate will post cure increased because the free radicals requires a break bond in a similar way, and that must be have a large amount of energy. The mobility of free radicals will be high when post cure increased and that is enable cured material to exhibit the best possible mechanical and physical properties such as Tg, hardness, modulus, electrical conductivity, thermal conductivity and strength . Which leads to increase the strength of adhesion between the fiber and the matrix this agreement with reference [60,61].
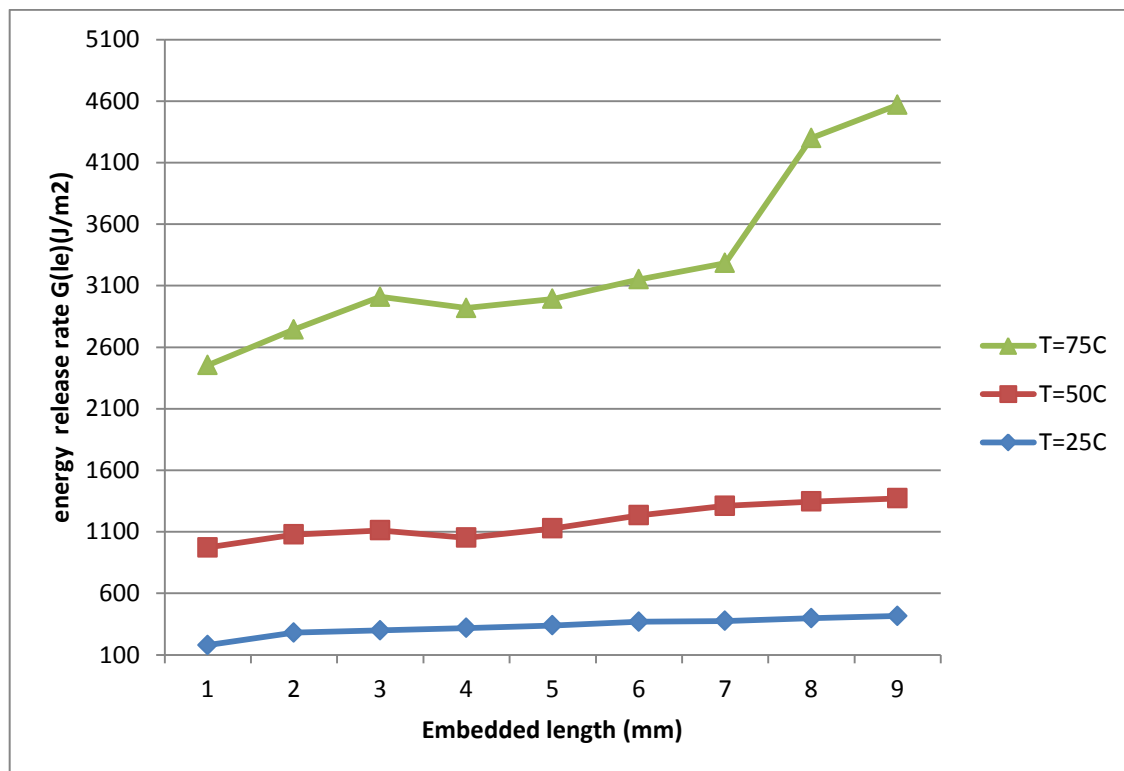
Fig (4-48) Effect of post cure on energy release rate for Epoxy-Carbon
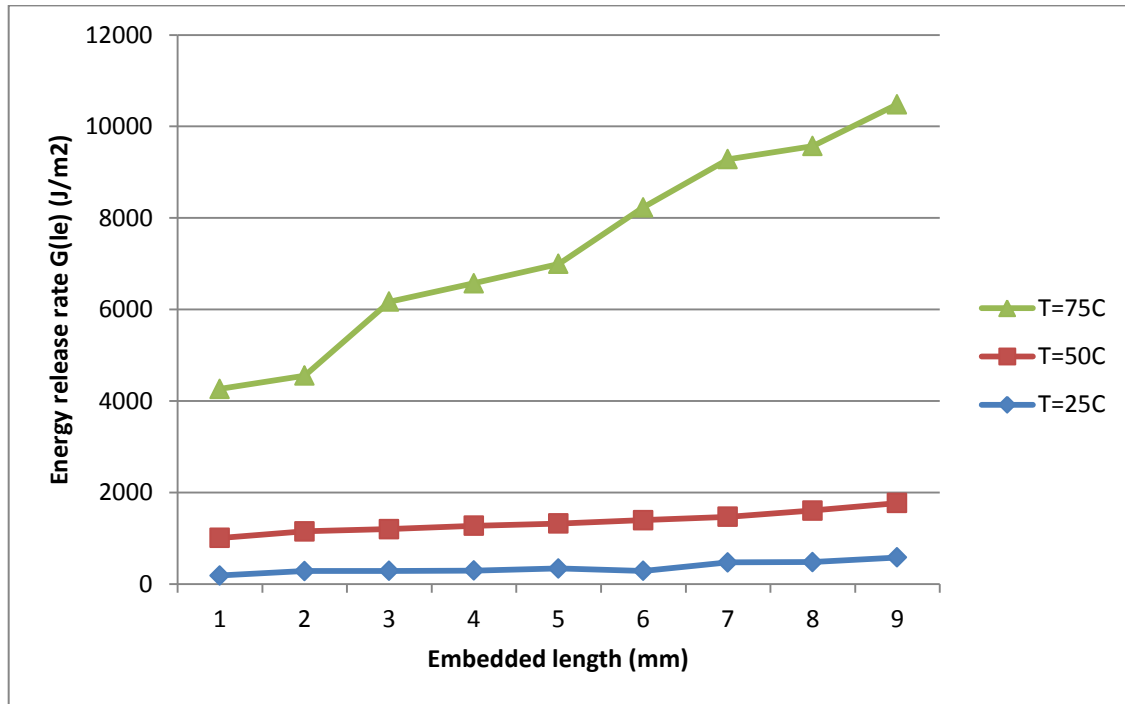
Fig (4-49) Effect of post cure on energy release rate for epoxy-kevlar fiber.
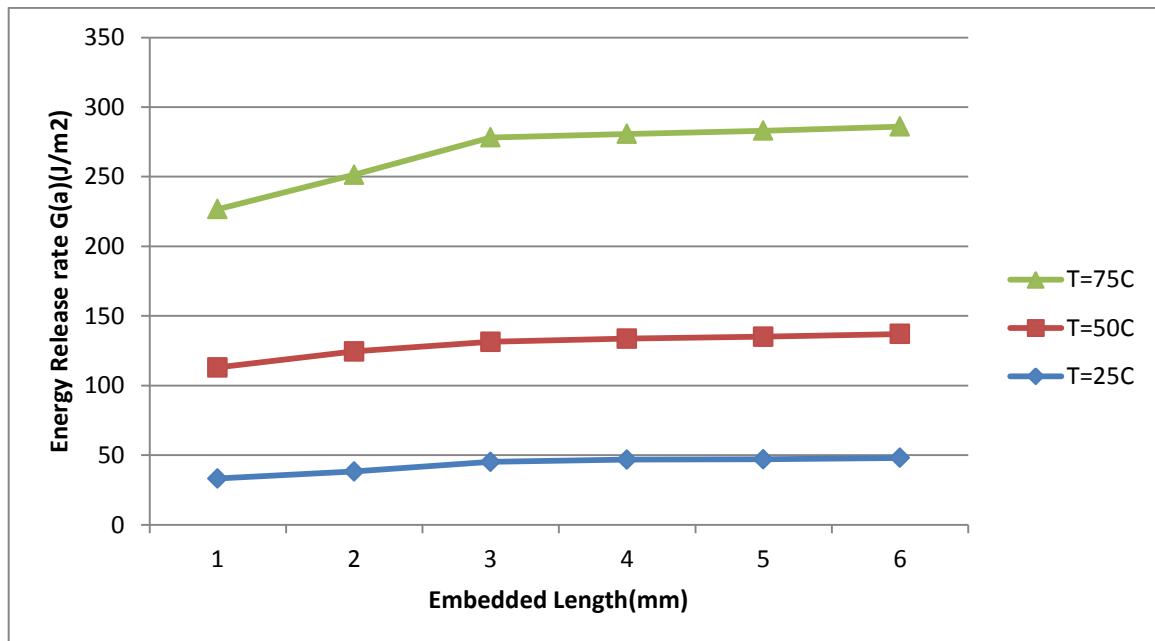
Fig (4-50) Effect of temperature on energy release rate for epoxy-polyethylene fiber.

The specimens of polyester matrix are cure in only at room temperature 25 ^{o}C.When polyester cure initially liquid resin is converted to a solid by cross-linking chains. This is done by creating free radicals at unsaturated bonds, which propagate in a chain reaction to other unsaturated bonds in adjacent molecules, linking them in the process. The initial free radicals are induced by adding a compound that easily decomposes into free radicals this agreement with refrencer [62, 63].

Chapter

Five

2-1 Introduction:

Study of interface in composite system is essential for the development of an understanding the science and technology of composite materials. The important property of interface that can greatly affect the mechanical behavior is strength of adhesive bonding between the reinforcement and the matrix in composite materials, when load is applied to fiber reinforced composite. The load is transferred between the fiber and matrix through the interface. Several micromechanical test methods have been developed to determine the interface properties of composite by measuring the level of adhesion between a reinforcing fiber and resin matrix [21].

The level of fiber–matrix interfacial adhesion in composites is traditionally evaluated by means of a stress-based parameter. Recently, it was suggested that an interfacial energy parameter might constitute a valid alternative. From an overview of the literature regarding the single-fiber composite fragmentation test, it appears that energy-based approaches have already been proposed in the past, but were either not successful, or not fully developed. In this work recent energy balance scheme, proposed for the analysis of the initial interface debonding which occurs at fiber breaks during a fragmentation test, is presented and expanded here. The effects of thermal residual stress in the fiber, and of friction in the debonded area, are now incorporated in the energy balance model. It can use a different shear-lag parameter proposed by Nayfeh rather than the commonly used Cox parameter [29].

The analysis of test data falls into substantially different approaches for quantitative characterization of interfacial strength. The first approach is the stress-based in which the mechanical stress at

interface is determined and interfacial strength is characterized by certain value of interfacial stress at which the interface fails. The second approach is the energy-based which depend on shear-lag analysis that calculates the stresses along the interface and fracture mechanics and based on the determination of amount of energy releases in specimen during interfacial debonding per unit debonding area. It is assumed that interfacial failure occurs when energy release rate reaches its critical value, which is assuming to be a characteristic of the strength of the interface or interfacial toughness [23].

To calculate interfacial shear strength from equation definition is the ratio of maximum measured force (F) over the total interfacial are

$$\tau_{iss} = \frac{F}{2\pi r_f l_e}$$ …….. (2-1)

Where r_f is the fiber radius and l_e is the embedded fiber length. Physically this term is the average interfacial shear stress at the time of failure. It might be useful for qualitative work, but it has several limitations when one desires more rigorous interfacial characterization [30,31]

The interfacial shear strength cannot be an adequate characteristic of shear stress that actually exists at interface. The interfacial shear stress is smaller than maximum shear stress at moment of debonding which is obtained by the stress distribution of shear-lag analysis. Moreover the maximum force measured by micromechanical tests in micorbond, drag-out and pull-out are test affected by embedded length, internal stress and friction effect. In the energy-based approach which is dependent on Nairn and Co-worker model, the failure of interface in two popular interface tests microbond and pull-out [24,25,26].

It can be represented by a cylindrical single fiber surrounded by a hollow cylindrical of matrix or two concentric cylinders, a shear-lag analysis used to derive a system of equations for finding axial and shear stresses of two concentric cylinders and an energy release equation of crack propagation including internal stress and friction effect derived. In the experimental test the fiber is subjected to tensile stress which leads to a critical debonding shear stress (shear strength) that can be calculated from force-displacement curve in Fig (2-1)[27].

Fig (2-1) A typical force–displacement curve for Twaron–epoxy system from the pull-out test. The 'kink' indicates crack initiation [35]

From each force–displacement curve, a schematic is given in Fig (2-1) the force at a "kink" in the initial slope F_{kink}, the force of debonding ($\mathbf{F_d}$) and the embedded length ($\mathbf{l_e}$)[35].

2-2 Drag-out Test Analysis:

The drag out configuration involves a sample that has a free length and two embedded fiber areas. A force is applied at a point on the free length in a direction perpendicular to the fiber, as shown in Fig (2-2). The balance of forces for this configuration is shown in Fig (2-3). A hook

applies a tensile force (**F**) at a distance **l₁** and **l₂** from the left (A) and right (B) edges, respectively. (**H**) is the distance perpendicular to the baseline AB. The force causes a tension (**T$_i$**) in the fiber. The subscripts 1 and 2 refer to the left and right sides, respectively. The tension is a vector with a component (**P$_i$**) parallel to the baseline AB and a component (**R$_i$**) perpendicular to AB. The parallel component is equal to the pull-out force that acts to debond the fiber from the matrix [13].

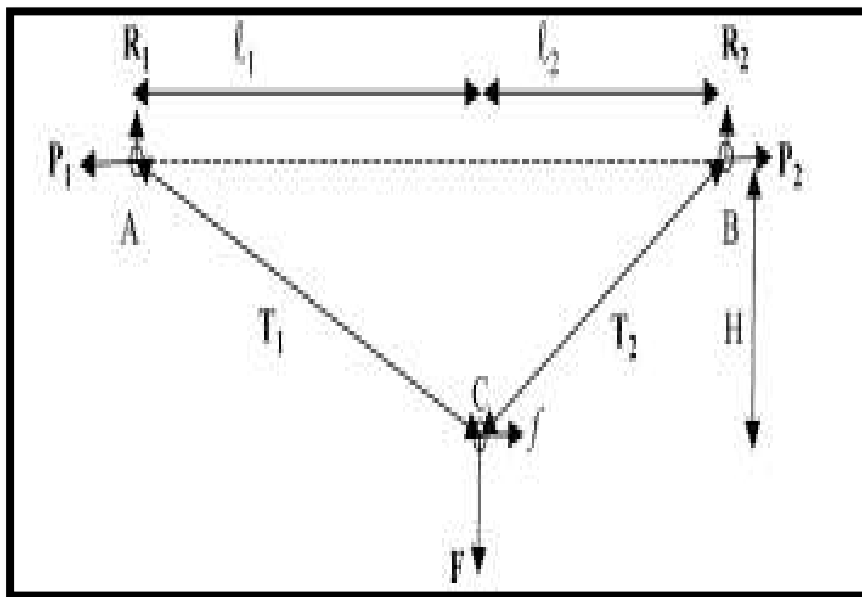**Fig (2-2) Force equilibrium for the drag-out configuration [13]**

If $l_1 \neq l_2$ then $P_1 \neq P_2$ and there is a horizontal balancing force f

$$p_1 = p_2 + f \qquad\qquad \text{.........(2-2)}$$

$$f = R_1 + R_2 \qquad\qquad \text{.........(2-3)}$$

From the torque balance get

$$R_1 l_1 = R_2 l_2 + fH \qquad\qquad \text{........(2-4)}$$

Inserting Eqs (2-3) in (2-2)

$$R_1 l_1 = (F - R_1) l_2 + fH \qquad\qquad\qquad ………(2\text{-}5)$$

$$R_1 = \frac{Fl_2 + fH}{l_1 + l_2} \qquad\qquad\qquad ……… (2\text{-}6)$$

$$R_2 = \frac{Fl_1 - fH}{l_1 + l_2} \qquad\qquad\qquad ……… (2\text{-}7)$$

The ratio between P and R is equal to the ratio between l and H

$$\frac{P_1}{R_1} = \frac{l_1}{H} \qquad\qquad\qquad ……… (2\text{-}8)$$

And

$$\frac{P_2}{R_2} = \frac{l_2}{H} \qquad\qquad\qquad ……… (2\text{-}9)$$

Isolating P in Eqs. (2-8) and (2-9) and inserting the expressions for R from Eqs. (2-6) and (2-7) gives:

$$P_1 = \frac{Fl_2 + fH}{l_1 + l_2} * \frac{l_1}{H} \qquad\qquad\qquad ………(2\text{-}10)$$

And

$$P_2 = \frac{Fl_1 - fH}{l_1 + l_2} * \frac{l_2}{H} \qquad\qquad\qquad ………(2\text{-}11)$$

If $l_1 = l_2 = l_{1/2}$ than $f = 0$ Eqs. (2-2), (2-8) and (2-9) become

$$R_1 = R_2 = \frac{F}{2} \qquad\qquad\qquad ……… (2\text{-}12)$$

$$P_1 = P_2 = \frac{F}{2} * \frac{l_{1\backslash 2}}{H} \qquad\qquad\qquad .... (2\text{-}13)$$

The tension T in the fiber is:

$$T_1 = \sqrt{P_1^2 + R_1^2} \qquad\qquad \ldots\ldots\ldots (2\text{-}14)$$

$$T_2 = \sqrt{P_2^2 + R_2^2} \qquad\qquad \ldots\ldots\ldots (2\text{-}15)$$

Assuming that no interfacial debonding is present under a small applied force F, we have:

$$\sqrt{H^2 + l_1^2} = l_1\left(1 + \frac{T_1}{AE}\right) \qquad\qquad \ldots\ldots (2\text{-}16)$$

$$\sqrt{H^2 + l_2^2} = l_2\left(1 + \frac{T_2}{AE}\right) \qquad\qquad \ldots\ldots\ldots (2\text{-}17)$$

The right-hand sides arise from the geometry, and the left side from Hooke's law

A is the fiber cross section and E is its Young's modulus.

If $l_1 = l_2 = l_{1/2}$ then $P_1 = P_2 = P$ and $T_1 = T_2 = T$

$$\sqrt{H^2 + l_{1\backslash2}^2} = l_{1\backslash2}\left(1 + \frac{\sqrt{p^2 + R^2}}{AE}\right) \qquad\qquad \ldots\ldots (2\text{-}18)$$

From Eqs (2-9)

$$\sqrt{H^2 + l_{1\backslash2}^2} = l_{1\backslash2}\left(1 + \frac{\sqrt{R^2\left(\frac{l_{1\backslash2}}{H}\right)^2 + R^2}}{AE}\right) \qquad\qquad \ldots\ldots\ldots (2\text{-}19)$$

In Eqs (2-3) $R_1 = R_2$ if $l_1 = l_2 = l_{1/2}$ then:

$$R = \frac{F}{2}$$

$$\sqrt{H^2 + l_{1\backslash2}^2} = l_{1\backslash2}\left(1 + \frac{F}{2AE}\sqrt{\left(\frac{l_{1\backslash2}}{H}\right)^2 + 1}\right) \qquad \ldots\ldots\ldots (2\text{-}20)$$

$$F = \frac{2AEH}{l_{1\backslash2}}\left(1 - \frac{l_{1\backslash2}}{\sqrt{H^2 + l_{1\backslash2}^2}}\right) \qquad \ldots\ldots\ldots (2\text{-}21)$$

From Eqs (2-8) if $l_1 = l_2 = l_{1/2}$ the pull-out force:

$$P = R\frac{l_{1\backslash2}}{H} = \frac{l_{1\backslash2}}{2} * \frac{F}{H} \qquad \ldots\ldots\ldots (2\text{-}22)$$

And

$$P = AE\left(1 - \frac{l_{1\backslash2}}{\sqrt{H^2 + l_{1\backslash2}^2}}\right) \qquad \ldots\ldots\ldots (2\text{-}23)$$

Where F is the applied force in drag-out test while P is the pull-out force component [13].

Equations (2-21), (2-23) are derived in elastic region and governed by Hooks law, before debonding between fiber and matrix occurs. The experimental data (drag-out force and the cross head displacement) indicates a knik point ($\mathbf{F_{Knik}}$) (the drag-out force at crack initiation) while the drag-out force at peak is the maximum force in Fig (2-1) and the drag-out force at peak ($\mathbf{F_d}$) point in which the crack equal approximately the length of embedded length as shown by Nairn[28].

2-3 Stress Analysis and Energy Release Rate

In Fig (2-3), show an idealized cylindrical model under test loading conditions. σ_f is the background fiber tensile stress or the stress on the fiber due to weight of the fiber below the droplet. σ_m is the stress applied to the droplet during the test. ξ and ζ represent the dimensionless radial and axial coordinates, respectively. The stresses on the top of the fiber and matrix cylinders are balanced with the σ_f stress on the bottom of the fiber. The net axial stress on any cross-section is $\sigma_0 = V_1\sigma_f$ where V_1 is the volume fraction of the fiber.

Fig (2-3) (A) microbond specimen of dimensionless length 2ρ, (B) Stress analysis [12].

A recent study has concluded that a critical energy release rate for interfacial crack growth failure criterion is more accurate than either an average shear or total energy failure criteria in predicting the failure load of microbond specimens. Recently derived variational mechanics analysis a new shear-lag analyses, two existing shear-lag analyses, and a simple

limiting model for long droplet lengths are all used to calculate the energy release rate for growth of an interfacial crack in the microbond specimen.

By assuming that debonding occurs when the energy release rate reaches a critical energy release rate, denoted as G_{ic}, predicted debond force as a function of droplet length for all[12,15].

2-3-1 Variation Mechanics stress Analysis

Used these equations because it is consistent with samples in the case around the drag-outt to pull-out. The droplet was assumed to be a cylinder on the fiber, the load was assumed to be applied uniformly over the top of the matrix cylinder. Axial ratio $\rho = l/2r_1$ where l is embeded length was analyzed by making only one assumption—that the axial stresses in the fiber and in the matrix cylinders depend only on the axial coordinate (z) and are independent of the radial coordinate (r), all stresses in the matrix and cylinder can be written in terms of a single unknown function, $\psi(\zeta)$, where $\zeta = z/r_1$ is a dimensionless axial coordinate normalized to the fiber radius, r_1. The stresses in the fiber are

$$\sigma_{zz,1} = \psi \qquad\qquad\qquad ……… (2\text{-}24)$$

$$\tau_{rz,1} = -\frac{\xi\psi'}{2} \qquad\qquad\qquad ……… (2\text{-}25)$$

$$\sigma_{rr,1} = \frac{\psi''}{16}\left(\xi^2(3+\upsilon_T)+\upsilon_m-\upsilon_T+\frac{2(1+\upsilon_m)\ln V_1}{V_2}-\frac{V_2 A_1}{V_1 A_0}\right)-\frac{V_2}{V_2}\left(\frac{A_3\psi+A_4\sigma_0+A_5\Delta T}{A_0}\right)$$

$$……….(2\text{-}26)$$

$$\sigma_{\theta\theta,1} = \frac{\psi''}{16}\left(\xi^2(1+3\upsilon_T) + \upsilon_m - \upsilon_T + \frac{2(1+\upsilon_m)\ln V_1}{V_2} - \frac{V_2 A_1}{V_1 A_0}\right) - \frac{V_2}{V_1}\left(\frac{A_3\psi + A_4\sigma_0 + A_5\Delta T}{A_0}\right).$$

……… (2-27)

The stresses in the matrix are

$$\sigma_{zz,2} = \frac{\sigma_0}{V_2} - \frac{V_1\psi}{V_2}$$

…..… (2-28)

$$\tau_{rz,2} = \frac{V_1\psi'}{2V_2}\left(\xi - \frac{1}{\xi V_1}\right)$$

……… (2-29)

$$\sigma_{rr,2} = \frac{\psi''}{16V_2}\left[(3+\upsilon_m)(1-\xi^2 V_1) + 2(1+\upsilon_m)\ln\xi^2 V_1 + \frac{V_2 A_1}{A_0}\left(1 - \frac{1}{\xi^2 V_1}\right) + \left(1 - \frac{1}{\xi^2 V_1}\right)\left(\frac{A_3\psi + A_4\sigma_0 + A_5\Delta T}{A_0}\right)\right]$$

……..(2-30)

$$\sigma_{\theta\theta,2} = \frac{\psi''}{16V_2}\left[(1+3\upsilon_m)(1-\xi^2 V_1) - 2(1-\upsilon_m)\ln\xi^2 V_1 + \frac{V_2 A_1}{A_0}\left(1 + \frac{1}{\xi^2 V_1}\right) + \left(1 + \frac{1}{\xi^2 V_1}\right)\left(\frac{A_3\psi + A_4\sigma_0 + A_5\Delta T}{A_0}\right)\right]$$

……… (2-31)

In these equations (2-24) and (2-25) refer to the fiber and matrix cylinders respectively, ν_m is the Poisson's ratio of the isotropic matrix, ν_T is the transverse Poisson's ratio of the transversely isotropic fiber, V_1 and V_2 are the volume fractions of the fiber and the matrix, A_1 to A_5 are material and geometry-specific constants[12].

σ_0 is the total stress applied in the z direction ($\sigma_0 = V1\sigma_f$ where σ_f is the background tensile stress), ΔT is the difference between the stress free temperature and the specimen temperature, and ξ is a dimensionless radial coordinate defined by $\xi = r/r_1$. By axisymmetry, the unspecified shear stresses are all zero. The stresses in Eqs (2-24)–(2-31) constitute an admissible stress state. By the principles of variational mechanics, the best approximation to the true stress state is found by finding the ψ (ζ)

that minimizes the total complementary strain energy. Depend only on mechanical properties of the fiber and matrix and on the geometry of the specimen physically, the constant ψ_0 is the far-field fiber stress or the stress that would exist in the fiber far from the ends of, an infinitely long droplet [12].

For energy release rate calculations, Need to calculate the total strain energy in the microbond specimen. Using the stresses in Eqs (2-24)–(2-31) to find the strain energy and integrating over the volume of the specimen gives the total strain energy. , the strain energy integral simplifies to

$$U(\rho) = \pi r_1^3 \int_{-\rho}^{\rho} d\zeta \left(C_{33}\psi^2 + 2C_{35}\psi\psi'' + C_{55}\psi''^2 + C_{44}\psi'^2 \right) \qquad \ldots\ldots\ldots (2\text{-}37)$$

In Eq. (2-37) assumed that $\sigma_f = \sigma_0 = 0$. This assumption follows the typical microbond experiment in which the background fiber stress σ_f is negligible. Eliminating σ_f leads to considerable simplification. If subsequent experiments show that σ_f is an important variable, the variational mechanics analysis can include its effects by rederiving the strain energy for non-zero σ_f. Substituting the known function $\psi(\zeta)$ and integrating gives[12]:

$$U(\rho) = 2C_{55}\rho\pi r_1^3 \left[\frac{D_3^2 \Delta T^2}{C_{33}^2} \left(\frac{C_{33}}{C_{55}} - \frac{X_e(\rho)}{\rho} \right) + \left(\frac{\sigma_m V_2}{2V_1} \right)^2 \left(\frac{X_e(\rho) + X_o(\rho)}{\rho} \right) \right] \quad \ldots (2\text{-}38)$$

2-3-2 Shear-Lag Stress Analysis:

The so-called "shear lag" method is often used for analysis of stress transfer problems in composites. The term "shear lag" can be traced, prior to its use in composites, to analysis of bending of I beams and T beams with wide flanges and to box beams. Simple beam theory

predicts that the axial displacements in the flanges of such beams are only a function of the distance from the neutral axis and independent of the distance from the web. This simple theory also predicts zero shear stress and zero shear strain in the flange. In reality, the true axial displacements "lag" behind the beam theory predictions. This "lag" is cause by load diffusion which can be viewed (using equilibrium arguments) as a consequence of non-zero shear stresses in the flange hence the term "shear-lag." In these beam analyses, "shear-lag" is an effect and not an analysis method. Many possible analysis methods can evaluate the "shear-lag" effect. These methods generally result in defining an effective flange width that is less than the actual flange width. [29,30].

A common problem analyzed by shear-lag methods is a solid fiber cylinder of radius r_1 embedded in a hollow matrix cylinder with inner radius r_1 and outer radius r_2

$$\frac{\partial^2 \tau_{rz}(r_1)}{\partial z^2} - \beta^2 \tau_{rz}(r_1) = 0 \qquad \ldots\ldots\ldots(2\text{-}39)$$

Where

$$\beta^2 = \frac{2}{r_1^2 E_A E_m} \left[\frac{E_A \upsilon_f + E_m \upsilon_m}{\dfrac{V_2}{4G_A} + \dfrac{1}{2G_m}\left(\dfrac{1}{V_2}\ln\dfrac{1}{V_1} - 1 - \dfrac{V_1}{2} \right)} \right] \qquad \ldots\ldots\ldots (2\text{-}40)$$

And V_1 and V_2 are the fiber and matrix volume fractions defined by

$$V_1 = \frac{r_1^2}{r_2^2} \qquad\qquad\qquad V_2 = \frac{r_2^2 - r_1^2}{r_2^2} \qquad \ldots\ldots\ldots (2\text{-}41)$$

E_A, E_m=Tensile Modulus

G_A, G_m= Axial shear modulus

The β^2 term Eq. (2-40), however, is very different than the one derived by Cox (1952) .The β^2 term here is identical to the one derived by Nayfeh and McCartney [31,.. ,34].

2-3-3 Energy Release Rate Analysis

The most widely used approach for analyzing failure in microbond specimens is to assume that the droplet shears off the fiber when the average shear stress at the interface, $\langle \tau_{rz}(\xi = 1) \rangle$, reaches the interfacial shear strength, τ_{ic}. By integrating the equations of stress equilibrium it is possible to derive an exact relation between $\langle \tau_{rz}(\xi = 1) \rangle$ and fiber force, F:

$$\langle \tau_{rz}(\xi = 1) \rangle = \frac{F}{2\pi r_1 l} \qquad \qquad \dots\dots\dots (2\text{-}42)$$

The force, Fd, or the stress, $\sigma_d = -\sigma_m V_2 / V_1$,in the fiber at the instant of debonding as a function of droplet length are thus predicted to be linear

$$F_d = 2\pi r_1 l \tau_{ic} \qquad \text{or} \qquad \sigma_d = 4\tau_{ic}\rho \qquad \dots\dots\dots(2\text{-}43)$$

There are two problems with Eq. (2-43). First, it is in poor agreement with experimental data over a wide range of droplet lengths. Second, despite that fact that Eq. (2-42) is an exact expression of stress equilibrium, the assumption that average shear stress determines failure is unrealistic. A variational stress analysis or a finite element analysis18 show that the shear stress is nonuniform and that there is a significant radial tensile stress concentration at the point where the fiber enters the droplet. It is probably incorrect to ignore these features of the stress state and attribute failure only to the level of average interfacial shear stress. It can be discuss a fracture mechanics method where debonding is predicted based on the energy release rate for initiation of an interfacial crack. The

highest interfacial stresses are at the point where the matrix is contacted by the microvise see in Fig (2-4) $\zeta = +\rho$. It is therefore logical to assume that debonding will be caused by initiation of an interfacial crack at $\zeta = +\rho$. This assumption agrees with experimental observations of microbond failures. In this section use the variational mechanics stress analysis and the shear-lag stress analysis to calculate the energy release rate for initiation of an interfacial crack G_i. By assuming that specimen failure occurs when G_i reaches the critical energy release rate for the interface, or the interfacial toughness, G_{ic}, further predict σ_d as a function of droplet length [17,35,36]

For a crack propagation analysis, we must consider a microbond specimen with an interfacial crack. Fig (2-4) shows an idealized microbond specimen with a crack of length a or dimensionless length 2δ where $\delta = a/2r_1$. The specimen is now divided into two regions—region I is the region within the interfacial crack and region II is the region with an intact interface. Our first step is to find the stresses and strain energies in each region. We begin by using the variational mechanics analysis.

Because the interfacial radial stress is tensile before crack formation, we assume the crack in Fig (2-4) opens and that the crack surfaces are stress free. The only possible stress state in region I in which σ_{zz} is independent of r is simple uniaxial tension. When σ_f is negligible, the axial stresses in the fiber and matrix are:

$$\sigma_{zz,1} = -\frac{\sigma_m V_2}{V_1} \qquad \text{and} \qquad \sigma_{zz,2} = \sigma_m \qquad \ldots\ldots\ldots(2\text{-}44)$$
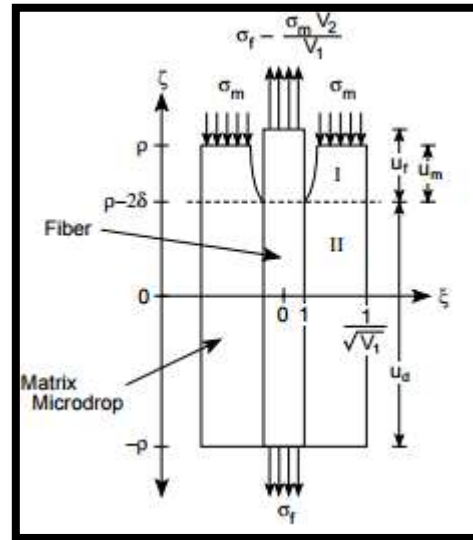
Fig (2-5) An idealized microbond specimen of dimensionless length 2ρ having an interfacial crack of dimensionless length 2δ emanating from the top of the droplet. Region I is the cracked region above the dashed line. Region II is the uncracked region below the dashed line [12].

Using the general composite fracture mechanics methods and applying them to the geometry in Fig. (2-5) with an interfacial debond of length (a), the energy release rate for debond growth in both the pull-out and microbond specimens can be written as [12].

$$G(a) = \frac{r_f}{2} C_{33s}(\sigma_d - ka)^2 + \frac{r_f}{2} D_{3s}(2 + C_T'(a))(\sigma_d - ka)\Delta T +$$

$$\frac{r_f}{2}\left[\left(\frac{D_3^2}{C_{33}} + \frac{V_2(\alpha_T - \alpha_m)^2}{V_1 A_0} + \frac{2D_3 D_{3s}}{C_{33}} C_T'(a)\right)\Delta T^2 - kD_{3s}C_T(a)\Delta T\right] \qquad .....(2\text{-}51)$$

$\Delta T =$ the different between stress free temperature and the specimen temperature

$C_T (a) =$ a stress-transfer function

Eq. (2-51) is essentially an exact result for debonding energy release rate in the concentric cylinders model including both the effects of residual thermal stresses and friction. Residual stresses are included by selecting

ΔT to match the true level of residual stresses in the specimen. Because rigorous modeling of coulomb friction is difficult, friction is included in an approximate manner. It is included by introducing a constant shear stress on the debond surface of τ_f. This frictional stress contributes to energy release rate by external work on the debond surfaces as the fiber and matrix slide by each other. In some experiments it is possible to measure τ_f and thus claim this approach can accurately include friction effects. The cumulative stress transfer function C_T (a) is defined [37…39]

$$C_T(a) = \int_0^{le-a} F(z)dz \qquad \text{……… (2-52)}$$

The model [9,12] ,suggested that an acceptable G(a=l) can be estimated by calculated G(a) from energy release rate curve for droplet has much larger than actual droplet. In reference [14] a well-behaved result got by calculation G(a) in long droplet limit or limit as $l_e\rightarrow\infty$ and the energy release rate G(a) in the limit as $l_e\rightarrow\infty$ could be calculated by found the limits on stress transfer function equations [40,41].

$$\lim_{le\rightarrow\infty} C_T(a) = \frac{1}{\beta} \quad \text{and} \quad \lim_{le\rightarrow\infty} C_T'(a) = 0$$

Substitute the results of above limits in Eq.(2-51)

$$G_\infty(a) = \frac{r_f}{2}\left[C_{33s}(\sigma_d - ka)^2 + D_{3s}(2\sigma_d - k(2a+\frac{1}{\beta})\Delta T + (\frac{D_3^2}{C_{33}} + \frac{V_2(\alpha_T - \alpha_m)^2}{V_1 A_0})\Delta T^2\right]$$

$$\text{…… (2-53)}$$

σ_d = the axial stress at peak force in force- displacement curve

$$\sigma_d = \frac{F_d}{\pi r_f^2}$$

k = the fractional stress transfer = $\dfrac{2\tau_f}{r_f}$ and $\quad \tau_f = \dfrac{F_r}{2\pi r_f l_e}$

a= crack length = embedded length l_e at peak force (F_d)

$V_f = V_1$ = fiber volume fraction

$V_m = V_2$ = matrix volume fraction

$$V_1 A_0 = \frac{V_2(1-v_T)}{E_T} + \frac{V_1(1-v_m)}{E_m} + \frac{1+v_m}{E_m}$$

v_T = transverse poissons ratio of fiber

E_T = transverse modulus of fiber

E_m = modulus of matrix

v_m = poissons ratio of matrix

$$A_3 = -\left(\frac{v_A}{E_A} + \frac{V_1 v_m}{V_2 E_m} \right)$$

v_A = axial poisson ratio of fiber

E_A = axial modulus of fiber

$$C_{33} = \frac{1}{2}\left(\frac{1}{E_A} + \frac{V_1}{V_2 E_m} \right) - \frac{V_2 A_3^2}{V_1 A_0}$$

$$C_{33s} = \frac{1}{2}\left(\frac{1}{E_A} + \frac{V_1}{V_2 E_m} \right)$$

$$D_3 = -\frac{V_2 A_3}{V_1 A_0}\left[\alpha_T - \alpha_m\right] + \frac{1}{2}\left[\alpha_A - \alpha_m\right]$$

α_T = transverse thermal expansion coefficient of fiber

α_T = axial thermal expansion coefficient of fiber

α_m = matrix thermal expansion coefficient

$$D_{3s} = \frac{1}{2}(\alpha_A - \alpha_m) \ [42,43]$$

It can be used the equation (2-1) to calculated interfacial shear stress τ_{ifss} and the energy release rate $G_\infty(a)$ from equation (2-53) used for pull-out component so using equation (2-22) to find the pull-out force to any drag-out force in force-displacement curve in drag-out test.

Reference

Reference

[1] Autar K. Kaw., "**Mechanics of Composite Materials** ", 2nd edition, Taylor &francis Group, *Boca Raton London New York*, *(2006)*.

[2] Mark V., and Brower P.E., "**Composite Materials**", The University of Alabama in Huntsville, *(2000)*.

[3] Sabu T., Kuruvilla J.,Malhotra S.K., Koichi G.,and SreekalaM.S.," **Polymer Composites**", Wiley-VCH VerlagGmbh&Co.KG, *(2012)*.

[4] Hull D.,Clyne T.W., "**An introduction Composite Materials**" 2nd edition, Cambridge University Press, *(1996)*.

[5] David I.B, "**An Introduction to polymer Physics**", Cambridge University Press.*(2002)*.

[6] Schaffer J. P., SaxenaA., AntolovichS.D., SandersT. H. , and WarnerS. B., "**The Science and Design of Engineering Materials**" , 2nd edition, WCB/McGraw-Hill, New York, *(1999)*.

[7] Oboigbaotor R.E., "**Polymer Science and Technology** " , University of Benin, CRC Press, *(2000)*.

[8] Jean P.H., Jacques V., and Roberto J.J., " **Thermosetting Polymers** " , Marcel Dekker,Inc, (*2002*).

[9] Nairn J.A., "Analysis **Fracture Mechanics of The Pull-Out Test Including The Effect OF Friction and Thermal Stress**" , Advanced Composites Letters, Vol. 9, No. 6, *(2000)*.

[10] Nuriel S., KatzA., and Wagner H.D., "**Measuring fiber–matrix interfacial adhesion by means of a 'drag-out' micromechanical test",Composites**: Part A ,36, PP.33-37,*(2005)* .

Reference

[11] Callister W.D.,"Materials Science and Engendering An Introduction",John Wiley & Sons, Inc, *(2007).*

[12] Scheer R.J., Nairn J.A., " **A Comparison of Several Fracture Mechanics Methods for Measuring Interfacial Toughness with Microbond Tests** ", J. Adhesion, Vol. 53 pp. 45–68, *(1995).*

[13] Nairn J.A., and Liu Y.C.,"**On the use of energy methods for interpretation of results of single-fiber fragmentation experiments** "J. Composite Interfaces, Vol 4,PP. 241–267,*(1996).*

[14] Liu C.H ., Nairn J.A., " **Analytical and Experimental Methods for a Fracture Mechanics Interpretation of The Microbond test Including The Effects Friction and Thermal Stresses**" International Journal of Adhesion & Adhesives ,19,PP .59-70,*(1999).*

[15] Zhandarov S., Pisanova E., Mäder E., andNairn J.A., " **Investigation of Load Transfer Between The Fiber and The Matrix in Pull-out Test With Fiber Having Differents** "J. Adhesion Sci. and Technology, in press,*(2000).*

[16] Nairn J.A., "**Fracture Mechanics of Composites with Residual Stresses, Imperfect Interface, and Traction-Loaded Cracks**" J. Composites Science and Technology, 61, PP. 2159-2167*, (2000).*

[17] Nairn J.A., Liu C.H., Mendels D.A., and Zhandarov S ., " **Fracture Mechanics Analysis of the Single-Fiber Pull-Out Test and the Microbond**" , Ann. Tech. Conf. of the Amer. Soc. Composites, VPI, Blacksburg VA, September 9-12, *(2001).*

[18] AL-Abdly H.A.A., Saleh N.J., AbdulRazak A.A., and Majdi H.S., "**Study the Adhesion Force of Tubular Shaped Fiber Reinforced Composites** ", Eng.&Tech.Vol.26,No.4,*(2008).*

Reference

[19] Hassan H. M. , " **The Stress-Based Model and The Energy-Based Model in Ultra High Polyethylene Fiber Reinforced Thermoset Polymer Composites** " , J.Alqadisiyah for pure science, vol.13 issue 1,PP.1-17, *(2008).*

[20] Al-Mullakhalaf M.S., Tolephih M.H., Ghani A.S., " **The Effect of Fiber Diameter on Debonding Force in Composite Material and Their Influence on Some Mechanical Properties**", Alteqani,Vol.24.ISSN:6, PP.1-11,*(2011).*

[21] Aruniit A., Kers J., Krumme A., Poltimae T., and Tall K., " **Preliminary Study of the Influence of Post Curing Parameters to the Particle Reinforced Composite's Mechanical and Physical Properties** ", J. Materials Science , Vol. 18, No. 3.PP.1392-1320,*(2012).*

[22] Kumar D.S., Shukla M.J., Mahato K.K.,Rathore D.K., Prusty R.K., and Ray B.C., " **Effect of post-curing on thermal and mechanical behavior of GFRP composites** " J.Materials Science and Engineering. 75, 012012,*(2015).*

[23] Nairn J. A., Mendels D.A., Leterrier Y., and Månson J.A.E., "**The Influenceof Internal Stresseson the Microbond Test II: Physical AgingandAdhasion**", J.Composite Materials, vol. 136,issue,14,*(2002).*

 [24] Wagner H.D., Nairn J.A.,and Zhou X.F., " **Fiber–matrix adhesion from the single-fiber composite test: nucleation of interfacial debonding** " Composites: Part A 30 ,PP.1387–1400,*(1999).*

[25] Nairn J.A., "**Fracture Mechanics Of Composites With Residual Stresses, Imperfect Interface, And Traction-Loaded Cracks**" J. Composites Science and Technology, 61,PP. 2159-2167*, (2000).*

Reference

[26] Cox H.L., "**The Elasticity and Strength of Paper and Other Fibrous Materials**" British J. of Applied Physics, 3, No.1, PP. 72-79,*(1952).*

[27]Nairn J.A., Kim B.W., "**Experimental Verification of the Effects of Friction and Residual Stress on the Analysis of Interfacial Debonding and Toughness in Single Fiber Composites** " Materials Science, 37, PP.3965-3972*, (2002).*

[28] Pisanova E., Zhandarov S.,Ma¨der E., Ahmad I., and Young R.J., " **Three techniques of interfacial bond strength estimation from direct observation of crack initiation and propagation in polymer–fiber systems**",J.Composites: Part A,PP. 32 435–443,*(2001).*

[29] Nairn J.A., " **Generalized Shear-Lag Analysis Including Imperfect Interfaces** "J. Material Science and Engineering, Adv. Comp. Letts., in press, *(2005).*

[30] Nairn J.A., Liu Y.C., and Galiotis C., " **Analysis of Stress Transfer from the Matrix to the Fiber Through an Imperfect Interface: Application to Raman Data and the Single-Fiber Fragmentation Test** "J. Fiber, Matrix, and Interface Properties, American Society for Testing and Materials, PP. 47–65, *(1996).*

[31] Nairn J.A., Mendels D.A., " **On the use of planar shear-lag methods for stress-transfer analysis of multilayered composites** " Mechanics of Materials 33 ,PP. 335-362,*(2001).*

[32] Nairn J.A., Wagner H.D., " **A Revised Shear-Lag Analysis of an Energy Model for Fiber-Matrix Debonding** ", J. Advanced Composite Letters,Vol 5, No. 5,PP. 131-135,*(1996).*

Reference

[33]Nairn J.A., Liu Y.C., "**Stresses Transfer In To A Fragmented, An Isotropic Fiber Through Am Imperfect Interface** ", J. Material Science and Engineering, Int. J. Solids Structures,Vol.34, No.10,PP.1255-1281,*(1996).*

[34] Nairn J.A., "**On the Use of Shear-Lag Methods for Analysis of Stress Transfer in Unidirectional Composites**" J.Material Science and Engineering ,26, pp. 63–80, *(1997).*

[35] Scheer R.J.,Nairn J.A., " **Variation Mechanics Analysis of Stresses and Failure in Microdrobond Debond Specimens**", J.CompositesEngineering, Volume 2 ,Issue 8, PP. 641-654,*(1992).*

[36] Rao V., Franco P.H., Ozzello A.D., and Drzal L.T., "**A Direct Comparison of the Fragmentation Test and the Microbond Pull-out Test for Determining the Interfacial Shear Strength** ", J. Adhesion, Vol. 34, pp 65-11,(1991).

[37] Nairn J.A., "**Energy release rate analysis for adhesive and laminate double cantilever beam specimens emphasizing the effect of residual stresses** ", J. of Adhesion & Adhesives ,Vol.20,PP.59-70,*(1999).*

[38]Nairn J.A., "**Fracture Mechanicsof Compositeswith Residual Stresses, Traction-Load Crack, andImperfect Interface**", J. Polymers and Composites,Proc. 2nd ESIS TC4 Conference, in press, *(1999).*

[39] Nairn J.A., "**Simulation of Crack Growth in Ductile Materials** " , J. Engineering Fracture Mechanic, in press,*(2004).*

[40] Nairn J.A., andLiu Y.C., "**On the use of energy methods for interpretation of results of single-fiber fragmentation experiments**" „J. Composite Interfaces, Vol 4,PP. 241–267,*(1996).*

Reference

[41] Nairn J.A., and Honglai T., **" Hierarchical, Adaptive, Material Point Method for Dynamic Energy Release Rate Calculations** ", J.Comput. Methods Appl. Mech. Engrg,191,PP. 2095–2109,*(2002).*

[42]Nairn J.A., "**Fracture Mechanics of Composites With Residual Thermal Stresses** ", J.Appl. Mech, Vol 64,PP. 804-810, *(1997).*

[43]Kim Y.K., Ye L., and phoa K., " **Interlaminar Fracture Toughness of CF/PEI and GF/PEI Composites at Elevated Temperatures** " Volume 11, Issue 3, pp 173–190,*(2004).*

[44] Flory P.J., "**Principles of Polymer Chemistry**", Cornell University Press, Ithaca, NY, *(1952).*

[45] Mark E.,Tuttle., "**Structural and Analysis of polymeric** ", Marcel Dekker, Inc., *(2004).*

[46] Rudin A., "**The Elements of Polymer Science and Engineering** ", Academic Press, New York, *(1982).*

[47] Mallick P.K.,"**Fiber-Reinforced Composites Materials Manufacturing and Design** ", Marcell Dekker, Inc., New York, *(1988).*

[48] Hyer M.W., " **Stress Analysis of Fiber-Reinforced Materials**", WCB McGraw–Hill, New York, *(1998).*

[49] Agrawal B.D., and Broutman L.J.,"**Analysis and Performance of Fiber Composites**", John Wiley & Sons, New York, *(1990).*

[50] Buchanan G.R.," **Mechanics of Materials**", HRW Inc., New York, *(1988).*

[51] Green G.,Feely C., "**Design And Manufacture of Composite Structures** ", Printed by Galliard Ltd.Great Yarmouth England, *(1994).*

Reference

[52] AL-shemery H. G., " **Calculations The Fracture Surface Energy of Polyethylene –Reinforced by Glass and Carbon Fiber** " M.Sc.Theses College of science University of Babylon, *(2000).*

[53] John L.,and Clarke," **Structural Design of Polymer Composites** ", Taylor& Francis e-Library, *(2005).*

[54] Mohamed M. I., Salah N.J., Mohamed L.H., "**studying The Mechanical properties of Epoxy Carbon Nanotubes Composite** ", NUCEJ Vol.18No.1, pp.84-90, *(2015)* .

[55] Zahid M. A. M.," **Toughening of High Density Polyethylene with Rubber and Reinforced with Glass fibers** "M.Sc.Theses College of Engineering University Babylon , *(2008).*

[56] Ishida H., and Bussi P., " **Surface-Induced Crystallization in Ultrahigh-Modulus Polyethylene Fiber Reinforced Polyethylene Composites** "J. Macromolecules, 24,PP. 3569-3577,*(1991).*

[57]Hassan H.M., "**The Effect of continuous sputtering on the Adhesion of Ultra High Polyethylene Fiber Reinforced Epoxy Matrix**" J.Alqadisiyah for pure science, vol.13 issue 4, PP.1-7,*(2008).*

[58]Ward I.M., and Ladizeeky N.H.L., " **Ultrahigh Modulus polyethylene composite** ", Pure &Appl. Chem. Vol 57,No11 ,PP. 1641-1649 ,*(1985).*

[59] Nairn.A., "**Residual Stresses Effect in Fractureof Compositeand Adhesives**" J. Mechanical Sci, 37, pp.3965-3972,*(2002).*

Reference

[60] Aijun G., Yizhuo G., Qing W., Chao Y., Min L., Zuoguang Z., " **Influence of processing temperature on interfacial behavior of HKT800 carbon fiber with BMI and epoxy matrices** " J.Chinese Journal of Aeronautics,28: 1255–1262,*(2015).*

 [61]Abas F.O., Abas R.O., and Ibrahim S.I., " **A Comparison Study of Different Ceramic Filler on Mechanical and Thermal Properties of Glass, Carbon, Kevlar / Polyester Composites** "J. Eng. & Tech. Journal ,Vol. 28, No. 12, *(2010).*

[62] Harith A.S., and AL-Ajaj E., " **The Effect of metals as additives on adhesion properties of epoxy resin** "J. Iraqi Journal of Physics, Vol. 9, No.15, PP. 55-62,*(2011).*

[63] Hachim T.M., Abullah Z.S., and Alausi Y.T., " **Evaluation of the effect of addition of polyester fiber on some mechanical properties of heat cure acrylic resin** " J. Baghdad College Dentistry, Vol. 25.PP.23-29,*(2013).*

الخلاصة

في فحص الانسحاب لليف لعينه على شكل حرف (U) لمادة بوليمريه مدعمة بليف مفرد تم حساب متانة القص البيني ومعدل الطاقة المتحررة عند المنطقة البينية تم علاجها في درجات حرارة($25،^oC$، 50^oC،75^oC) التي تتضمن تأثير الاحتكاك و التأثير الحراري حيث أعطت مؤشر على متانة قوى التلاصق في المنطقة البينية. لتحضير العينات، استخدمت قوالب حديدية ذات عرض مختلف لغرض صنع قوالب مطاطية من مادة البولي سالوكسين واستخدمت الاخيرة لعمل العينات من مادتي الايبوكسي والبولي استر حيث دعمت بألياف الزجاج والكاربون والكفلر والبولي اثلين. جميع العينات تم استخدام أطوال وأقطار مختلفة لليف المدعم، تم فحص العينات باستخدام جهاز فحص الشد للحصول على رسوم بيانية تبين العلاقة بين قوه سحب الليف مع طول الليف المنسلخ. تم الدمج بين الطريقة العملية في فحص الليف المنسلخ والنظرية المستخدمة لنايرن لغرض حساب كل من متانة القص البيني والطاقة البينية المتحررة من الانسلاخ الليف والمتضمنة لكل من الإجهاد الحراري و الاحتكاك، وقد أظهرت النتائج زيادة العلاج يؤدي الى زيادة الالتصاق بين الألياف و المادة الحاضنة وهذا يؤدي الى زياد معدل تحرير الطاقه. افضل ماده مركبة تم الحصول عليها هي الايبوكسي-كفلر

شد القص البيني ومعدل القياس للطاقة المتحررة لمواد ليفيه الأساس المسحوبة من البوليمر المركب

رسالة مقدمة

إلى كلية التربية/قسم الفيزياء/جامعه القادسية

كجزء من متطلبات نيل درجه الماجستير في الفيزياء

من قبل

إيلاف عادل عبد علي البديري

بكلوريوس جامعه القادسية ٢٠١٤

بأشراف

الأستاذ المساعد الدكتور هشام محمد علي حسن البيرماني

٢٠١٧ م   ١٤٣٨هـ